# Dilution Effects of Highly Concentrated Electrolyte with Fluorinated Solvents on Charge/Discharge Characteristics of Ni-rich Layered Oxide Positive Electrode

**Ziyang Cao**

March, 2020

# Contents

**CHAPTER 3**

Dilution Effects of Highly Concentrated Dimethyl Carbonate-based Electrolytes with a Hydrofluoroether on Charge/Discharge Properties of $LiNi_{0.8}Co_{0.1}Mn_{0.1}O_2$ Positive Electrode

## CHAPTER 4

Dilution Effects of Highly Concentrated $LiBF_4$/DMC with Fluorinated Esters on Charge/Dishcharge Properties of Ni-rich $LiNi_{0.8}Co_{0.1}Mn_{0.1}O_2$ Positive Electrode

## CHAPTER 5

## General Conclusions and Publication List

# CHAPTER 1

# General Introduction

## 1.1 Background

With the explosion of population and economic growth, human demand for energy is increasing. At present, the energy consumed in the world mainly comes from fossil energy such as coal, oil and natural gas. On one hand, fossil energy is limited in global reserves and it is non-renewable energy. On the other hand, fossil fuels produce a large amount of $CO_2$, $SO_x$, $NO_x$, and other exhaust gases in the combustion process, which not only cause serious pollution to the environment, but also cause the greenhouse effect. In view of the above problems, we should not only continuously improve the utilization efficiency of existing fossil energy, but also should develop new green renewable energy sources, such as solar energy, wind energy, hydropower, and geothermal energy. In the development and utilization of these new energy sources, people need chemical energy storage devices with high

energy conversion efficiency, that is, batteries. Among storage batteries, lithium ion batteries have attracted extensive attention due to their advantages of high energy density, long service life, low self-discharge and no memory effect. Since Sony Corp. successfully commercialized lithium-ion battery technology for the first time in 1991, lithium-ion batteries have been widely used in mobile phones, laptop computers, digital cameras and other consumer electronic devices. In recent years, China, Korea, Japan, the United States, the European Union and other governments around the world have realized the increasingly serious pollution caused by traditional internal combustion engine vehicles, and have begun to issue various supportive and encouraging policies to vigorously promote the development of electric vehicles, resulting in the explosive growth of lithium-ion batteries.

## 1. 2 Lithium ion batteries

### *1.2.1 Configuration of lithium ion batteries*

Depending on different applications in the current market, lithium ion batteries can be divided into four types according to their shapes: cylindrical cells, prismatic cells, coin cells and thin film cells. They are all composed of a positive electrode material, a negative electrode material, an electrolyte and a separator. Lithium transition metal oxides, such as $LiCoO_2$, $LiMn_2O_4$, $LiNiO_2$ and $LiNi_{1-x-y}Mn_xCo_yO_2$[x+y=1], in which lithium ions can be reversibly intercalated, are used as positive electrodes. Graphite, silicon and lithium titanate (LTO) are used as negative electrodes. The electrolyte is mainly a mixed electrolyte solution formed by

dissolving lithium salt ($LiPF_6$, $LiBF_4$, LiTFSI) in organic solvents. Porous films made of polyethylene (PE), polypropylene (PP) and their copolymers are used as separators. Their functions are to allow ions to pass through and to prevent short circuit between the positive and negative electrodes.

### *1.2.2 Working principle of lithium ion batteries*

The working principle of a lithium ion battery is shown in Fig. 1-1. When the battery is charged, the positive electrode releases lithium ions, which flow through the electrolyte to the negative electrode to be stored. The lithium ion battery stores energy during this process. When the battery is discharged, lithium ions within the negative electrode pass through the electrolyte and go back to the positive electrode, producing energy to power the lithium ion battery. The charge/discharge reactions of a lithium ion battery using a $LiCoO_2$ positive electrode and a graphite negative electrode are described as:

$$\text{Cathode:} \quad LiCoO_2 \underset{\text{Discharge}}{\overset{\text{Charge}}{\rightleftarrows}} Li_{1-x}CoO_2 + xLi^+ + xe^- \qquad (1\text{-}1)$$

$$\text{Anode:} \quad 6C\ (\text{Graphite}) + xLi^+ + xe^- \underset{\text{Discharge}}{\overset{\text{Charge}}{\rightleftarrows}} Li_xC_6 \qquad (1\text{-}2)$$

$Li^+$ ions are de-intercalated from $LiCoO_2$ during charging and intercalated between the graphite layers of the graphite negative electrode as in Eqs. (1-1) and (1-2). The reverse reactions occur during discharging. In this scheme, only $Li^+$ ions move between the positive and negative electrodes, which is the reason for the name “Lithium ion batteries”.

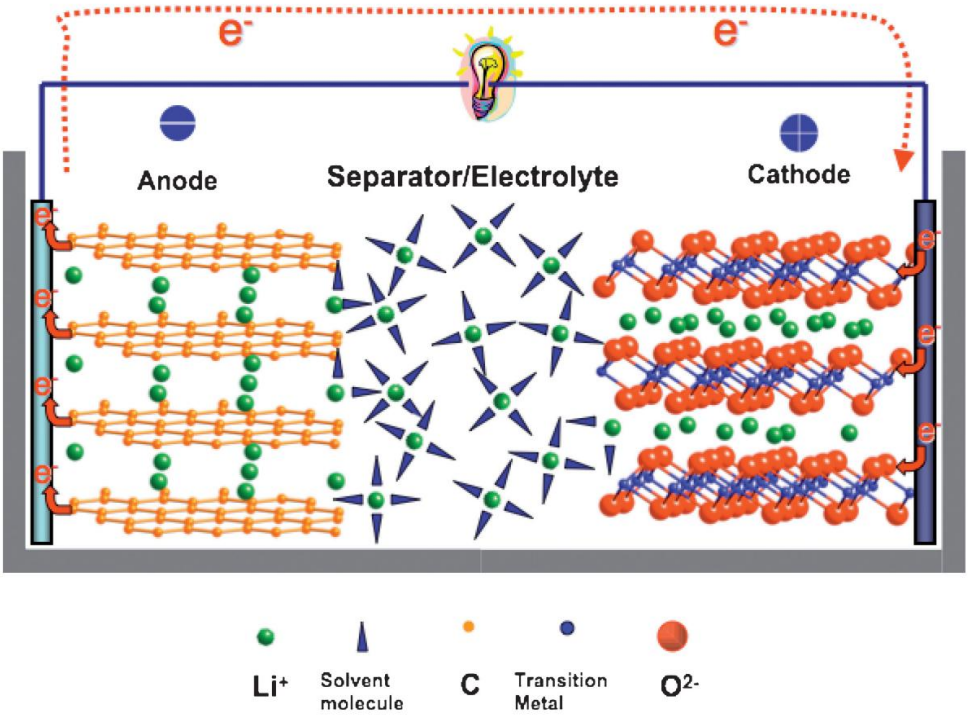


**Fig. 1-1.** Illustration of the components in a lithium ion cell. From *Energy Environ. Sci.,* **2**, A589 (2009)

## 1.3 Positive electrodes

### *1.3.1 $LiCoO_2$*

Figure 1-2 shows the crystal structure of $LiCoO_2$, which is an oxide having an $\alpha$-$NaFeO_2$-type layered structure. The crystal structure belongs to a hexagonal system with a space group of $R\bar{3}m$ and can be viewed as an "ordered rock salt" in which alternate layers of $Li^+$ and $Co^{3+}$ ions occur in the octahedral sites within the cubic close packed oxygen array. $Li^+$ ions can be reversibly de-intercalated from and intercalated into this structure, creating or annihilating vacancies within the triangular lattice formed by $Li^+$ ions in a plane.[1-3] When all $Li^+$ ions were de-intercalated from the lattice, $LiCoO_2$ has a theoretical capacity of 274 mAh $g^{-1}$. However, the practical capacity of $LiCoO_2$ is about 150 mAh $g^{-1}$. This is because when more than 50% of

lithium ions were de-intercalated, the octahedral layered structure of $CoO_6$ becomes unstable, changes to spinel phase, and internal defects of crystal grains increase. Meanwhile, part of the oxide ions escapes in a free state and generates oxygen gas, resulting in rapid capacity decay. In order to increase the reversible capacity, researchers usually use bulk doping,[4,5] surface coating[6,7] and increasing the potential windows by the use of oxidation-resistant electrolytes.[8,9]

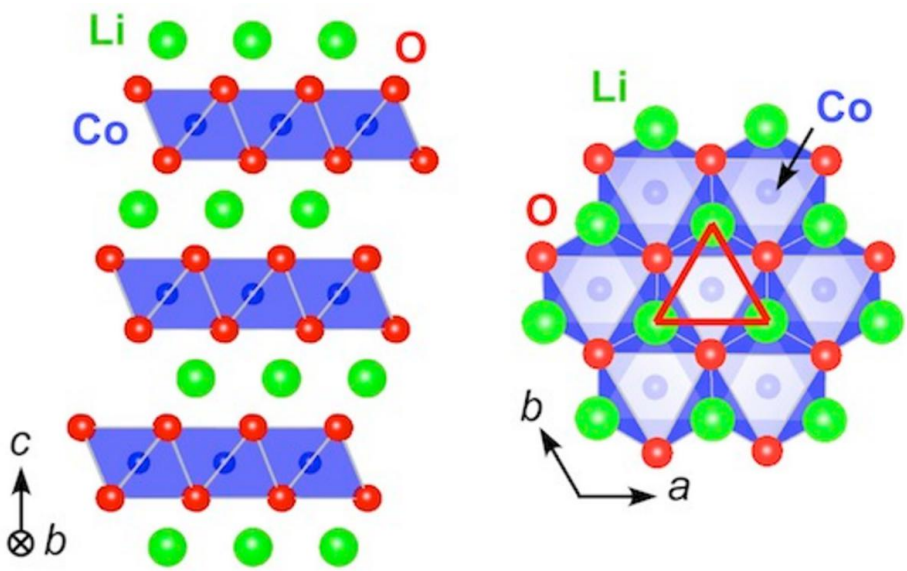


**Fig. 1-2.** Crystal structures of an α-$NaFeO_2$-type insertion electrode ($LiCoO_2$). Form *Phys. Rev. Lett.* **111**, 126104 (2013).

### *1.3.2 Other positive electrode materials*

At present, the positive material used in commercial lithium ion batteries is mainly $LiCoO_2$. $LiCoO_2$ has advantages of easy synthesis and stable cycling performance, but cobalt has the problems of poor resources, high price and high toxicity. Therefore, researchers are actively developing alternative positive electrode

materials that can replace $LiCoO_2$. $LiNiO_2$ has the same layered structure and a similar theoretical capacity as $LiCoO_2$, but the practical capacity is higher than that of $LiCoO_2$ (about 200 mAh $g^{-1}$).[10,11] Due to its low cost and less toxicity. $LiNiO_2$ is a very promising positive electrode material for lithium ion batteries. However, it is very difficult to synthesize stoichiometric $LiNiO_2$ because it easily decomposed to a lithium-deficient $Li_{1-x}Ni_{1+x}O_2$ during high temperature calcination due to the instability of $Ni^{3+}$ ions.[12] The tendency for formation of antisite defects from occupation of $Ni^{2+}$ ions in the $Li^+$ sites, which hinders $Li^+$ diffusion and occurs the cation disorder of $Ni^{2+}/Li^+$, resulting in the deterioration of the cycling performance. Therefore, it is necessary to synthesize $LiNiO_2$ at a low temperature, under enriched oxygen atmosphere with an excessive lithium source to inhibit lithium defect formation and the cation disorder of $Ni^{2+}/Li^+$. On the other hand, using other transition metal elements (such as Co, Al, Mg) to replace part of Ni to form multi-metal compounds can significantly improve electrochemical performance.[13-15]

Lithium manganese oxide, such as $LiMn_2O_4$ and $LiMnO_2$, are often suggested as cathode materials for lithium ion batteries, because the replacement of cobalt by manganese will provide cheaper and less toxic materials. The spinel-type lithium manganese oxide ($LiMn_2O_4$) with a theoretical capacity 148 mAh $g^{-1}$ exhibits a good stability of cycle performance.[16] However, it cannot meet the growing demand for the development of high energy density batteries. In contrast, $LiMnO_2$ positive material has two structure-types, orthorhombic $LiMnO_2$ ( *o*-$LiMnO_2$, space group *Pmnm* ) and monoclinic $LiMnO_2$ ( *m*-$LiMnO_2$, space group *C2/m*), both of which can be used as

positive electrodes for lithium ion batteries with a higher theoretical capacity (285 mAh $g^{-1}$) than that of $LiMn_2O_4$.[17,18] Especially monoclinic $LiMnO_2$ has a layered structure, through which lithium ions move easily. Unfortunately, monoclinic $LiMnO_2$ is a metastable phase, which slowly transforms to tetragonal $Li_2Mn_2O_4$ and *o*-$LiMnO_2$ upon annealing at a high temperature by solid-state reaction methods, leading to a decrease of capacity. The stable layered structure is only obtained by doping other metal elements, such as Co, Al and Cr.[19-21]

According to the above discussion, single layered structures ($LiCoO_2$, $LiNiO_2$, $LiMnO_2$) have their own inevitable disadvantages and are difficult to be used in a large scale in the field of power batteries. Similar to $LiCoO_2$, $LiNi_{1-x-y}Co_xMn_yO_2$ (NCM) ternary materials have a layered structure. Ni, Mn and Co ions randomly occupy the 3b sites of the lattice. Oxide ions occupy the 6c sites, forming $MO_6$ octahedra. Li ions occupy the 3a sites, forming $LiO_6$ octahedra. $Li^+$ ions are located between the $MO_6$ octahedral layers and can be reversibly de-intercalated and intercalated between the layers.[22-26] Due to the obvious synergistic effect among Ni, Co and Mn, NCM is considered as one of the most promising new cathode materials with better performance than single component layered cathode materials. The three elements have different effects on the electrochemical performance of the material. Generally, the presence of Ni is helpful to improve the capacity, but too high a content of Ni causes cation mixing with $Li^+$, resulting in deterioration of cycle performance and rate performance. Co can effectively stabilize the layered structure of the ternary materials, inhibit cation mixing, improve the electronic conductivity of materials and

improve the cycle performance. The existence of Mn can reduce the cost and improve the structural stability and safety of the material. According to the proportional relationship among Ni, Co and Mn, there are several kinds of NCM materials: NCM111, NCM523, NCM622, NCM811 and $LiNi_{0.8}Co0._{15}Al_{0.05}O_2$ (NCA). With the increase of energy density requirements, ternary materials are developing towards a high nickel content (generally Ni-rich ternary materials refer to ternary materials with a Ni content above 60 mol.%). At high potentials, various side reactions between positive material and electrolyte are more severe and the safety becomes worse.[27-28] A lack of electrolytes that are stable at high potentials has greatly restricted the market application of the Ni-rich ternary materials. Comparing the development of Ni-rich ternary materials, the oxidation resistance of electrolyte is slowly. Noh et al. synthesized a series of $Li(Ni_xCo_yMn_z)O_2$ (x = 1/3, 0.5, 0.6, 0.7, 0.8) materials by a co-precipitation method, and studied the influence of Ni content on its electrochemical performance, structure and thermal stability.[29] They found that electrochemical performance and thermal performance are closely related to the Ni content. Figure 1-3 shows that the specific capacity of NCM ternary materials increases with Ni content. However, the capacity retention and safety decrease with Ni content. DSC analysis showed that its structural stability is related to thermal and electrochemical stability, as shown in Fig. 1-4.

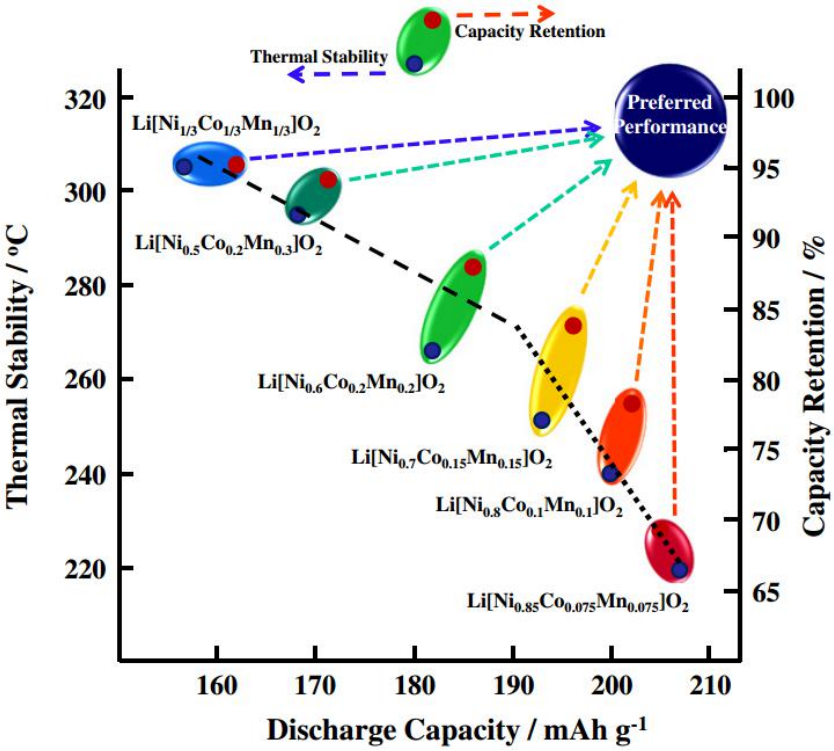


**Fig. 1-3.** A map of relationship between discharge capacity, and thermal stability and capacity retention of Li/Li[$Ni_xCo_yMn_z$]$O_2$ (x = 1/3, 0.5, 0.6, 0.7, 0.8 and 0.85).[29]

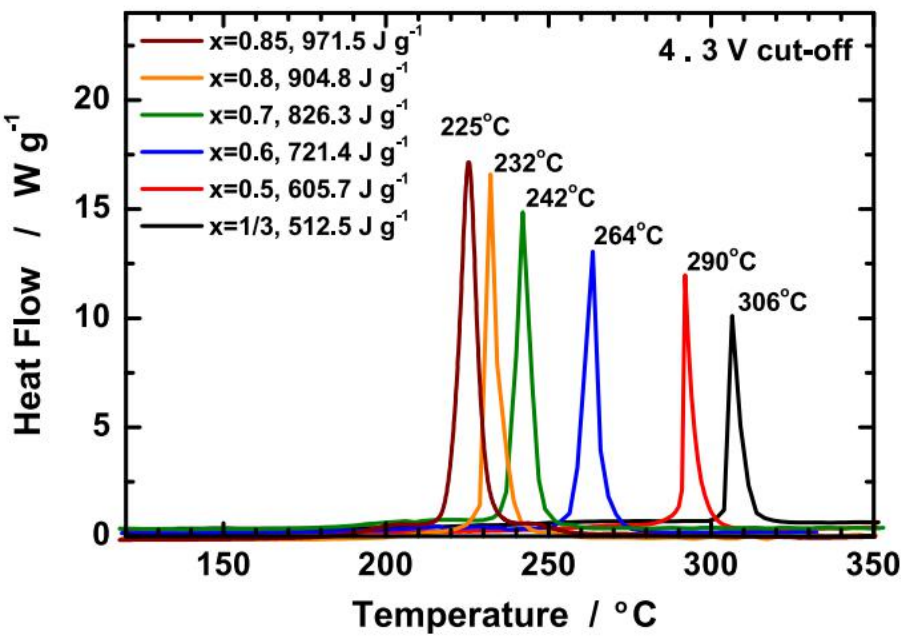


**Fig. 1-4.** DSC results of the $Li_{1-d}$[$Ni_xCo_yMn_z$]$O_2$ materials (x= 1/3, 0.5, 0.6, 0.7, 0.8 and 0.85). [29]

Although the Ni-rich ternary material has advantages over other positive electrode materials in terms of energy density, it also inherits some disadvantages of $LiNiO_2$, such as cation disorder of $Ni^{2+}/Li^{+}$ in the synthesis process, easy transition to the spinel structure in the cycle process, resulting in poor cycle performance, safety performance and storage performance of the Ni-rich material, which hinders the large-scale application of the Ni-rich ternary materials in the field of power batteries. Many studies have shown that the main degradation factors of the ternary materials are as follows:

(1) Cation disorder of $Ni^{2+}/Li^{+}$

Similar to the problems existing in $LiNiO_2$, part of $Ni^{2+}$ ions occupy the $Li^{+}$ sites in the synthesis process of the Ni-rich ternary materials, forming the cation disorder of $Ni^{2+}/Li^{+}$. In addition, in the process of precipitation, Ni ions of low valence in the transition element layer migrate to the lithium layer, occupying Li vacancies and forming the cation disorder of $Ni^{2+}/Li^{+}$.[30] At present, most of researchers believe that $Ni^{2+}$ ions occupying the $Li^{+}$ sites hinder the deintercalation of Li ions and decrease the electrochemical performance of the layered ternary materials.[31-33] Therefore, researchers have proposed a variety of methods to reduce the degree of the $Ni^{2+}/Li^{+}$ disorder, such as increasing the average valence of Ni in the product by using a $Ni_{0.8}Co_{0.15}Al_{0.05}OOH$ precursor,[34] adjusting the lithium content with an excess amount[32] and sintering under oxygen-enriched atmosphere.[35]

(2) Poor thermal stability

The thermal stability of the material is directly related to the safety performance of the battery, and the thermal decomposition temperature of the positive electrode material is often the main factor affecting the thermal runaway of the battery. Recent researches show that the higher the Ni contents in ternary materials, the worse the thermal stability. For example, the decomposition temperature is 306℃ for NCM111, and decreases with the Ni content (NCM523: 290 ℃, NCM811: 232 ℃) when charged to 4.3 V, which is also accompanied by a sharp increase in the amount of heat released.[29] In order to solve this problem, researchers mainly improve the structural stability of the material by ion doping, especially in the lithium-removed (discharged) state, and further improve the thermal stability, especially by the doping of Zr, Nb, Al, F.[36-39] In addition, the surface oxide coating of the material powder with $Li_2ZrO_3$,[40] $TiO_2$,[41] $Sb_2O_3$,[42] $AlPO_4$,[43] $Al_2O_3$,[44] $Li_3PO_4$,[45] can reduce the direct contact between the material and the electrolyte, inhibit the side reaction of the electrolyte, and also improve the thermal stability of the material.

(3) Unstable surface structure

The lithium deintercalation of positive electrode materials starts from the surface, and excessive lithium deintercalation phenomenon occurs in the surface layer structure as charging progresses. As a result, the layered structure of the Ni-rich ternary material changes to a spinel structure or a rock salt structure.[46-48] Usually, after the previous charging and discharging, the surface layer of the material forms a

thicker inert layer. In addition, high valence transition metal ions with high oxidative ability on the surface cause serious side reactions with the electrolyte, which will also increase the polarization of the battery and rapid capacity decay.[49] In order to solve this problem, researchers can effectively stabilize the surface crystal structure of the ternary materials by surface coating.[43,47] Another important method to improve the surface structure of ternary materials is to synthesize gradient materials.[50-51] The surface layer is composed of stable Mn-rich composition, which gradually changes into high-capacity Ni-rich composition inside the particles. Gradient materials can not only maintain the high capacity of ternary materials, but also improve the stability of materials.

(4) Microcrack formation of secondary particles

At present, the precursors of the ternary materials are mostly synthesized by a co-precipitation method, and the co-precipitation is characterized by the aggregation and growth of nano-scale primary particles into secondary particles.[52] In the co-precipitation process, vigorous stirring leads to disordered distribution and agglomeration of primary particles, and hence different degrees of strain and distortion remain in secondary particles. Researches show that with deintercalation of $Li^+$ ion, the volume contraction of ternary materials can reach about 3.9%, which is enough to cause crack formation near the grain boundaries inside the particles. New cracks appearing continuously in the material particles expose fresh surfaces and continue to cause side reactions with electrolyte, eventually causing pulverization of

electrode materials and battery failure.[53,54] Generally, the volume change of Ni-rich ternary materials is larger during cycling, and hence it is easier to cause material failure due to microcrack propagation.[55] Watanabe et al. found that the formation of microcracks in the particles during long-term cycling is directly related to the depth of charge and discharge.[56] The deeper the depth of charge and discharge, the faster the crack propagation and the faster the decay of cycling capacity. Therefore, the charging and discharging depths of the material need to be adjusted by controlling the charging and discharging potentials in practical use to prolong the life of the battery. In addition, a suitable surface coating can also relieve the volume change of the material during the charging and discharging process and inhibit microcrack formation during cycling, thus improving the cycling performance of the material.[57]

(5) Alkali residues on the surface

The basicity of nickel ions in the ternary material is higher than the other transition metal ions, and is easy to absorb moisture and $CO_2$ when exposed to the air, and reacts with residual lithium on the surface to generate LiOH and $Li_2CO_3$, which further increases the pH value of the material and seriously affects the electrochemical performance of the ternary material.[58-60] The higher the nickel content in the ternary material, the more residual alkali on the surface. For example, the pH value of the NCM111 surface is 8-9, while the pH values of NCM811 and NCA are as high as 11-12. On one hand, excessively high pH values are easy to cause slurry gelation in the process of preparing electrode sheets, resulting in uneven coating. On the other

hand, the lithium residues on the surface of the material particles have poor conductivity, which will also increase the polarization of the battery.[61] Xiong et al. proposed that washing NCM811 particles with ethanol solution of $(NH_4)_2HPO_4$ can effectively remove the lithium residues on the surface of particles without destroying the layered structure of NCM811 and effectively improving the electrochemical performance of the material.[62]

### 1.4 Electrolytes

Electrolyte is one of the four key materials of lithium ion batteries. It is called blood of lithium ion batteries and guarantees the high voltage, high specific energy and other advantages of lithium ion batteries. The electrolyte is mainly prepared from high-purity organic solvent, lithium salt and functional additives. The commercial electrolyte commonly employs 1 mol $dm^{-3}$ (1 M) $LiPF_6$/ethylene carbonate (EC)-based electrolytes and the electrolyte formula has been confined over the past 25 years.[63] This is because the combination of $LiPF_6$ and EC has an irreplaceable position in lithium ion batteries. Aluminum current collector is easily corroded at high potentials; however, a hydrolysis reaction of $LiPF_6$ with a trace amount of water can produce HF, which subsequently reacts with Al to form a stable $ALF_3$ film on the surface.[64] The reductive decomposition of EC can form a solid electrolyte interphase (SEI), which can effectively prevent the solvent cointercalation of graphite or continuous electrolyte decomposition at low potentials.[65]

### *1.4.1 Organic solvents*

The electrolyte of lithium ion batteries commonly employs a mixture of organic solvents with a high dielectric constant solvent (to dissolve the lithium salt) and a low viscosity solvent (to facilitate ion transport), while still meeting the requirements of interfacial stability on both positive and negative electrodes. Organic solvents commonly used in lithium ion battery electrolyte include ethylene carbonate (EC), propylene carbonate (PC), diethyl carbonate (DEC), dimethyl carbonate (DMC), methyl ethyl carbonate (EMC), ethyl acrylate (EA), methyl acrylate (MA), etc.[63] The quality of the organic solvent must be strictly controlled before use. The purity of the solvent is closely related to the stable potential window. The water content of the organic solvent plays a decisive role in the preparation of qualified electrolyte. Using molecular sieve adsorption, atmospheric or vacuum distillation and inert gas introduction, the moisture content can meet these requirements.

### *1.4.2 Lithium salts*

Lithium salt accounts for the largest cost (about 40%) of the electrolyte. Commonly used electrolyte lithium salts include lithium hexafluorophosphate ($LiPF_6$),[66] lithium perchlorate ($LiCO_4$),[67] lithium tetrafluoroborate ($LiBF_4$),[66] lithium bis(oxalato)borate (LiBOB),[68] lithium bis(fluorosulfonyl)imide (LiFSI)[69] and lithium bis(trifluoromethanesulfonyl)imide (LiTFSI).[70] Of these lithium salts, $LiPF_6$ has an outstandingly high ionic conductivity, better oxidation stability and lower environmental pollution. Hence $LiPF_6$ has been widely used as the Li salt for

commercially available lithium ion batteries. However, it has a serious shortcoming: that is, it is very sensitive to trace moisture and generates HF in the electrolyte. HF contributes to the dissolution of transition metal ions from positive electrode materials, whereas the metal ions and their complexes cross over to the negative electrode and ruin the important properties of the SEI.[71] Therefore, the control of moisture in the electrolyte should be very strict. In addition to $LiPF_6$, the physicochemical properties of $LiBF_4$, LiBOB, LiFSI, LiTFSI salts are summarized as:[63]

$LiBF_4$: The low temperature performance is better, but the price is expensive and the dissociation in carbonate solutions is poorer, resulting in lower ion conductivity.

LiBOB: The high-temperature performance is better, especially the cointercalation of solvent molecules within the negative electrode can be inhibited, but the solubility is too low.

LiFSI: It is not only environmentally friendly, but also has good thermal stability, high sensitivity to moisture and causing the corrosion of aluminum foil current collector.

LiTFSI: Good electrochemical stability, high ionic conductivity, good thermal stability and the stability for hydrolysis. However, it corrodes aluminum foil current collector.

### *1.4.3 Concentrated electrolytes*

In order to improve the energy density of lithium ion batteries for electric vehicles application, increasing the working voltage of positive electrode materials is

inevitable. However, the commercial $LiPF_6$/EC-based electrolytes easily decompose at potentials higher than 4.3 V vs. $Li/Li^+$, and they do not meet the current demand for high-voltage positive electrodes. At present, various functional additives are added to the electrolyte to form a stable cathode/electrolyte interphase (CEI) on the surface of the positive electrode to prevent the oxidative decomposition of the electrolyte.[72-79] These additives should meet the following requirements: (1) the additive is chemically stable in the electrolyte, (2) the additive has a lower oxidation potential than those of electrolyte solvents, (3) the additive decomposes and can form a stably CEI on the surface of the positive electrode, (4) the additive has no harmful influence on anode in charge/discharge cycles, and (5) the resulting CEI has a good ion conductivity so that $Li^+$ ions and easily intercalated and de-intercalated.

Recently highly concentrated electrolyte solutions have attracted more and more attention by researchers. Researchers found that the concentrated electrolytes have unusual physicochemical and electrochemical properties that are remarkably distinct from conventional diluted (1 M-level) electrolytes. The electrochemical window of concentrated electrolyte is wider than that of the traditional electrolyte solution. The reason is that free solvent molecules have a higher HOMO energy than solvent molecules coordinating $Li^+$ ion, the former of which decompose easier in the electrolyte. As the concentration of Li salt increases, solvent molecules coordinate more strongly to $Li^+$ ions, which give higher stability against the oxidative decomposition during cycling. Wang et al. reported that the use of concentrated LiFSI/DMC suppresses the corrosion of Al current collector at high potentials and

showed an excellent stability against oxidation for $LiNi_{0.5}Mn_{1.5}O_4$ positive electrode at 5 V vs. $Li/Li^+$.[80] In addition, they used concentrated LiFSI/trimethyl phosphate (TMP) electrolyte for $LiNi_{0.5}Mn_{1.5}O_4$/graphite cell and obtained good capacity retention up to the 100th cycle.[81] Doi. et al. found that the solubility of $LiBF_4$ in PC was higher than $LiPF_6$, and the nearly saturated $LiBF_4$/PC electrolyte can suppress the irreversible capacity and gave a good cycleability of the 5 V-class $LiNi_{0.5}Mn_{1.5}O_4$ positive electrode.[82]

Unfortunately, the use of highly concentrated electrolyte causes some problems, such as a high viscosity, a low ionic conductivity and a high cost that limit their use in practical applications. To solve these problems, researchers adopt diluents to decrease the high viscosity of concentrated electrolytes. Fluorinated ethers have been studied in recent years,[83-86] because they hardly coordinate to $Li^+$ ions due to the low donor numbers (DNs), and hence it is believed that the local solvate structure of $Li^+$ ion does not change from that in a highly concentrated electrolyte solution. Meanwhile, fluorinated ethers own other good physicochemical properties, such as nonflammability and high stability against oxidation. Ma et al. reported that a highly concentrated LiTFSI/DMC electrolyte diluted to a normal concentration by 1,1,1,3,3,3-hexafluoro-2-methoxypropane (HFME) behaves like a concentrated electrolyte in chemistry and electrochemistry, while it behaves like a dilute electrolyte in physics. The HFME-diluted electrolyte also can suppress the Al current collector corrosion. $LiNi_{1/3}Co_{1/3}Mn_{1/3}O_4$|graphite cell in the diluted electrolyte exhibited a better cycleability and rate-capability than those in concentrated electrolytes.[86]

## 1.5 Outline of the work

As discussed in previous sections, Ni-rich ternary materials have higher capacity than the commercial $LiCoO_2$ positive electrode, and therefore they are promising candidates for the positive electrode material of lithium ion batteries for use in EVs. In order to improve the cycling performance of the Ni-rich ternary materials, bulk doping, surface coating and optimization of synthesis methods have been adopted so far. However, not only to modify the material itself, but also to develop oxidation resistant electrolytes at high potentials is very important. In this thesis, the author focused on highly concentrated electrolytes and their diluted electrolytes with fluorinated solvents to improve the cycling performance of a Ni-rich ternary $LiNi_{0.8}Co_{0.1}Mn_{0.1}O_2$ (NCM811) for practical application. Dilution effects of the concentrated electrolytes on the charge/discharge properties of NCM811 were discussed in detail from the viewpoint of the solvation structure in the electrolyte.

In Chapter 2, charge/discharge characteristics of nickel-rich $LiNi_{0.8}Co_{0.1}Mn_{0.1}O_2$ cathode was investigated in highly concentrated $LiBF_4$/DMC electrolyte. On the basis of the Raman spectroscopic results, the influence of the solvation structure in the electrolyte on the electrochemical performance of the electrolyte was discussed.

In Chapter 3, 1,1,2,2‐tetrafluoroethyl 2,2,3,3‐tetrafluoropropyl ether (HFE) was chosen to dilute highly concentrated $LiBF_4$/DMC and $LiPF_6$/DMC electrolytes. The cycling performance of $LiNi_{0.8}Co_{0.1}Mn_{0.1}O_2$ positive electrode was investigated in the

diluted electrolytes. The influence of HFE on the solvation structure in the diluted $LiBF_4$/DMC and $LiPF_6$/DMC was investigated by Raman spectra.

In Chapter 4, 3,3,3-trifluoropropionate (CF3CH2COOCH3, 3FMP), methyl tetrafluoropropionate (CF3CHFCOOCH3, 4FMP), and methyl perfluoropropionate (CF3CF2COOCH3, 5FMP)) were used for diluting the concentrated $LiBF_4$/DMC electrolyte. The solvation structures in these diluted electrolytes were investigated by Raman spectroscopy, and the influence on the cycling performance of $LiNi_{0.8}Co_{0.1}Mn_{0.1}O_2$ was discussed.

In Chapter 5, the dilution effects of concentrated electrolyte with fluorinated solvents on the charge/discharge characteristics of NCM811 positive electrode obtained in this thesis were summarized, and the prospects for their use in practical application were proposed.

**References**

[1] K. Mizushima, P. C. Jones, P. J. Wiseman, and J. B. Goodenough, "$Li_xCoO_2$ (0< x ≤1): A new cathode material for batteries of high energy density." *Solid State Ionics*, **3/4**, A171 (1981).

[2] Z. Wang, Z.Wang , W. Peng, H. Guo, X. Li, J. Wang, and A. Qi, "Structure and electrochemical performance of $LiCoO_2$ cathode material in different voltage ranges." *Ionics*, **20**, A1525 (2014).

[3] Y. Meng, and M. Dompablo, "First principles computational materials design for energy storage materials in lithium ion batteries." *Energy Environ. Sci.*, **2**, A589 (2009).

[4] M. Zou, M. Yoshio, S. Gopukumar, and J. Yamaki, "Synthesis of high-voltage (4.5 V) cycling doped $LiCoO_2$ for use in lithium rechargeable cells." *Chem. Mater.*, **15**, A4699 (2003).

[5] S. A. Needhama, G. X. Wang, H. K. Liu, V. A. Drozd, and R. S. Liu, "Synthesis and electrochemical performance of doped $LiCoO_2$ materials." *J. Power Sources*, **174**, A828 (2007).

[6] J. Cho, Y. Kim, and B. Park, "Novel $LiCoO_2$ cathode meterial with $Al_2O_3$ coating for a Li ion cell." *Chem. Mater.*, **12**, A3788 (2002).

[7] Y.-K. Sun, J.-M. Han, S.-T. Myung, S.-W. Lee, and K. Amine, "Significant improvement of high voltage cycling behavior $AlF_3$-coated $liCoO_2$ cathode." *Electrochem. Commun.*, **8**, A821 (2006).

[8] Z. Chen, and J.R. Dahn, "Methods to obtain excellent capacity retention in $LiCoO_2$ cycled to 4.5 V." *Electrochimica Acta*, **49**,A1079 (2004).

[9] F. Wang, Y. Lin, L. Suo, X. Fan, T. Gao, C. Yang, F. Han, Y. Qi, K. Xu, and C. Wang, "Stabilizing high voltage $LiCoO_2$ cathode in aqueous electrolyte with

interphase-forming additive." *Energy Environ. Sci.*, **9**, A3666 (2016).

[10] S. Yamada, M. Fujiwara, and M. Kanda, "Synthesis and properties of $LiNiO_2$ as cathode material for secondary batteries." *J. Power Sources*, **54**, A209 (1995).

[11] C. Yoon, D.-W. Jun, S.-T. Myung, and Y.-K. Sun, "Structural Stability of $LiNiO_2$ Cycled above 4.2 V." *ACS Energy Lett.*, **2**, A1150 (2017).

[12] G. X. Wang, S. Zhong, D. H. Bradhurst, S. X. Dou, and H. K. Liu, "Synthesis and characterization of $LiNiO_2$ compounds as cathodes for rechargeable lithium batteries." *J. Power Sources*, **76**, A141 (1998).

[13] E. Zhcheva, and R. Stoyanova, "Stabilization of the layered crystal structure of $LiNiO_2$ by Co-substitution." *Solid State Ionics*, **66**, A143 (1993).

[14] M. Guilmard, A. Rougier, M. Grune, L. Croguennec, C. Delmas, "Effects of aluminum on the structural and electrochemical properties of $LiNiO_2$." *J. Power Sources*, **115**, A305 (2003).

[15] B. V. R. Chowdari G. V. Subba Rao, and S. Y. Chow, "Cathodic behavior of (Co, Ti, Mg)-doped $LiNiO_2$." *Solid State Ionics*, **140**, A55 (2001).

[16] M.-J. Lee, S. Lee, P. Oh, Y. Kim, and J. Cho, "High Performance $LiMn_2O_4$ Cathode Materials Grown with Epitaxial Layered Nanostructure for Li-Ion Batteries." *Nano Lett.*, **14**, A993 (2014).

[17] I. Koetschau, M. N. Richard, and J.R. Dahn, "Orthorhombic $LiMnO_2$ as a High Capacity Cathode for Li-Ion Cells." *J. Electrochem Soc.*,**14**, A2906 (1995).

[18] S. Zhao, H. Liu, S. Ouyang, and Q. Li, "Synthesis and Performance of $LiMnO_2$ as Cathodes for Li-ion batteries." *J. Wuhan Univ. Techno*., **18**, A5 (2003).

[19] J. N. Reimers, E. W. Fuller, E. Rossen, and J. R. Dahn, "Synthesis and electrochemical studies of $LiMnO_2$ prepared at low temperatures." *J. Electrochem Soc.*, **140**, A3396 (1993).

[20] Y.-I. Jang, B. Huang, Y.-M. Chiang, and D. R. Sadoway "Stabilization of $LiMnO_2$ in the α–$NaFeO_2$ structure type by $LiAlO_2$ addition." *Electrochemical and Solid-State Letters*, **1**, A13 (1998).

[21] B. Ammundsen, J. Desilvestro, T. Groutso, D. Hassell, J. B. Metson, E. Regan, R. Steiner, and P. J. Pickering, "Formation and structural properties of layered LiMnO2 cathode materials." *J. Electrochem Soc.*, **147**, A1078 (2000).

[22] X. Cao, Y. Zhao, L. Zhu, L. Xie, X. Cao, S. Xiong, and C. Wang, "Synthesis and Characterization of $LiNi_{1/3}Co_{1/3}Mn_{1/3}O_2$ as Cathode Materials for Li-Ion Batteries via an Efficacious SolGel Method." *Int. J. Electrochem. Sci.*, **11**, A5267 (2016).

[23] M. Noh and J. Cho, "Optimized synthetic conditions of $LiNi_{0.5}Co_{0.2}Mn_{0.3}O_2$ cathode materials for high rate lithium batteries via co-precipitation method." *J. Electrochem Soc.*, **160**, A105 (2013).

[24] H. Cao, Y. Zhang, J. Zhang, and B. Xia, "Synthesis and electrochemical characterstics of layered $LiNi_{0.6}Co_{0.2}Mn_{0.2}O_2$ cathode material for lithium ion batteries." *Solid State Ionics*, **176**, A1207 (2005).

[25] L. Li, X. Li,, Z. Wang, H. Guo, P. Yue, W. Chen, and L. Wu, "A simple and effective method to synthesize layered $LiNi_{0.8}Co_{0.1}Mn_{0.1}O_2$ cathode materials for lithium ion battery." *Powder Techno.*, **206**, A353 (2011).

[26] W. Liu, G. Hu, Z. Peng, Ke Du, Y. Cao, and Q. Liu, "Synthesis of spherical $LiNi_{0.8}Co_{0.15}Al_{0.05}O_2$ cathode materials for lithium-ion batteries by a co-oxidation-controlled crystallization method." *Chinese Chemical Letters*, **22**, A1099 (2011).

[27] S. Wang, J. Liu, X. Yu, J. Liu, J. Rong, C. Zhu, Q. Wang, Z. Yuan, and Y. Zhang, "Electrochemical Behavior of 3,4-ethylenedioxythiophene as an Anti-overcharge Additive for Lithium-ion Batteries." *Int. J. Electrochem. Sci.*, **14**,

A9527 (2019).

[28] J. Laveda, J. Low, F. Pagani, E. Stilp, S. Dilger, V. Baran, M. Heere, and C. Battaglia, "Stabilizing Capacity Retention in NMC811/Graphite Full Cells via TMSPi Electrolyte Additives." *Appl. Energy Mater.*, **2**, A7036 (2019).

[29] H.-J. Noh, S. Youn, C. S. Yoon, and Y.-K. Sun, "Comparison of the structural and electrochemical properties of layered $Li[Ni_xCo_yMn_z]O_2$ (x=1/3, 0.5, 0.6, 0.7, 0.8 and 0.85) cathode material for lithium-ion batteries." *J. Power Sources.*, **233**, A121 (2013).

[30] F. Wu, Jun Tian, Y. Su, J. Wang, C. Zhang, L. Bao, Tao He, Jinghui Li, and S. Chen, "Effect of $Ni^{2+}$ content on lithium/nickel disorder for Ni-rich cathode materials." *ACS Appl. Mater. Interfaces*, **7**, A7702 (2015).

[31] K. Kang, and G. Ceder, "Factors that affect li mobility in layered lithium transition metal oxides." *Physical Review* B, **74**, 094105 (2006).

[32] C. Fu, G. Li, D. Luo, Q. Li, Jianming Fan, and L. Li, "Nicke-rich layered microspheres cathodes: Lithium/nickel disordering and electrochemical performance." *ACS Appl. Mater. Interfaces*, **6**, A15822 (2014).

[33] P. Xiao, T. Lv, X. Chen, and C. Chang, "$LiNi_{0.8}Co_{0.15}Al_{0.05}O_2$: Enhanced electrochemical performance from reduced cationic disordering in Li slab." *Scientific Reports*, **7**, A1408 (2017).

[34] G. Hu, W. Liu, Z. Peng, K. Du, and Y. Cao, "Synthesis and electrochemical properties of $LiNi_{0.8}Co_{0.15}Al_{0.05}O_2$ prepared from the precursor $Ni_{0.8}co_{0.15}Al_{0.05}OOH$." *J. Power Sources.*, **198**, A258 (2012).

[35] Q. Du, Z. Tang, X. Ma, Y. Zang, X. Sun, Y. Shao, Z. Wen, and C. Chen, "Improving the electrochemical properties of high-energy cathode material $Li_{0.5}Co_{0.2}Mn_{0.3}O_2$ by Zr doping and sintering in oxygen." *Solid State Ionics*, **279**, A11

(2015).

[36] F. Schipper, M. Dixit, Daniel, and D, Aurbach et al. "Stabilizing nickel-rich layered cathode materials by a high-charge cation doping strategy: zirconium-doped $LiNi_{0.6}Co_{0.2}Mn_{0.2}O_2$." *J. Mater. Chem. A*, **4**, A16073 (2016).

[37] H. Kaneda, Y. Koshika, T. Nakamura, H. Nagata, R. Ushio, and K. Mori, "Improving the cycling performance and thermal stability of $LiNi_{0.6}Co_{0.2}Mn_{0.2}O_2$ cathode materials by Nb-droping and surface modification." *Int. J. Electrochem. Sci.*, **12,** A4640 (2017).

[38] D. Aurbach, O. Srur-Lavi, and A. Garsuchc et al., "Studies of aluminum-doped $LiNi_{0.5}Co_{0.2}Mn_{0.3}O_2$: electrochemical behavior, aging, structural transformations, and thermal characteristics." *J. Electrochem Soc.*, **162,** A1014 (2015).

[39] X. Lia, Z. Xiea, W. Liua, W. Gea, H. Wang, and M. Qu, "Effects of fluorine doping on structure, surface chemistry, and electrochemical performance of $liN_{i0.8}Co_{0.15}Al_{0.05}O_2$." *Electrochimica Acta,* **174**, A1122 (2015).

[40] J. Zhang, Z. Li, R. Gao, Z. Hu, and X. Liu, "High rate capability and excellent thermal stability of $Li^+$-conductive $Li_2ZrCo_{1/3}Mn_{1/3}O_2$ via a synchronous lithiation strategy." *J. Phys. Chem. C*, **119**, A20350 (2015).

[41] Y. Choa, Y.-S. Leea, S.-A. Park, Y, Lee, and J. Choa, "$LiNi_{0.8}Co_{0.15}Al_{0.05}O_2$ cathode materials prepared by $TiO_2$ nanoparticle coatings on $Ni_{0.8}Co_{0.15}Al_{0.05}(OH)_2$ precursors." *Electrochimica Acta,* **56, A**333 (2010).

[42] Z. Han, J. Yu, H. Zhan, X. Liu, and Y. Zhou, "$Sb_2O_3$-modified $LiNi_{1/3}Co_{1/3}Mn_{1/3}O_2$ material with enhanced thermal safty and electrochemical property." *J. Power Sources*, **254**, A106 (2014).

[43] J. Cho, T. Kim, J. Kim, M. Noh, and B. Park, "Synthesis, thermal, and electrochemical properties of $AlPO_4$-coated $LiNi_{0.8}Co_{0.1}Mn_{0.1}O_2$ cathoide materials for

a Li-ion cell." *J. Electrochem Soc.*, **151**, A1899 (2004).

[44] Y. Shi, M, Zhang, D, Qian, and Y. Meng, "Ultrathin $Al_2O_3$ coatings for improved cycling performance and thermal stability of $LiNi_{0.5}Co_{0.2}Mn_{0.3}O_2$ cathode material." *Electrochimica Acta*, **203**, A154 (2016).

[45] Z. Tang, R. Wu, P. Huang, Q. Wang, and C. Chen, "Improving the electrochemical performance of ni-rich cathode material $liNi_{0.815}Co_{0.15}Al_{0.035}O_2$ by removing the lithium residues and forming $Li_3PO_4$ coating layer." *J. Alloys and Compounds*, **693**, A1157 (2017).

[46] S. Hwang, W. Chang, S. Kim, D. Su, D. Kim, J. Lee, K. Chung, and E. Stach, "Investigation of changes in the surface structure of $Li_xNi_{0.8}Co_{0.15}Al_{0.05}O_2$ cathode materials induced by the initial charge." *Chem. Mater.*, **26**, A1084 (2014).

[47] A. Yano, S. Aoyama, M. Shikano, H. Sakaebe, K. Tatsumi, and Z. Ogumi, "Surface structure and high-voltage charge/discharge characteristics of Al-oxide coated $LiNi_{1/3}Co_{1/3}Mn_{1/3}O_2$ cathodes." *J. Electrochem Soc.*, **162,** A3137 (2015).

[48] S. Sallis, N. Pereira, P. Mukherjee, N. F. Quackenbush, N. Faenza, C. Schlueter, T.-L. Lee, W. L. Yang, F. Cosandey, G. G. Amatucci, L. and F. J. Piper, "Surface degradation of $Li_xNi_{0.8}Co_{0.15}Al_{0.05}O_2$ cathodes: correlating charge transfer impedance with surface phase transformations." *Appl. Phys. Lett.*, **108**, A263902 (2016).

[49] Y. M. Lee, K.-M. Nam, E.-H. Hwang, Y.-G. Kwon, D.-H. Kang, S.-S. Kim, and S.-W. Song, "Interfacial origin of performance improvement and fade for 4.6 V $LiNi_{0.5}Co_{0.2}Mn_{0.3}O_2$ battery cathodes." *J. Phys. Chem. C*, **118**, A10631 (2014).

[50] B.-B. Lim, S.-J. Yoon, K.-J. Park, C.- S. Yoon, S.-J. Kim, J.- J. Lee, and Y.-K. Sun, "Advanced concentration gradient cathode material with two-slope for high-energy and safe lithium batteries." *Adv. Functional mater.*, **25**, A4673 (2015).

[51] P. Hou, H. Zhang, Z. Zi, L. Zhang, and X. Xu, "Core–shell and concentration-gradient cathodes prepared via co-precipitation reaction for advanced lithium-ion batteries." *J. Mater. Chem. A*, **5**, A4254 (2017).

[52] Y. Yang, S. Xu, M. Xie, Y. He, G. Huang, and Y. Yang, "Growth mechanisms for spherical mixed hydroxide agglomerates prepared by co-precipitation method: A case of $Ni_{1/3}Co_{1/3}Mn_{1/3(}OH)_2$." *J. Alloys and Compounds*, **619**, A846 (2015).

[53] S. Zheng, R. Huang, Y. Makimura, Y. Ukyo, C. A. J. Fisher, T. Hirayama, and Y. Ikuhara, "Microstructural changes in $LiNi_{0.8}Co_{0.15}Al_{0.05}O_2$ positive electrode material during the first cycle." *J. Electrochem. Soc.*, **158**, A357 (2011).

[54] J.-M. Lim, T. Hwang, D. Kim, M.-S. Park, K. Cho, and M. Cho, "Intrinsic origins of crack generation in Ni-rich $LiNi_{0.8}Co_{0.1}Mn_{0.1}O_2$ layered oxide cathode material." *Scientific Reports*, **7**, A39669 (2017).

[55] K. Mukai, "Pseudo zero-strain insertion materials for Li-ion batteries: cross-sectional observations of $LiNi_{1/2}Co_{1/2}O_2$, $liNi_{1/3}Co_{1/3}Mn_{1/3}O_2$ and $LiNi_{0.8}Co_{0.15}Al_{0.05}O_2$." *Ionics*, **24**, A2181 (2018).

[56] S. Watanabe, M. Kinoshita, T. Hosokawa, K. Morigaki, and K. Nakura, "Capacity fading of $LiAl_yNi_{1-x-y}Co_xO_2$ cathode for lithium-ion batteries during accelerated calendar and cycle life tests (effect of depth of discharge in charge-discharge cycling on the suppression of the micro-crack generation of $LiAl_yNi_{1-x-y}Co_xO_2$ particle)." *J. Power Sources*, **260**, A50 (2014).

[57] H. Kim, M.-G. Kim, H.-Y. Jeong, H. Nam, and J. Cho, "A new coating method for alleviating surface degradation of $LiNi_{0.6}Co_{0.2}Mn_{0.2}O_2$ cathode material: nanoscale surface treatment of primary particles." *Nano Lett.*, **15**, A2111 (2015).

[58] G. Zhuang, G. Chen, J. Shim, X. Song, P. Ross, and T. Richardson, "$Li_2CO_3$ in $LiNi_{0.8}Co_{0.15}Al_{0.05}O_2$ cathodes and its effects on capacity and power." *J. Power*

*Sources*, **134**, A293 (2004).

[59] N. Mijung, Y. Lee, and J. Choa, "Water adsorption and storage characteristics of optimized $LiCoO_2$ and $LiNi_{1/3}Co_{1/3}Mn_{1/3}O_2$ composite cathode material for Li-ion cells." *J. Electrochem. Soc.*, **153**, A935 (2006).

[60] K. Shizuka, C. Kiyohara, K. Shima, and Y. Takeda, "Effect of $CO_2$ on layerd $Li_{1+z}Ni_{1-x-y}Co_xM_yO_2$ (M=Al, Mn) cathode materials for lithium ion batteries." *J. Power Sources*, **166**, A233 (2007).

[61] X. Xiong, Z. Wang, P. Yue, H. Guo, F. Wu, J. Wang, and X. Li, "Washing effects on electrochemical performance and storage characteristic of $LiNi_{0.8}Co_{0.1}Mn_{0.1}O_2$ as cathode material for lithium-ion batteries." *J. Power Sources*, **222**, A318 (2013).

[62] X. Xiong, D. Ding, Y. Bu, Z. Wang, B. Huang, H. Guo, and X. Li, "Enahnced electrochemical properties of a $LiNiO_2$-based cathode material by removing lithium residues with $(NH_4)_2HPO_4$." *J. Mater. Chem. A*, **2**, A11691 (2014).

[63] K. Xu, "Nonaqueous liquid electrolytes for lithium-based rechargeable batteries." *Chem. Rev*, **104**, 4303 (2004).

[64] S.-Y. Myung, Y. Sasaki, S. Sakurada, Y.-K. Sun, and H. Yashiro, "Electrochemical behavior of current collectors for lithium batteries in non-aqueous alkyl carbonate solution and surface analysis by ToF-SIMS." *Electrochim. Acta*, **55**, A288 (2009).

[65] R. Fong, U. V. Sacken, and J. R. Dahn, "Studies of lithium intercalation into carbons using nonaqueous electrochemical cells." *J. Electrochem. Soc.*, **137**, A2009 (1990).

[66] R. Marom, Ortal Haik, D. Aurbach, and I. C. Halalay, "Revisiting $LiClO_4$ as an Electrolyte for Rechargeable Lithium-Ion Batteries." *J. Electrochem. Soc.*, **157**, A972 (2010).

[67] S. S. Zhang, K. Xu, and T. R. Jow, "Study of $LiBF_4$ as an Electrolyte Salt for a Li-Ion Battery." *J. Electrochem. Soc.*, **149**, A586 (2002).

[68] T. Corina, F. Meike, W.-M. Margret, W. Ulrich, and B. Thorsten, "LiBOB as Electrolyte Salt or Additive for Lithium-Ion Batteries Based on $LiNi_{0.8}Co_{0.15}Al_{0.05}O_2$/Graphite." *J. Electrochem. Soc.*, **157**, A721 (2010).

[69] H. Han, S. Zhou, and Z. Zhou et al., "Lithium bis(fluorosulfonyl)imide (LiFSI) as conducting salt for nonaqueous liquid electrolytes for lithium-ion batteries: Physicochemical and electrochemical properties." *J. Power Sources*, **196**, A3623 (2011).

[70] S. F. Lux, L. Terborg, O. Hachmoller, T. Placke, H.-W. Meyer, S. Passerini, M. Winter, and S. Nowak, "LiTFSI Stability in Water and Its Possible Use in Aqueous Lithium-Ion Batteries: pH Dependency, Electrochemical Window and Temperature Stability." *J. Electrochem. Soc.*, **160**, A1694 (2013).

[71] A. Gueguen, D. Streich, M. He, M. Mendez, F. F. Chesneau, Petr Novak, and E. J. Berga, "Decomposition of $LiPF_6$ in High Energy Lithium-Ion Batteries Studied with Online Electrochemical Mass Spectrometry." *J. Electrochem. Soc.*, **163**, A1095 (2016).

[72] H. Kim, M. G. Kim, H. Y. Jeong, H. l. Nam, and J. Cho, "A New Coating Method for Alleviating Surface Degradation of $LiNi_{0.6}Co_{0.2}Mn_{0.2}O_2$ Cathode Material: Nanoscale Surface Treatment of Primary Particles." *Nano Lett.*, **15**, A2111 (2015).

[73] S. Chen, T. He, Y. Sun, Y. Lu, L. Bao, L. Chen, Q. Zhang, J. Wang, R. Chen, and F. Wu, "Ni-Rich $LiNi_{0.8}Co_{0.1}Mn_{0.1}O_2$ Oxide Coated by Dual-Conductive Layers as High Performance Cathode Material for Lithium-Ion Batteries." *Appl. Mater. Interfaces*, **9**, A29732 (2017).

[74] K. Abe, Y. Ushigoe, H. Yoshitake, and M. Yoshio, "Novel type additives for cathode materials, providing high cycleability performance." *J. Power Sources*, **153**, A328 (2006).

[75] N. S. Choi, J. G. Han, S. Y. Ha, I. Park, and C. K. Back, "Recent advances in the electrolytes for interfacial stability of high-voltage cathodes in lithium-ion batteries." *RSC Adv.*, **5**, A2732 (2015).

[76] Y. K. Han, J. Yoo, and T. Yim, "Why is tris(trimethylsilyl) phosphite effective as an additive for high-voltage lithium-ion batteries?" *J. Mater. Chem. A*, **3**, A10900 (2015).

[77] C. Peebles, R. Sahore, J. A. Gilbert, J. C. Garcia, A. Tornheim, J. Bareno, H. Iddir, C. Liao, and D. P. Abraham, "Tris(trimethylsilyl) Phosphite (TMSPi) and Triethyl Phosphite (TEPi) as Electrolyte Additives for Lithium Ion Batteries: Mechanistic Insights into Differences during $LiNi_{0.5}Mn_{0.3}Co_{0.2}O_2$-Graphite Full Cell Cycling." *J. Electrochem. Soc.*, **164,** A1579 (2017).

[78] W. D. Qiu, J. Xia, L. P. Chen, and J. R. Dahn, "A study of methyl phenyl carbonate and diphenyl carbonate as electrolyte additives for high voltage $LiNi_{0.8}Mn_{0.1}Co_{0.1}O_2$/graphite pouch cells." *J. Power Sources*, **318**, A228 (2016).

[79] D. Y. Wang, J. Xia, L. Ma, K. J. Nelson, J. E. Harlow, D. J. Xiong, L. E. Downie, R. Petibon, J. C. Burns, A. Xiao, W. M. Lamanna, and J. R. Dahn, "A Systematic Study of Electrolyte Additives in $Li[Ni_{1/3}Mn_{1/3}Co_{1/3}]O_2$ (NMC)/Graphite Pouch Cells." *J. Electrochem. Soc.*, **161**, A1818 (2014).

[80] Y. Yamada, and A. Yamada. “Review — Superconcentrated Electrolytes for Lithium Batteries.” *J. Electrochem Soc.*, **162**, A2406 (2015).

[81] J. Wang, Y. Yamada, K. Sodeyama, E. Watanabe, K. Takada, Y. Tateyama, and A. Yamada, “Fire-extinguishing organic electrolytes for safe batteries.” *Nature Energy*, **3**, A22 (2018).

[82] T. Doi, R. Masuhara, M. Hashinokuchi, Y. Shimizu, and M. Inaba, “Concentrated $LiPF_6$/PC electrolyte solutions for 5-V $LiNi_{0.5}Mn_{1.5}O_4$ positive electrode in lithium-ion batteries.” *Electrochim. Acta.*, **209**, A219 (2016).

[83] T. Doi, Y. Shimizu, M. Hashinokuchi, and M. Inaba, “Dilution of highly concentrated libf4/propylene carbonate electrolyte solution with fluoroalkyl ethers for 5-V $LiNi_{0.5}Mn_{1.5}O_4$ positive electrodes.” *J. Electrochem Soc*., **164**, A6412 (2017).

[84] T. Doi, R. Matsumoto, Z. Cao, M. Hashinokuchi, and M. Inaba, “Fluoroalkyl ether-diluted dimethyl carbonate-based electrolyte solutions for high-voltage operation of $LiNi_{0.5}Co_{0.2}Mn_{0.3}O_2$ electrodes in lithium ion batteries.” *Sustainable Energy Fuels*, **2**, A1197 (2018).

[85] S. Chen, J. Zheng, D. Mei, K. S. Han, M. H. Engelhard, W. Zhao, W. Xu, J. Liu, and J.-G. Zhang, “High-Voltage Lithium-Metal Batteries Enabled by Localized High-Concentration Electrolytes.” *Adv. Mater.*, **30**, A1706102 (2018).

[86] G. Ma, L. Wang, X. He, J. Zhang, H. Chen, W. Xu, and Y. Ding, “Pseudoconcentrated Electrolyte with High Ionic Conductivity and Stability Enables High-Voltage Lithium-Ion Battery Chemistry.” *ACS Appl. Energy Mater*., **1**, A5446 (2018).

# CHAPTER 2

# Improved Cycle Performance of $LiNi_{0.8}Co_{0.1}Mn_{0.1}O_2$ Positive Electrode Material in Highly Concentrated $LiBF_4$/DMC

## 2.1 Introduction

With the depletion of natural resources, such as oil and gas, and the aggravation of environmental pollution, it is urgent to develop new environmentally friendly energy to substitute for traditional energy. Lithium-ion batteries (LIBs) are widely used as power sources of electric vehicles (EVs) including battery electric vehicles (BEVs), plug-in hybrid electric vehicles (PHEVs) and hybrid electric vehicles (HEVs).[1-3] Previous researches indicate that nickel-rich layered lithium transition metal oxides such as $LiNi_{0.8}Co_{0.1}Mn_{0.1}O_2$ (NCM811) is one of the most promising candidates for the cathode material of LIBs mounted in EVs because of their higher energy density, a lower cost, and more environmentally friendly than the conventional $LiCoO_2$, $LiNi_{1/3}Co_{1/3}Mn_{1/3}O_2$, and $LiMn_2O_4$ cathode materials.[4,5] Unfortunately, poor cycle performance of $LiNi_{0.8}Co_{0.1}Mn_{0.1}O_2$ limits its use in commercial applications.

The main reasons for the degradation are classified into the following three. The first one is the decomposition of electrolyte solution at high potentials,[6,7] which deteriorates the active material during cycling. The second one is surface structural reconstruction, such as $Ni^{2+}/Li^{+}$ cation disorder and oxygen non-stoichiometry, which leads to severe capacity decay upon cycling.[8,9] The third one is crack formation of the secondary particles of NCM811 caused by expansion/shrinkage during cycling, which results in particle disintegration and loss of electronic contact.[10,11] To overcome these problems, various additives that form a stable cathode/electrolyte interphase (CEI)[12-15] and the modification of the active material surface, for example, with an oxide thin layer have been proposed.[16-20] The surface modification not only inhibits the oxidation reaction of the electrolyte solution on the active material, but also suppresses the surface phase transformations from the layered to a disorder spinel and a rock-salt structure. In contrast to these, crack formation is a mechanical property of the secondary particles and hence it has been believed that an improvement of the mechanical strength is needed to attain good cycleability.

Highly concentrated electrolyte solutions have been attracted by more and more researchers in recent years because of their unique properties.[21-23] One of the advantages of concentrated electrolyte is that the electrochemical window is wider than the traditional 1 mol $dm^{-3}$-level electrolyte solutions.[24-31] Because almost all the solvent molecules coordinate $Li^{+}$ ions in highly concentrated electrolytes, their anodic or cathodic stability is improved compared with the traditional electrolyte solutions that contain a large amount of free solvent molecules. In our previous studies, we

reported that highly concentrated propylene carbonate (PC), γ-butyrolactone (GBL) and dimethylcarbonate (DMC) based electrolytes exhibit high anodic stability against high potentials of 5-V class $LiNi_{0.5}Mn_{1.5}O_4$ and 4.6 V-charged $LiNi_{0.5}Co_{0.2}Mn_{0.3}O_2$.[28-31] Even though the charging limit of NCM811 is lower (4.3 V vs. $Li/Li^+$) than these cathode materials, the high stability against oxidation of highly concentrated electrolytes should improve the cycling performance of NCM811 cathode.

In Chapter 2, DMC was used for dissolving a $LiBF_4$ salt, because it owns a low viscosity and $LiBF_4$ has a high solubility (> 8.67 mol $kg^{-1}$ at 25 °C) in DMC. The $LiBF_4$ salt has good thermal and oxidative stability and is less sensitive to trace water. Hence it hardly generates HF and prevents the dissolution of the transition metal ions in the electrolyte solution.[32,33] Charge and discharge characteristics of NCM811 cathode were investigated in $LiBF_4$/DMC electrolytes of different concentrations. We found that the use of the highly concentrated $LiBF_4$/DMC suppressed not only solvent decomposition at the cathode particle surface, but also particle disintegration by crack propagation, and is an effective way to improve the cycleability of NCM811.

## 2.2 Experimental

### *2.2.1 Preparation of electrolyte solution*

DMC (Kishida Chemical Co. Ltd) was used without further purification. $LiBF_4$ (Kishida Chemical Co. Ltd) was dissolved in DMC to prepare 0.93 (ca. 1 M), 2.22 and 8.67 mol $kg^{-1}$ (nearly saturated) electrolyte solution. The molar ratios (DMC/Li)

were 11.9, 5.00 and 1.28, respectively. 1 mol $dm^{-3}$ (ca. 1 M) $LiPF_6$/EC+DMC (1:1 by volume) was purchased form Kishida Chemical Co., Ltd and used as a reference electrolyte.

### *2.2.2 Characterization of electrolyte solutions*

The viscosity of electrolyte solution was measured with an Ubbelohde capillary viscometer at room temperature in an Ar-filled glove box (MDB-1NKP-DS, Miwa Mfg). Raman spectra of the electrolyte solutions were obtained with a Raman spectrometer (LabRAM HR Evolution, Horiba) equipped with a multichannel charge coupled device detector. The spectra were recorded using a 785-nm semiconductor laser (100 mW) through an objective lens. The solvation and HOMO energies of different solvated states of the solvents interacting with $Li^+$, as well as $BF_4^-$ anion, were estimated by a first-principle calculation using the Gaussian 09W(B3LYP/ 6-31G(d)).

The ionic conductivity was measured with an a.c. impedance analyzer (VersaSTAT 3, Princeton Applied Research) using a symmetrical cell with two Pt plate electrodes. Stability against oxidation was evaluated by linear sweep voltammetry, which was performed at a scan rate of 1 mV $s^{-1}$ between 3.0 and 6.0 V (vs. $Li/Li^+$) using a three-electrode cell with a Pt disk (10 mm in diameter) as a working electrode and Li foils as a reference and a counter electrode.

### *2.2.3 Charge and discharge tests*

The slurry consisting of 80 mass% $LiNi_{0.8}Co_{0.1}Mn_{0.1}O_2$ powder as an active material, 10 mass% graphitized Ketjenblack (FD-7001D, Lion Specialty Chemicals) as a conductor, 10 mass% poly[(vinylidenefluoride)-co-chorotrifluoroethylene] (P(VdF-CtFE)) as a binder and 1-methyl-2-pyrrolidone (NMP) as a solvent was cast onto an aluminum foil. The sheet was dried at 80°C for 18 h in a vacuum oven, and was punched into discs of 13 mm in diameter. The disc electrode as a working electrode was used to assemble a two-electrode coin-type cell with lithium foil (Honjo Metal Co., Ltd, 15 mm in diameter) as a counter electrode. A glass filter (GF/D, Whatman®) was used as a separator and dipped in the electrolyte solution, prior to assembling the coin-type cells in the Ar-filled glove box. Charge and discharge tests were performed with a two-electrode coin-type cell between 3.0 V and 4.3 V vs $Li/Li^+$ at 30°C using a battery test system (TOSCAT-3100, Toyo system Co., Ltd.) at a C/10 rate. Electrochemical impedance was measured with using the a.c. impedance analyzer in a three-electrode coin-type cell.

After charge and discharge tests, the coin-type cell was disassembled in the Ar-filled glove box. The NCM811 electrode was washed with DMC to remove residual solvent and $LiBF_4$ salt, and then dried for one day. Surface morphology observation and elemental analysis of the NCM811 electrode were carried out with a scanning electron microscope (SEM) (SU8220, HITACHI Ltd.) equipped with an energy dispersive X-ray spectroscopy (EDX, XFlash5060FQ, Bruker).

## 2.3 Results and discussions

### *2.3.1 Characterization of concentrated electrolytes*

Figure 2-1 shows the Raman spectra (890-960 $cm^{-1}$) of pure DMC solvent and $LiBF_4$/DMC electrolytes in the concentration range of 0.93 (ca. 1 mol $dm^{-3}$) to 8.67 mol $kg^{-1}$ (DMC/$Li^+$ from 11.9 to 1.28). Pure DMC solvent showed only one band at around 916 $cm^{-1}$ in this range, which is assigned to the O-$CH_3$ stretching vibration mode of free DMC molecule. On the spectra of $LiBF_4$/DMC electrolytes, another band appeared at around 933 $cm^{-1}$, which derived from DMC molecules coordinating with $Li^+$. With decreasing the molar ratio of DMC/Li, the scattering intensity of the solvated DMC band increased, while that of the free DMC band gradually decreased. In the nearly saturated 8.67 mol $kg^{-1}$ $LiBF_4$/DMC (DMC/Li = 1.28), the free DMC band became extremely small, indicating that almost all the DMC molecules coordinated with $Li^+$ in the highly concentrated electrolyte solution.

The coordination numbers of DMC molecules toward $Li^+$ were evaluated from the intensities of the bands at 916 and 933 $cm^{-1}$ (i.e., stretching vibration modes of free and coordinating DMC, respectively) using the method reported by Homma et al.,[34] and Yamada et al.,[35] the details of which is described in Supporting Information. The variation of the coordination number of DMC with molar ratio DMC/Li is shown in Fig. 2-2. At low concentrations (i.e. high DMC/Li), the coordination number was close to 2, which is similar to that reported by Chapman et al.[36] At molar ratios of DMC/Li lower than 4, the coordination number gradually decreased. The decrease in the coordination number is attributed to the formation of aggregates including $Li^+$ ions,

$BF_4^-$ anions and DMC solvent molecules, which is discussed in the following paragraph.

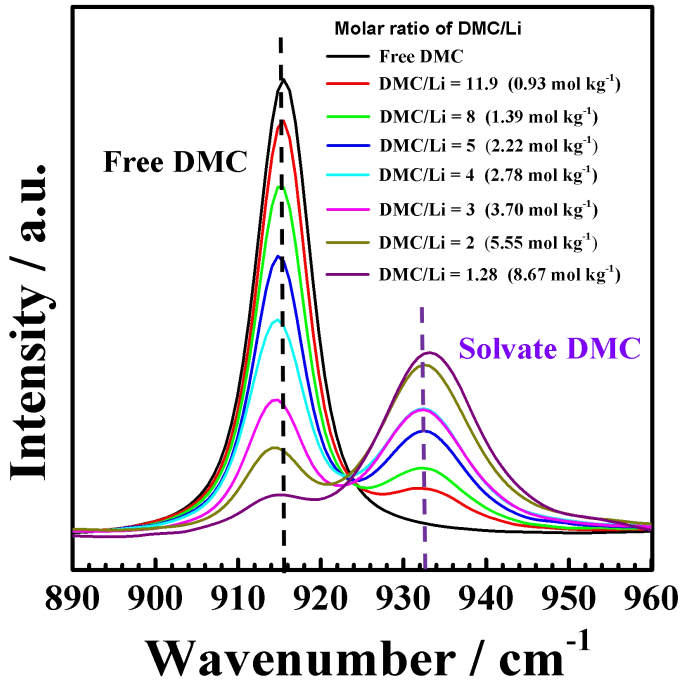


**Fig. 2-1.** Raman spectra (890-960 $cm^{-1}$ ) of pure DMC and $LiBF_4$/DMC of different DMC/Li molar ratios.

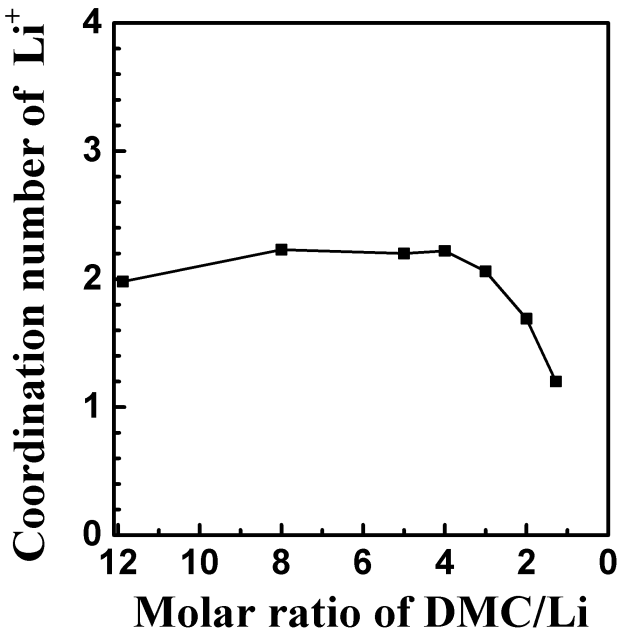


**Fig. 2-2.** Calculated coordination numbers for $LiBF_4$/DMC of different DMC/Li molar ratios.

Figure 2-3 shows the Raman spectra in the range of 750 to 815 $cm^{-1}$. Three peaks relating to the B-F symmetric vibration band from $BF_4^-$ anion were observed at 764, 773, and 781 $cm^{-1}$. These bands can be assigned to the vibration modes of solvent-separated ion pairs (SSIP), contact ion pairs (CIP) and aggregates (AGG), respectively.[37,38] The peak appeared at 799 $cm^{-1}$ is not relevant to $BF_4^-$ anion, but is assigned to the rocking vibration of $OCO_2$ in the DMC molecule.[39] Peak fitting of these bands enabled us to obtain the percentage of these components, and the results are shown in Fig. 2-4. It is clear that $Li^+$ ions, $BF_4^-$ anions and DMC solvent molecules are likely to form aggregates, and their formation is enhanced at molar ratios of DMC/Li lower than 4. In the aggregates, $BF_4^-$ anion would preferentially coordinate to at least one $Li^+$ ion because of high electron affinity of F atom and inhibit DMC molecule from coordinating to $Li^+$ ion, leading to lowering the coordination number of DMC.[38] The solvation energy of $Li(DMC)_nBF_4$ (n = 1, 2) is higher than $Li(DMC)_n$ (Fig. S2-2a in Supplementary Information), which confirmed the above tendency. When the solvation number DMC/Li decreases, the HOMO energy was gradually lowered for both $Li(DMC)_nBF_4$ and $Li(DMC)_n$ (Fig. S2-2b), which suggests that the anodic stability of the electrolyte solution should increase with an increase in salt concentration.

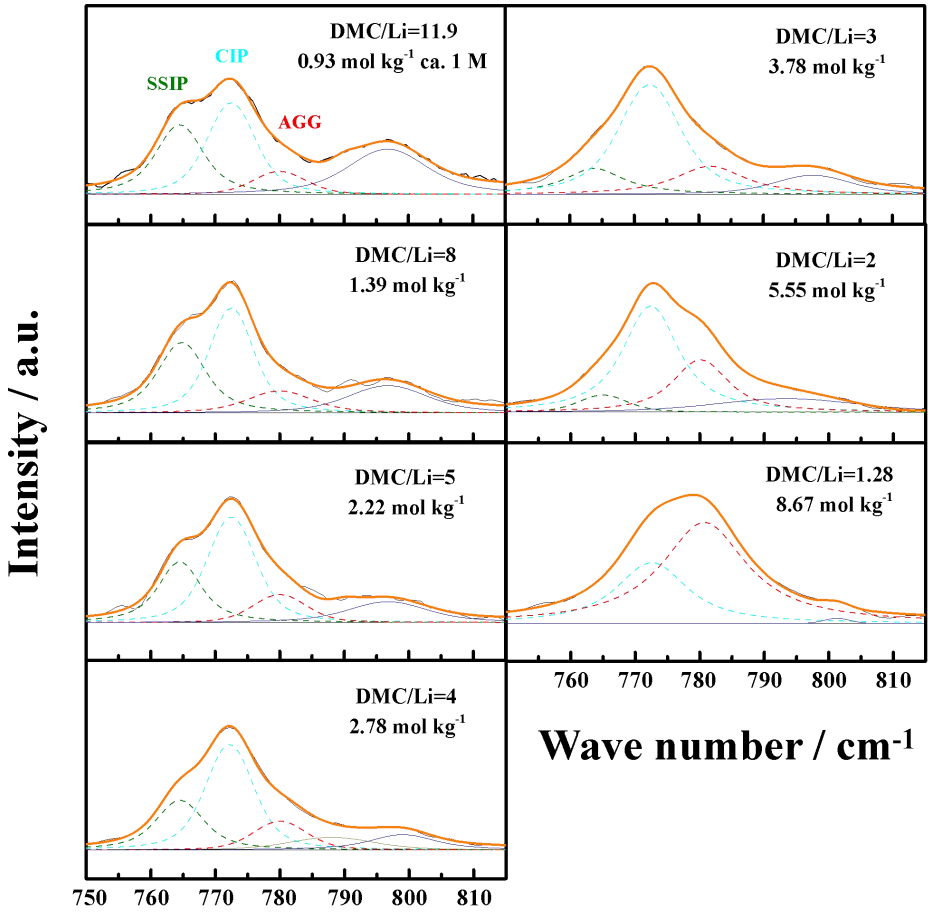


**Fig. 2-3.** Raman spectra (750-815 $cm^{-1}$) of $LiBF_4$/DMC of different salt/solvent molar ratios.

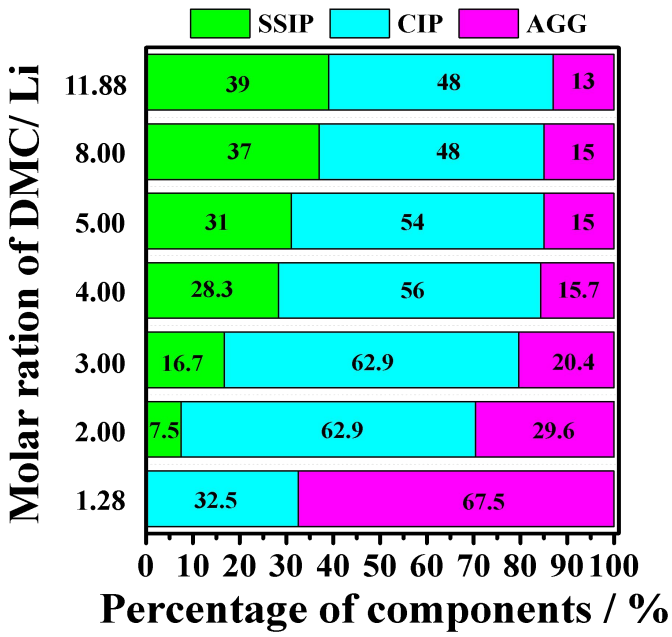


**Fig. 2-4.** Calculated percentage of different kinds of $BF_4^-$ anions in $LiBF_4$/DMC of different molar ratios (DMC/Li).

The anodic stability of $LiBF_4$/DMC electrolytes of different concentrations was investigated using LSV, and the results are shown in Fig. 2-5. In 0.93 mol $kg^{-1}$ $LiBF_4$/DMC, a small anodic peak appeared at around 4 V vs $Li/Li^+$ before the oxidation of the electrolyte solution at around 5.0 V, which is mainly due to the oxidation of free solvent molecules and $BF_4^-$ anions. As $LiBF_4$ salt concentration increased, the anodic peak at 4 V became smaller. In the nearly saturated 8.67 mol $kg^{-1}$ $LiBF_4$/DMC, the anodic peak at 4 V disappeared and the oxidation current of the electrolyte solution at potentials higher than 5.0 V was remarkably lower than that in 0.93 or 2.22 mol $kg^{-1}$ $LiBF_4$/DMC. These facts exhibited the outstanding anodic stability of the nearly saturated $LiBF_4$/DMC electrolyte, which is in agreement with the fact that no free anions are present and almost all DMC solvent molecules form AGGs with $Li^+$ and $BF_4^-$ anions in the nearly saturated solution as shown in Fig. 2-4.

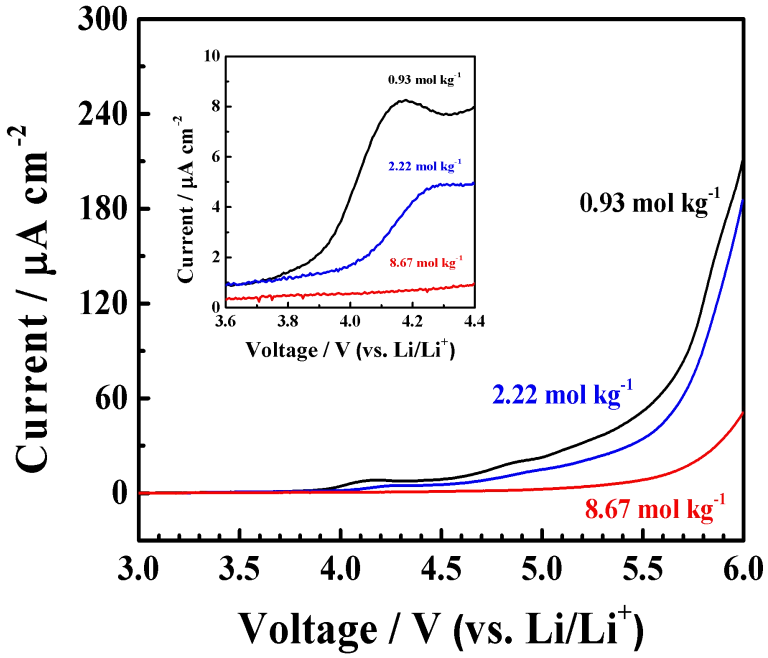


Fig. 2-5. Linear sweep voltammograms of Pt in (a) 0.93 mol $kg^{-1}$ (ca. 1 M), (b) 2.22 mol $kg^{-1}$, and (c) nearly saturated 8.67 mol $kg^{-1}$ $LiBF_4$/DMC.

### *2.3.2 Charge and discharge properties*

The charge/discharge curves of NCM811|Li cells using 1 M $LiPF_6$/EC+DMC and 0.93, 2.22 and 8.67 mol $kg^{-1}$ $LiBF_4$/DMC electrolytes between 3.0 and 4.3 V for 50 cycles are shown in Fig. 2-6. The initial charge and discharge capacities and coulombic efficiencies in the first cycle are summarized in Table 2-1. In each electrolyte, a discharge capacity of ca. 200 mAh $g^{-1}$ was obtained in the first cycle, which is typical of nickel-rich NCM811 cathode. The initial coulombic efficiency in 0.93 mol $kg^{-1}$ $LiBF_4$/DMC was 90.3%, which was higher than that in 1 M $LiPF_6$/EC+DMC (82.3%), but was poorer than those in 2.22 mol $kg^{-1}$ and 8.67 mol $kg^{-1}$ $LiBF_4$/DMC (90.9% and 91.8%, respectively). Though the discharge capacity of ca. 200 mAh $g^{-1}$ was obtained in the first cycle in each electrolyte, it decreased significantly upon repeated cycling in 0.93, 2.22 mol $kg^{-1}$ $LiBF_4$/DMC and 1 M $LiPF_6$/EC+DMC, while the capacity fading was remarkably suppressed in the nearly saturated 8.67 mol $kg^{-1}$ $LiBF_4$/DMC. Also the polarization (overvoltage) increased significantly upon repeated cycles in 0.93, 2.22 mol $kg^{-1}$ $LiBF_4$/DMC and 1 M $LiPF_6$/EC+DMC, whereas it did not appreciably increase up to the $50^{th}$ cycle in the nearly saturated 8.67 mol $kg^{-1}$ $LiBF_4$/DMC. These results indicated that the oxidative decomposition of the electrolyte solution was suppressed in highly concentrated $LiBF_4$/DMC, especially at the nearly saturated concentration (8.67 mol $kg^{-1}$).

**Table 2-1.** Initial charge/discharge performance of NCM811| Li cell using 0.93, 2.22, 8.67 mol kg$^{-1}$ $LiBF_4$/DMC and 1 mol dm$^{-3}$ $LiPF_6$/EC+DMC electrolyte solutions.

| $LiBF_4$/DMC | | | | Initial charge/discharge performance | | | |
|---|---|---|---|---|---|---|---|
| Conc. (mol kg$^{-1}$) | DMC/Li Molar ratio | Viscosity (mPa s) | Ionic conductivity (mS cm$^{-1}$) | Charge capacity (mAh g$^{-1}$) | Discharge capacity (mAh g$^{-1}$) | Irreversible capacity (mAh g$^{-1}$) | Coulombic efficiency (%) |
| 0.93 | 11.9 | 0.91 | 0.47 | 216 | 195 | 21 | 90.3 |
| 2.22 | 5 | 4.18 | 2.19 | 220 | 200 | 20 | 90.9 |
| 8.67 | 1.28 | 226 | 0.75 | 220 | 202 | 18 | 91.8 |
| 1 mol dm$^{-3}$ $LiPF_6$/EC+DMC (1:1 by volume) | | | | 221 | 182 | 39 | 82.3 |

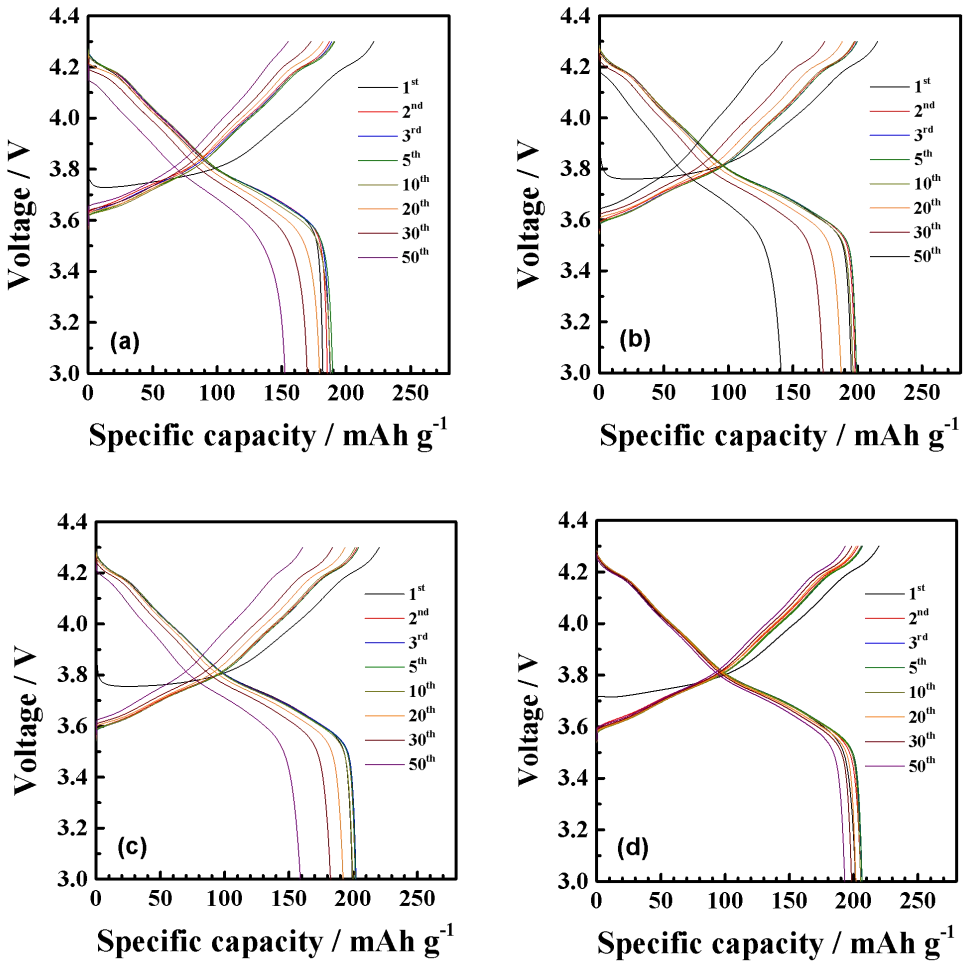


**Fig. 2-6.** Charge/discharge curves of $LiNi_{0.8}Co_{0.1}Mn_{0.1}O_2$ cathode in (a) 1 M $LiPF_6$/EC+DMC, and (b) 0.93, (c) 2.22 and (d) 8.67 mol kg$^{-1}$ $LiBF_4$/DMC at 30°C.

Figure 2-7 showed the variations of discharge capacity and coulombic efficiency of NCM811|Li cells using 0.93, 2.22, 8.67 mol $kg^{-1}$ $LiBF_4$/DMC and 1 M $LiPF_6$/EC+DMC. In each solution, the discharge capacity increased slightly in a few initial cycles, and reached the maximum capacity. In 0.93, 2.22 mol $kg^{-1}$ $LiBF_4$/DMC and 1 M $LiPF_6$/EC+DMC, the discharge capacity significantly decreased to 70.7%, 72.2%, and 80.5% respectively, after 50 cycles. On the other hand, the capacity retention was 93.3% (193 mAh $g^{-1}$) after 50 cycles in 8.67 mol $kg^{-1}$ $LiBF_4$/DMC. The average coulombic efficiency for 50 cycles in 8.67 mol $kg^{-1}$ $LiBF_4$/DMC persisted at 99.7 %, which was higher than those using 0.93, 2.22 mol $kg^{-1}$ $LiBF_4$/DMC and 1 M $LiPF_6$/EC+DMC (98.9%, 99.2 %, and 98.2% respectively). These results showed that oxidative electrolyte decomposition was suppressed in the highly concentrated $LiBF_4$/DMC.

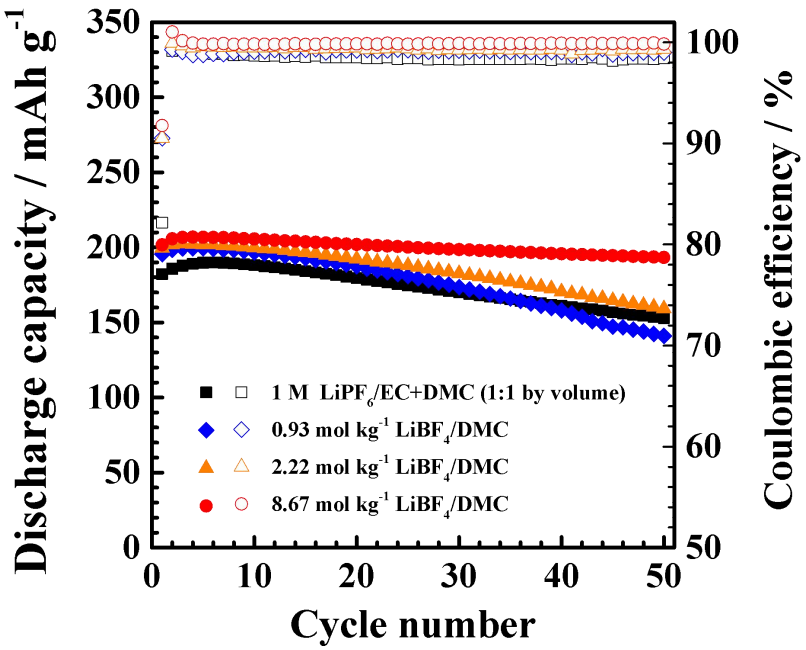


**Fig. 2-7.** Cycle performance of $LiNi_{0.8}Co_{0.1}Mn_{0.1}O_2$ cathode in 1 M $LiPF_6$/EC+DMC, and 0.93, 2.22 and 8.67 mol $kg^{-1}$ $LiBF_4$/DMC electrolytes.

The rate performance of NCM811|Li cells using $LiBF_4$/DMC electrolytes of different concentrations are shown in Fig 2-8. At low rates (0.1 and 0.2C), no obvious differences were observed among the NCM811|Li cells using 0.93, 2.22 and 8.67 mol $kg^{-1}$ $LiBF_4$/DMC. However, at higher rates (≥ 1 C), the discharge capacity increased with an increase in salt concentration. The nearly saturated 8.67 mol $kg^{-1}$ $LiBF_4$/DMC electrolyte gave a high capacity of 153 mAh $g^{-1}$ even at 2 C in spite of a high viscosity (226 mPa s) and a low ionic conductivity (0.75 mS $cm^{-1}$). The poor rate performance in 0.93 mol $kg^{-1}$ $LiBF_4$/DMC may be correlated with increased interfacial impedance owing to oxidative decomposition of electrolyte solution as will be discussed later.

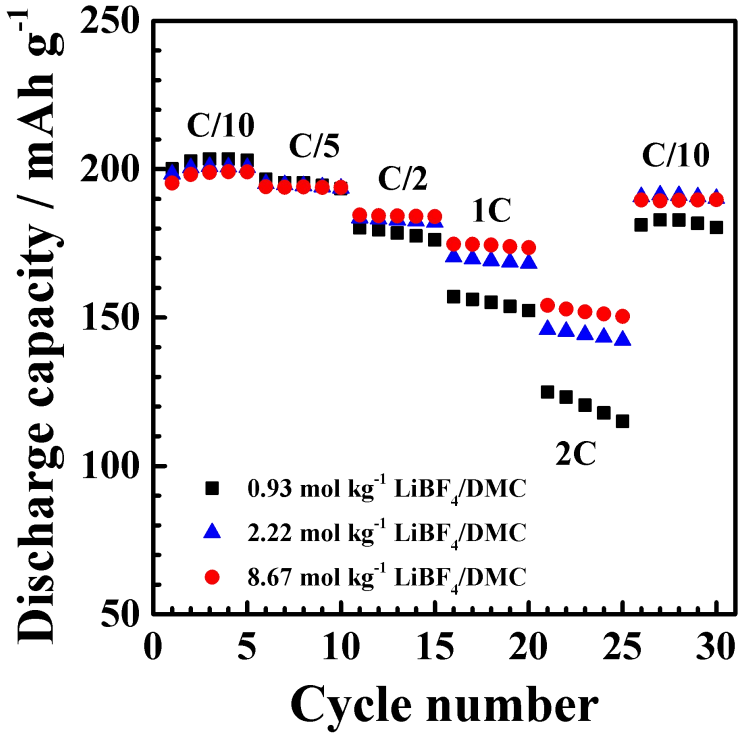


**Fig. 2-8.** Rate-capability of $LiNi_{0.8}Co_{0.1}Mn_{0.1}O_2$ cathode in 0.93, 2.22 and 8.67 mol $kg^{-1}$ $LiBF_4$/DMC electrolytes.

Figure 2-9 shows SEM images and EDX F-mapping profiles of NCM811 electrodes before cycling and after 50 cycles in 0.93 and 8.67 mol $kg^{-1}$ $LiBF_4$/DMC. The primary particles of about 300 nm in size were clearly seen on the surface before cycling. However, after 50 cycle in 0.93 mol $kg^{-1}$ $LiBF_4$/DMC, the shape of the primary particles became obscure (Fig. 2-9e) due to the large amount of F-containing precipitates on the surface as seen in (Fig. 2-9f). On the other hand, the surface morphological change of NCM811 cycled in 8.67 mol $kg^{-1}$ $LiBF_4$/DMC (Fig. 2-9i) was smaller than that in 0.93 mol $kg^{-1}$ $LiBF_4$/DMC and F-containing precipitates on the surface significantly decreased (Fig. 2-9j). The F-containing precipitates came from the oxidative decomposition of $BF_4^-$ anions, which indicated that the anodic stability of $BF_4^-$ anions was remarkably improved in the high concentrated electrolyte due to the absence of free $BF_4^-$ anions as shown in Fig. 2-4. The surface of the particle was covered by a less amount of oxidative decomposition products in the highly concentrated electrolyte, so that $Li^+$ ions were easily transported at the surface of the active material and the high rate-capability was obtained as shown in Fig. 2-8.

In cross-sectional images, some cracks were formed along the grain boundaries in both samples, which were due to the repeated volume expansion/shrinkage of NCM811 grains during cycling. However, the amount of F-containing decomposition products inside the particle, especially along the grain boundaries, was much larger for the sample cycled in 0.93 mol $kg^{-1}$ $LiBF_4$/DMC. This fact clearly shows that the electrolyte solution penetrated inside of the particle and decomposed at the cracks to form decomposition products. The decomposition products accumulated at the cracks

accelerated particle disintegration and resulted in the faster deterioration of NCM811 cathode as shown in Fig. 2-7.

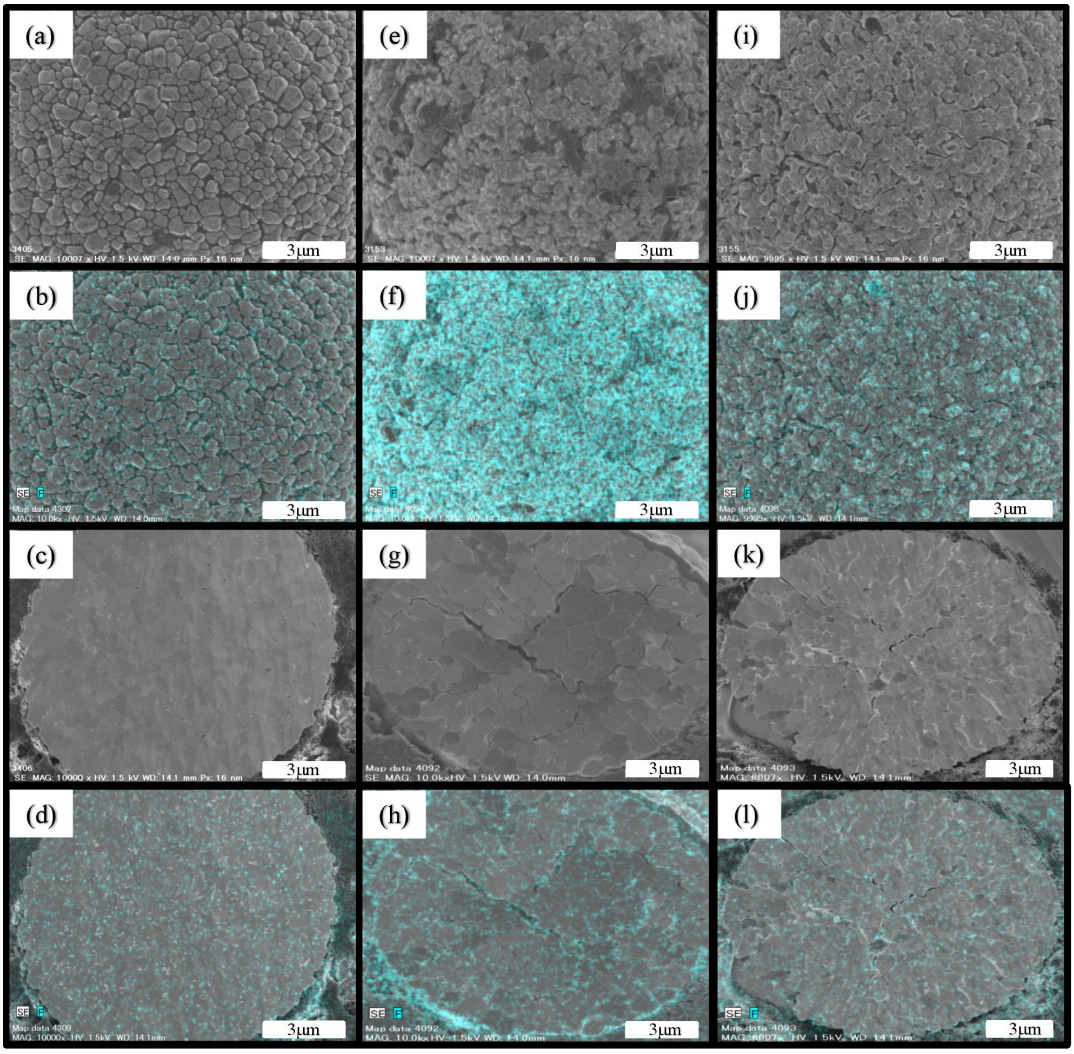


**Fig. 2-9.** SEM images (a,c,e,g,i,k) and EDX mappings (b,d,f,h,j,l) of the surfaces (a,e,i) and the cross-sections (e,g,k) of $LiNi_{0.8}Co_{0.1}Mn_{0.1}O_2$ particles before cycling (a-d), and in 0.93 (e-h) , 8.67 mol $kg^{-1}$ (i-l) $LiBF_4$/DMC electrolytes after 50 cycles at 30°C.

Impedance spectra of the NCM811 electrode during cycling are shown in Fig. 2-10. The impedance was measured at a discharge state of 3.7 V after the 1st, 20th and 50th cycle. The high frequency intercept with *x*-axis corresponds to the ohmic resistance ($R_\Omega$), which involves resistances for the lithium ion transport in the electrolyte solution (closely related to the ionic conductivity) and for the electron transport in the electrode, current collector, etc. The $R_\Omega$ for 0.93 mol $kg^{-1}$ (ca. 1 M) was almost the same as that of the saturated 8.67 mol $kg^{-1}$ $LiBF_4$/DMC at the 20th cycle, suggesting that the difference in the ionic conductivity was small as shown in Table.2-1.

The high- and low-frequency semicircles are assigned to the resistances of the SEI ($R_{SEI}$) that was formed by the oxidative decomposition of the electrolyte and the interfacial Li-ion transport ($R_{ct}$) at the NCM811/electrolyte interface, respectively. At the first cycle, both $R_{SEI}$ and $R_{ct}$ in 8.67 mol $kg^{-1}$ $LiBF_4$/DMC were much lower than those in 0.93 mol $kg^{-1}$. As discussed earlier, free $BF_4^-$ anions were oxidized at potentials higher than 4 V and a larger amount of F-containing precipitates were generated on the secondary particle surface in 0.93 mol $kg^{-1}$ $LiBF_4$/DMC. This caused a significant increase of $R_{SEI}$ in 0.93 mol $kg^{-1}$ $LiBF_4$/DMC up to the 50th cycles. On the contrary, $R_{SEI}$ did not change appreciably up to the 50th cycle in 8.67 mol $kg^{-1}$ $LiBF_4$/DMC, because $BF_4^-$ anions, mostly in the aggregate form as shown in Fig. 2-4, were hardly oxidized in the high concentration electrolyte as shown in Fig. 2-5. In each electrolyte, $R_{ct}$ increased with cycle number. However, the growth of $R_{ct}$ in 8.67 mol $kg^{-1}$ $LiBF_4$/DMC was less remarkable than 0.93 mol $kg^{-1}$ $LiBF_4$/DMC. This is due

to the suppression of solvent decomposition inside the particles in the concentrated electrolyte solution, which suppressed particle disintegration and electronical isolation of the grains.

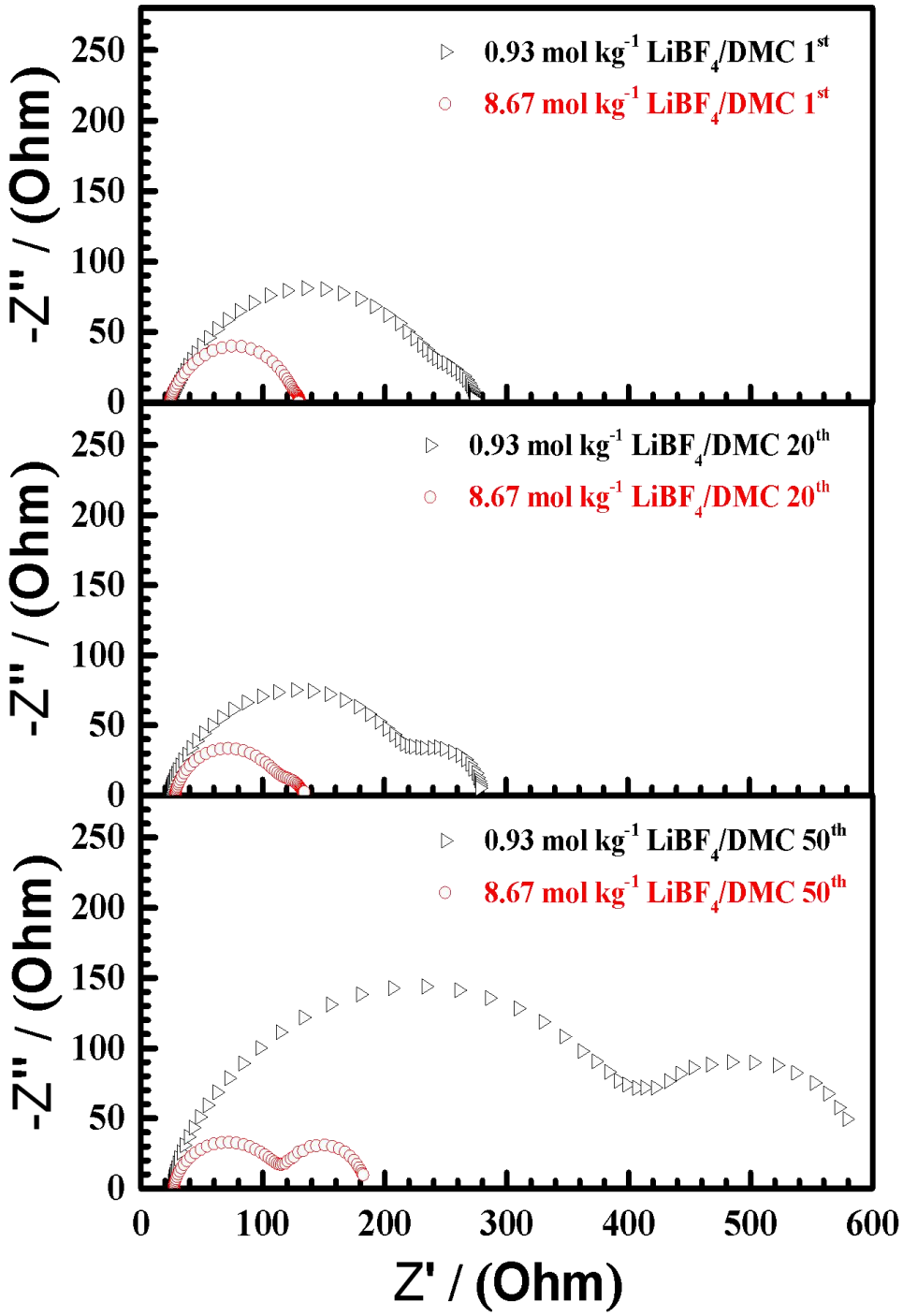


**Fig. 2-10.** Nyquist plots of $LiNi_{0.8}Co_{0.1}Mn_{0.1}O_2$ cathode in 0.93, and 8.67 mol $kg^{-1}$ $LiBF_4$/DMC measured at 3.7 V after the 20th and 50th cycles.

## 2.4 Conclusions

In Chapter 2, it was found that the nearly saturated 8.67 mol $kg^{-1}$ $LiBF_4$/DMC electrolyte solution exhibited higher anodic stability upon charging of the NCM811 electrode to 4.3 V than 0.93 and 2.22 mol $kg^{-1}$ $LiBF_4$/DMC. One reason is that almost all DMC solvent molecules solvate $Li^+$ ions and stabilized against oxidation. The other reason is that most of $BF_4^-$ anions form aggregations, which are also stable against oxidation, in highly concentrated electrolytes. The high stability of the nearly saturated 8.67 mol $kg^{-1}$ $LiBF_4$/DMC gave a good cycle performance to the NCM811 cathode with high coulombic efficiencies. It was found that the particle disintegration of NCM811 caused by crack formation is accelerated by the electrolyte decomposition at the cracks inside the particles in 0.93 mol $kg^{-1}$ $LiBF_4$/DMC. The high stability of the nearly saturated 8.67 mol $kg^{-1}$ $LiBF_4$/DMC reduced the solvent decomposition not only on the particle surface, but also inside the particles, which is one of the reasons for the improved cycleability. Unfortunately the nearly saturated 8.67 mol $kg^{-1}$ $LiBF_4$/DMC have a high viscosity and hence is difficult to be used in practical batteries. As we reported recently,[28,31] highly concentrated electrolytes can be diluted with fluorinated solvent, such as 1,1,2,2–tetrafluoroethyl 2,2,3,3–tetrafluoropropyl ether (HFE), without losing the high stability against oxidation. The effects of the dilution of the concentrated $LiBF_4$/DMC on the performance of NCM811 cathode are discussed in Chapters 3 and 4.

## References

[1] H. Horie, T. Abe, T. Kinoshita, and Y. Shimoida, "A study on advanced lithium ion battery system for EVs." *World Electr. Veh. J.*, **2**, A25 (2008).

[2] T. P. Narins, "The battery business: Lithium availability and the growth of global electric car industry." *Extr. Ind. Soc.*, **4**, A321 (2017).

[3] V. Etacheri, R. Marom, R. Elazari, G. Salitra, and D. Aurbach, "Challenges in the development of advanced Li-ion batteries: a review." *Energy Environ. Sci.*, **4**, A3243 (2011).

[4] H.-J. Noh, S. Youn, C. S. Yoon, and Y.-K. Sun, "Comparison of the structural and electrochemical properties of layered $Li[Ni_xCo_yMn_z]O_2$ (x=1/3, 0.5, 0.6, 0.7, 0.8 and 0.85) cathode material for lithium-ion batteries." *J. Power Sources*, **233**, A121 (2013).

[5] Y. Xia, J. Zheng, C. Wang, and M. Gu, "Designing principle for Ni-rich cathode materials with high energy density for practical applications." *Nano Energy*, **49**, A434 (2018).

[6] M. Ue, M. Takeda, M. Takehara, and S. Mori, "Electrochemical Properties of Quaternary Ammonium Salts for Electrochemical Capacitors." *J. Electrochem. Soc.*, **144**, A2684 (1997).

[7] K. Xu, "Nonaqueous Liquid Electrolytes for Lithium-Based Rechargeable Batteries." *Chem. Rev.*, **104**, A4303 (2004).

[8] P. H. Duvigneaud, and T. Segato, "Synthesis and Characterisation of $LiNi_{1-x-y}Co_xAl_yO_2$ Cathodes for Lithium-Ion Batteries by the PVA Precursor Method." *J. Eur. Ceram. Soc.*, **24**, A1375 (2004).

[9] J. Zheng, J. Xiao, and J. Zhang, "The roles of oxygen non-stoichiometry on the electrochemical properties of oxide-based cathode materials." *Nano Today*, **11**, A678 (2016).

[10] H. Kim, M. G. Kim, H. Y. Jeong, H. l. Nam, and J. Cho, "A New Coating Method for Alleviating Surface Degradation of $LiNi_{0.6}Co_{0.2}Mn_{0.2}O_2$ Cathode Material: Nanoscale Surface Treatment of Primary Particles." *Nano Lett.*, **15**, A2111 (2015).

[11] S. Chen, T. He, Y. Sun, Y. Lu, L. Bao, L. Chen, Q. Zhang, J. Wang, R. Chen, and F. Wu, "Ni-Rich $LiNi_{0.8}Co_{0.1}Mn_{0.1}O_2$ Oxide Coated by Dual-Conductive Layers as High Performance Cathode Material for Lithium-Ion Batteries." *Appl. Mater. Interfaces*, **9**, A29732 (2017).

[12] K. Abe, Y. Ushigoe, H. Yoshitake, and M. Yoshio, "Novel type additives for cathode materials, providing high cycleability performance." *J. Power Sources*, **153**, A328 (2006).

[13] N. S. Choi, J. G. Han, S. Y. Ha, I. Park, and C. K. Back, "Recent advances in the electrolytes for interfacial stability of high-voltage cathodes in lithium-ion batteries." *RSC Adv.*, **5**, A2732 (2015).

[14] A. Cresce, and K. Xu, "Electrolyte additive in support of 5 V Li ion chemistry." *J Electrochem Soc.*, **158**, A337 (2011).

[15] M. Xu, L. Zhou, Y. Dong, Y. Chen, J. Demeaux, A. D. MacIntosh, A. Garsuch, and B. L. Lucht, "Development of novel lithium borate additives for designed surface modification of high voltage $LiNi_{0.5}Mn_{1.5}O_4$ cathodes." *Energy Environ. Sci.*, **9**, A1308 (2016).

[16] B. Zhang, P. Dong, H. Tong, Y. Yao, J. Zheng, W. Yu, J. Zhang, and D. Chu, "Enhanced electrochemical performance of $LiNi_{0.8}Co_{0.1}Mn_{0.1}O_2$ with lithium-reactive $Li_3VO_4$ coating." *J. Alloys Compd.*, **706**, A198 (2017).

[17] X. Xiong, Z. Wang, G. Yan, H. Guo, and X. Li, "Role of $V_2O_5$ coating on $LiNiO_2$-based materials for lithium ion battery." *J. Power Sources*, **245**, A183 (2014).

[18] W. Cho, S. M. Kim, J. H. Song, T. Yim, S. G. Woo, K. W. Lee, J. S. Kim, and Y. J. Kim, "Improved electrochemical and thermal properties of nickel rich $LiNi_{0.6}Co_{0.2}Mn_{0.2}O_2$ cathode materials by $SiO_2$ coating." *J. Power Sources*, **282**, A45 (2015)

[19] X. Xiong, Z. Wang, X. Yin, H. Guo, and X. Li, "A modified LiF coating process to enhance the electrochemical performance characteristics of $LiNi_{0.8}Co_{0.1}Mn_{0.1}O_2$ cathode materials." *Mater. Lett.*, **110**, A4 (2013).

[20] Y. Xu, Y. Liu, Z. Lu, H. Wang, D. Sun, and G. Yang, "The preparation and role of $Li_2ZrO_3$ surface coating $LiNi_{0.5}Co_{0.2}Mn_{0.3}O_2$ as cathode for lithium-ion batteries." *Appl. Surf. Sci.*, **361**, A150 (2016).

[21] Y. Yamada, K. Furukawa, K. Sodeyama, K. Kikuchi, M. Yaegashi, Y. Tateyama, and A. Yamada, "Unusual Stability of Acetonitrile-Based Superconcentrated Electrolytes for Fast-Charging Lithium-Ion Batteries." *J. Am. Chem. Soc.*, **136**, A5039 (2014).

[22] Y. Yamada, and A. Yamada. "Review−Superconcentrated Electrolytes for Lithium Batteries." *J. Electrochem Soc.*, **162**, A2406 (2015).

[23] J. Wang, Y. Yamada, K. Sodeyama, C. H. Chiang, Y. Tateyama, and A. Yamada,

"Superconcentrated electrolytes for a high-voltage lithium-ion battery." *Nature Commun.*, **7**, A12032 (2016).

[24] J. Wang, Y. Yamada, K. Sodeyama, E. Watanabe, K. Takada, Y. Tateyama, and A. Yamada, *"*Fire-extinguishing organic electrolytes for safe batteries." *Nature Energy*, **3**, A22 (2018).

[25] K. Dokko, N. Tachikawa, K. Yamauchi, M. Tsuchiya, A. Yamazaki, E. Takashima, J.-W. Park, K. Ueno, S. Seki, N. Serizawa, and M. Watanabe, "Solvate Ionic Liquid Electrolyte for Li-S Batteries*." J. Electrochem. Soc.*, **160**, A1304 (2013).

[26] T. Doi, Y. Shimizu, M. Hashinokuchi, and M. Inaba, "$LiBF_4$-Based concentrated electrolyte solutions for suppression of electrolyte decomposition and rapid lithium-ion transfer at $LiNi_{0.5}Mn_{1.5}O_4$/electrolyte interface." *J. Electrochem Soc.*, **163**, A2211 (2016).

[27] T. Doi, Y. Shimizu, M. Hashinokuchi, and M. Inaba, "Dilution of highly concentrated libf4/propylene carbonate electrolyte solution with fluoroalkyl ethers for 5-V $LiNi_{0.5}Mn_{1.5}O_4$ positive electrodes." *J. Electrochem Soc.*, **164**, A6412 (2017).

[28] T. Doi, M. Hahsinokuchi, and M. Inaba, *"*Solvation-controlled ester-based concentrated electrolyte solutions for high-voltage lithium-ion batteries." *Current Option in Electrochemistry*, **9**, A49 (2018).

[29] T. Doi, R. Masuhara, M. Hashinokuchi, Y. Shimizu, and M. Inaba, "Concentrated $LiPF_6$/PC electrolyte solutions for 5-V $LiNi_{0.5}Mn_{1.5}O_4$ positive electrode in lithium-ion batteries." *Electrochim. Acta.,* **209**, A219 (2016).

[30] T. Doi, Y. Shimizu, M. Hashinokuchi, and M. Inaba, "Low-Viscosity

γ-Butyrolactone-Based Concentrated Electrolyte Solutions for $LiNi_{0.5}Mn_{1.5}O_4$ Positive Electrodes in Lithium-Ion Batteries." *Chem Electro Chem.,* **4**, A2398 (2017).

[31] T. Doi, R. Matsumoto, Z. Cao, M. Hashinokuchi, and M. Inaba, "Fluoroalkyl ether-diluted dimethyl carbonate-based electrolyte solutions for high-voltage operation of $LiNi_{0.5}Co_{0.2}Mn_{0.3}O_2$ electrodes in lithium ion batteries." *Sustainable Energy Fuels,* **2**, A1197 (2018).

[32] S. S. Zhang, K. Xu, and T, R. Jow, "Enhanced Performance of Li-Ion Cell with $LiBF_4$-PC Based Electrolyte by Addition of Small Amount of LiBOB." *J. Power Sources,* **152**, A629 (2006).

[33] S. Karaal, H. Kose, A. Aydın, and H. Akbulut, "The effect of $LiBF_4$ concentration on the discharge and stability of $LiMn_2O_4$ half cell Li ion batteries." *Mater Sci Semicond Process*, **38**, A397 (2015).

[34] O. Homma, Y. Amino, T. Miyajima, T. Enta, E. Murotani, and Y. Onozaki, *Res. Reports Asahi Glass Co., Ltd.*, 67, A33 (2017) (in Japanese) .

[35] Y. Yamada, Y. Takazawa, K. Miyazaki, and T. Abe, "Electrochemical Lithium Intercalation into Graphite in Dimethyl Sulfoxide-Based Electrolytes: Effect of Solvation Structure of Lithium Ion." *J. Phys. Chem. C,* **114**, A11680 (2010).

[36] N. Chapman, O. Borodim, T. Yoon, C. C. Nguyen, and B. L. Lucht, "Spectroscopic and Density Functional Theory Characterization of Common Lithium Salt Solvates in Carbonate Electrolytes for Lithium Batteries." *J. Phys. Chem. C,* **121**, A2135 (2017).

[37] D.M. Seo, O. Borodin, S.-D Han, Q, Ly, P. D. Boyle, W. and A. Henderson,

"Electrolyte Solvation and Ionic Association." *J. Electrochem Soc.*, **159**, A553 (2012).

[38] D. M. Seo, P. D. Boyle, J. L. Allen, S.-D Han, E. Jónsson, P. Johansson, and W. A. Henderson, "Solvate Structures and Computational/Spectroscopic Characterization of $LiBF_4$ Electrolyte." *J. Phys. Chem. C,* **118** , A18377 (2014).

[39] L. Doucey, M. Evault, A. Lautié, A. Chaussé, and R. Messina, "A study of the $Li/Li^+$ couple in DMC and PC solvents Part 1: Characterization of $LiAsF_6$/DMC and $LiAsF_6$/PC solutions." *Electrochim. Acta,* **44**, A2371 (1999).

## Supporting Information

### *Determination of the coordinating number of DMC molecules toward $Li^+$*

The coordinating numbers of DMC molecules toward $Li^+$ were evaluated from the intensities of the bands at 916 and 934 $cm^{-1}$ (i.e., stretching vibration mode of free and coordinating DMC, respectively) using the method reported by Homma et al.,[34] and Yamada et al.[35] The Raman intensities of the bands at 916 $cm^{-1}$ ($I_{free}$) and 933 $cm^{-1}$ ($I_{coordinating}$) were determined by the numbers of free DMC molecules ($N_{free}$) and coordinating DMC molecules ($N_{coordinating}$), respectively, per one $Li^+$ in the solution as:

$$N_{total} = N_{free} + N_{coordinating} \tag{S2-1}$$

$$I_{free} = \sigma_{free} N_{free} \tag{S2-2}$$

$$I_{coordinating} = \sigma_{coordinating} N_{coordinating} \tag{S2-3}$$

where $N_{total}$ denotes the total number of DMC molecules per $Li^+$, and $\sigma_{free}$ and $\sigma_{coordinating}$ the Raman scattering coefficients for free and coordinating DMC molecules, respectively. For calculation, we need the Raman intensity of a band that is not affected by coordination, and here we employed a Raman band at 690 $cm^{-1}$ that is assigned to the $OCO_2$ rocking mode of DMC.[S1] The Raman intensity of the unaltered 690 $cm^{-1}$ band ($I_{unaltered}$) is given by the product of $N_{total}$ and the Raman scattering coefficient ($I_{unaltered}$) of the 690 $cm^{-1}$ band as:

$$I_{unaltered} = \sigma_{unaltered} N_{total} \tag{S2-4}$$

From Eqs (S2-1) ,(S2-2) and (S2-3), the following equation (Eq. (S2-5)) is given:

$$N_{coording} = N_{total} \frac{\dfrac{I_{coordinating}}{\sigma_{coordinating} / \sigma_{free}}}{\dfrac{I_{coordinating}}{\sigma_{coordinating} / \sigma_{free}} + I_{free}} \tag{S2-5}$$

The value of $N_{coordinating}$ can be calculated by the ratio of $\sigma_{coordinating}/\sigma_{free}$. From Eqs. (S2-2) ,(S2-3) and (S2-4), the following equation (Eq. (S2-6)) is given:

$$\frac{I_{coordinating}}{I_{unaltered}} = -\frac{\sigma_{coordinating}}{\sigma_{free}}\frac{I_{free}}{I_{unaltered}} + \frac{\sigma_{coordinating}}{\sigma_{unaltered}} \qquad \text{(S2-6)}$$

Here, the intensities of $I_{\text{coordinating}}$ and $I_{\text{free}}$ are normalized by the intensity of $I_{unaltered}$ at 690 $cm^{-1}$. The slope of the $I_{coordinating}/I_{unaltered}$ *vs* $I_{free}/I_{unaltered}$ plot gives the value of the $\sigma_{coordinating}/\sigma_{free}$ value (Fig. S2-1) and imported the value into Eq. (S2-5) to obtain $N_{coordinating}$ of DMC in different concentrated $LiBF_4$/DMC electrolyte solutions are shown in Fig.2- 2 in the main text.

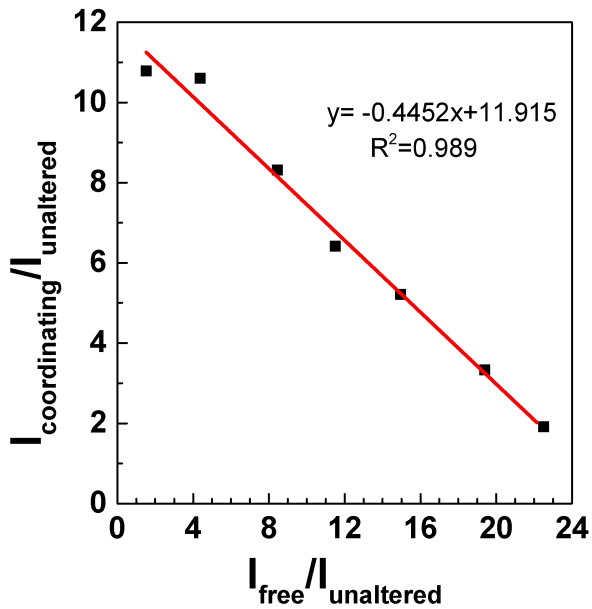


**Fig. S2-1.** $I_{coordinating}/ I_{unaltered}$ vs. $I_{free}/ I_{unaltered}$ plot of DMC molecules in $LiBF_4$/DMC of different molar ratios.

[S1] L. Doucey, M. Evault, A. Lautié, A. Chaussé, and R. Messina, "A study of the Li/Li couple in DMC and PC solvents Part 1: Characterization of $LiAsF_6$/DMC and $LiAsF_6$/PC solutions." *Electrochim. Acta*, **44**, A2371 (1999)

***Computational detail***

The clusters including $Li^+$ are optimized at the B3LYP/6–31G(d) level. Once the optimized geometry is obtained, we analyze the optimized parameters in the first step. To confirm each optimized and stationary points and make zero-point energy corrections, frequency analyses are done with the same basis set. Gibbs free energies are obtained at 298.15 K. The solvation energy ($\Delta G_{solv}$) of $Li^+$ solvated by solvent (DMC) and anion ($BF_4^-$) using the equation:

$$\Delta G_{solv} = G[Li^+(SOL)_n(AN)_m] - G[Li^+] - n \times G[SOL] - m \times G[AN] \qquad \text{(S2-7)}$$

where, $G[Li^+(SOL)_n(AN)_m]$, $G[Li^+]$, G[SOL] and G[AN] are total energy of $Li^+$-SOL-AN clusters, $Li^+$, solvent (DMC) molecule and anion ($BF_4^-$), respectively. *n* and *m* are the number of solvent(DMC) and anion($BF_4^-$)) molecules. In addition, the solvation energy ($\Delta G_{solv}$) of $Li^+$ solvated by solvent (PC) were estimated in the same manner.

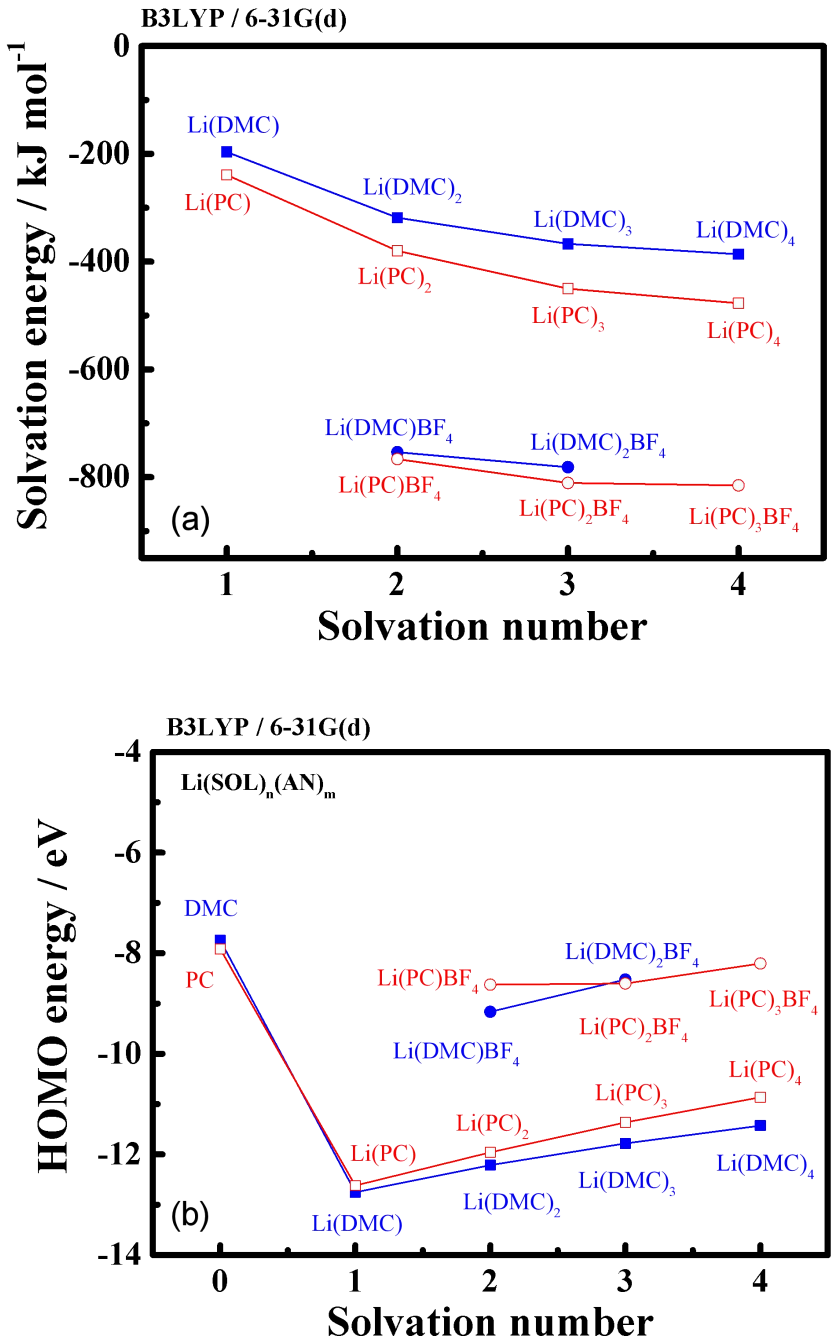


**Fig.S2-2.** Solvation energies (a) and HOMO energies (b) of different solvate $Li^+$ ions plotted against solvation number (calculated by B3LYP/6-31G(d)).

*Viscosity of electrolyte solution measurement*

The viscosity of each electrolyte solution was measured with an Ubbelohde capillary viscometer at room temperature in an Ar-filled glove box (MDB-1NKP-DS, Miwa Mfg).

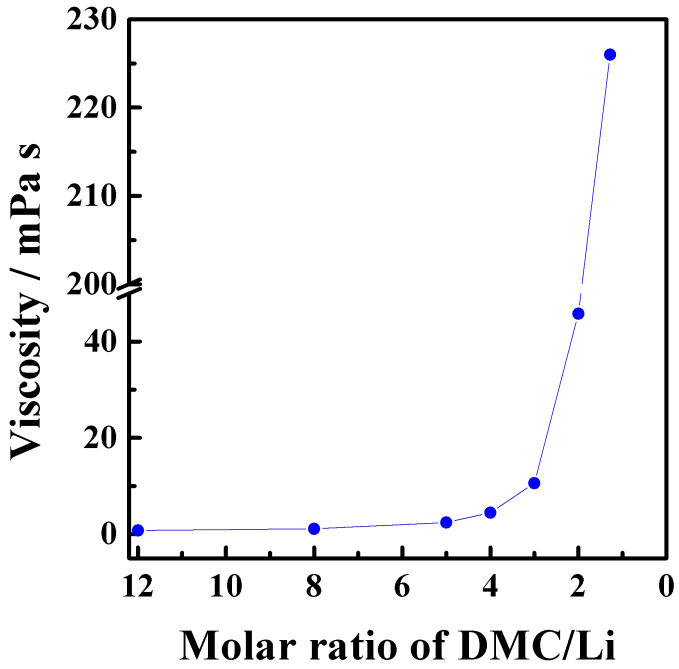


**Fig. S2-3.** Variations of viscosity of $LiBF_4$/DMC of different DMC/Li ratios.

# CHAPTER 3

# Dilution Effects of Highly Concentrated Dimethyl Carbonate-based Electrolytes with a Hydrofluoroether on Charge/Discharge Properties of $LiNi_{0.8}Co_{0.1}Mn_{0.1}O_2$ Positive Electrode

## 3.1 Introduction

Lithium-ion batteries (LIBs) have been commercialized and applied to various electronic devices since 1990s.[1-3] It is now expected that electric vehicles (EVs) will replace traditional internal combustion engine vehicles to solve the global warming problem. However, $LiCoO_2$, which has been used as a positive electrode material in commercially available LIBs, does not satisfy the demand on the energy density of EVs. Because $LiCoO_2$ delivers relatively a low capacity of about 145 mAh $g^{-1}$ with working potentials up to around 4.3 V vs. $Li/Li^+$.[4-9] In order to improve the energy density of LIBs for EV application, increasing the working voltage and/or the specific capacity of positive electrode materials is effective. In recent years, several promising candidates for positive electrode materials have been proposed in substitute for the conventional cathode materials, such as high capacity nickel-rich layered transition

metal oxides ($LiNi_{1-x-y}Co_xMn_yO_2(1-x-y\geq0.5)$)[10-15] and a high voltage spinel-type lithium nickel-manganese oxide ($LiNi_{0.5}Mn_{1.5}O_4$).[16,17] Among the nickel-rich layered transition metal oxides, $LiNi_{0.8}Co_{0.1}Mn_{0.1}O_2$ (NCM811) is the most promising because it can provide a high specific capacity close to 200 mAh $g^{-1}$ when charged to 4.3 V vs. $Li/Li^+$.[18,19] Unfortunately, the traditional 1 mol $dm^{-3}$ (M)-level electrolyte solution is not suitable for NCM811 to be charged to 4.3 V because surface reactions (such as oxidative decomposition of the electrolyte solution) enhance the structural degradation (such as crack formation) of the cathode particles, which results in poor cycle performance.[20]

To overcome the severe degradation problem, the use of the highly concentrated electrolyte solution is considered to be an effective in recent years because it reduces side reactions at high voltages.[21-30] The highly concentrated electrolyte solutions have chemical windows wider than conventional 1 M-level electrolyte solutions. For example, we reported that highly concentrated lithium hexafluorophosphate ($LiPF_6$)/propylene carbonate (PC) can suppress the irreversible capacity and gave a good cycleability of the 5-V class $LiNi_{0.5}Mn_{1.5}O_4$ cathode, because almost all of the solvent molecules strongly coordinate to $Li^+$ ions at high concentrations and have a high stability against oxidation owing to the electron withdrawing effects of $Li^+$.[29] Wang et al. also reported that the use of superconcentrated lithium bis(fluorosulfonyl)amide (LiFSA)/dimethylcarbonate (DMC) suppresses the corrosion of Al substrate at high potentials and enables reversible $Li^+$ de-intercalation/intercalation reactions of $LiNi_{0.5}Mn_{1.5}O_4$.[30]

However, the use of highly concentrated electrolyte causes some problems, such as a high viscosity, a low ionic conductivity and a high cost, that limit the use in practical applications. To solve these problems, fluorinated ethers were used for diluting the highly concentrated electrolytes in recent years.[31-34] Fluorinated ethers own low donor numbers by which they hardly coordinate to $Li^+$ ion, and hence it is believed that the local solvate structure of $Li^+$ ion does not change from that in a highly concentrated electrolyte solution. Meanwhile, they also own other good physicochemical properties, such as nonflammability and high stability against oxidation.

In Chapter 2,[20] it was found that highly $LiBF_4$/DMC electrolyte solution for $LiNi_{0.8}Co_{0.1}Mn_{0.1}O_2$ at a cut-off voltage of 4.3 V gave good cycle performance with a low irreversible capacity. The highly concentrated electrolyte solution effectively suppressed not only oxidative decomposition of the electrolyte on the particle surface, but also the particle fracture caused by crack propagation. In Chapter 3, a hydrofluoroether (1,1,2,2–tetrafluoroethyl 2,2,3,3–tetrafluoropropyl ether, HFE) was used for diluting the highly concentrated $LiBF_4$/DMC electrolyte to 0.96 mol $kg^{-1}$ (ca. 1 mol $dm^{-3}$ = 1 M) that is commonly used in commercially available LIBs. We chose concentrated $LiBF_4$/DMC and $LiPF_6$/DMC systems and discussed the effects of lithium salts on the dilution effects. The diluted $LiBF_4$/DMC+HFE electrolyte gave a poor cycleability for the NCM811 cathode, whereas excellent cycle performance was obtained in the diluted $LiPF_6$/DMC+HFE electrolyte. It was found that the local salt/solvent structure in the electrolyte is strongly affected by the

dissociative/associative character of the salts, which determined the stability against oxidation.

## 3.2 Experimental

### *3.2.1 Preparation of electrolyte solution*

$LiBF_4$, $LiPF_6$ and DMC (Kishida Chemical Co. Ltd), HFE (Daikin Industries, Ltd.) were of lithium battery grade and used without further purification. $LiBF_4$ and $LiPF_6$ were dissolved in DMC to prepare electrolyte solutions in the range of 0.96 mol $kg^{-1}$ (about 1 mol $dm^{-3}$) to a nearly saturated concentration (8.67 mol $kg^{-1}$ for $LiBF_4$/DMC and 5.05 mol $kg^{-1}$ for $LiPF_6$/DMC). The DMC/Li molar ratios of the nearly saturated solutions were 1.28 and 2.2, respectively.

$LiBF_4$ and $LiPF_6$ were dissolved in a mixed solvent of DMC and HFE with a volume ratio of 1: 2. The concentration of the salts was 0.96 mol $kg^{-1}$ (ca. 1 M), and the DMC/Li ratio was 3.00, which was equal to that in 3.70 mol $kg^{-1}$ for $LiBF_4$/DMC and $LiPF_6$/DMC. All electrolytes were prepared in an Ar filled glove box (DBO-1.5KP-DID, Miwa Mfg).

### *3.2.2 Characterization of electrolyte solutions*

The viscosity of the electrolytes was measured with an Ubbelohde capillary viscometer at room temperature in an Ar-filled glove box (MDB-1NKP-DS, Miwa Mfg). Raman spectra of the electrolytes were obtained with a Raman spectrometer (LabRAM HR Evolution, Horiba) equipped with a multichannel charge coupled

device detector. The spectra were recorded using a 785-nm semiconductor laser (100 mW) through an objective lens.

The ionic conductivity was measured with an a.c. impedance analyzer (VersaSTAT 3, Princeton Applied Research) using a symmetrical cell consisting of two Pt plate electrodes. The stability of the electrolytes against oxidation was evaluated on a Pt disk working electrode (10 mm in diameter) by linear sweep voltammetry, which was performed at a scan rate of 1 mV $s^{-1}$ between 3.0 and 5.0 V (vs. $Li/Li^{+}$) using a three-electrode cell with two Li foils as a reference and a counter electrode.

### *3.2.3 Preparation of NCM811 electrode*

The slurry consisting of 80 mass% $LiNi_{0.8}Co_{0.1}Mn_{0.1}O_2$ powder as an active material, 10 mass% graphitized Ketjenblack (FD-7001D, Lion Specialty Chemicals) as a conductor, 10 mass% poly[(vinylidenefluoride)-co-chorotrifluoroethylene] (P(VdF-CtFE)) as a binder and 1-methyl-2-pyrrolidone (NMP) as a solvent was cast onto an aluminum foil. The sheet was dried at 80°C for 18 h in a vacuum oven, and was punched into discs of 13 mm in diameter. The active material mass loading was 1.6-2.3 mg $cm^{-2}$ and the electrode thickness was 15-20 μm.

### *3.2.4 Charge and discharge tests*

The disc electrode as a working electrode was used to assemble a two-electrode coin-type cell with a lithium foil (Honjo Metal Co., Ltd, 15 mm in diameter) as a counter electrode. A glass filter (GF/D, Whatman®) was used as a separator and dipped in the electrolyte prior to assembling the coin-type cells in the Ar-filled glove box. Charge and discharge tests were performed between 3.0 V and 4.3 V vs $Li/Li^+$ at 30°C using a battery test system (TOSCAT-3100, Toyo system Co., Ltd.) at a C/10 rate unless otherwise noted. After charge and discharge tests, the coin-type cell was disassembled in the Ar-filled glove box. The NCM811 electrode was washed with pure DMC to remove residual solvent and Li salt, and then dried overnight in the glove box. The cross-sectional SEM images of NCM811 particles were obtained with a cross-section polisher (JEOL, SM-09010DM) and a scanning electron microscope (SEM) (SU8220, HITACHI Ltd.).

## 3.3 Result and Discussion

### *3.3.1 Charge and discharge characteristics*

The charge/discharge curves of NCM811|Li cells using the nearly saturated $LiBF_4$/DMC (8.67 mol $kg^{-1}$, DMC/Li = 1.28) and $LiPF_6$/DMC (5.05 mol $kg^{-1}$, DMC/Li = 2.2), and the diluted electrolytes (0.96 mol $kg^{-1}$, DMC:HFE = 1:2 by volume, DMC/Li = 3.00) are shown in Fig. 3-1. The variations of the discharge capacity and the coulombic efficiency are summarized in Fig. 3-2. The viscosity and ionic conductivity values of these electrolytes are summarized in Table S3-1 in

Supporting Information. For the $LiBF_4$/DMC system, the initial discharge capacity in the diluted electrolyte (192 mAh $g^{-1}$) was slightly lower than that in the nearly saturated electrolyte (197 mAh $g^{-1}$), which suggested that the low ionic conductivity of the diluted electrolyte (0.13 mS $cm^{-1}$) affected $Li^+$ de-intercalation/intercalation reactions to some extent. In the nearly saturated electrolyte, good cycleability was obtained up to the 50$^{th}$ cycle with a high average coulombic efficiency of 99.7% (Fig. 3-2(a)). However, the discharge capacity in the diluted electrolyte gradually decreased to 152 mAh $g^{-1}$ (capacity retention: 79.2 %) at the 50$^{th}$ cycle and the average coulombic efficiency for 50 cycles was 99.5%. These results indicated that the dilution of concentrated $LiBF_4$/DMC with HFE gives some harmful effects on the anodic stability of the electrolyte and the cycleability of NCM811.

In the nearly saturated 5.05 mol $kg^{-1}$ $LiPF_6$/DMC, the discharge capacity was low (179 mAh $g^{-1}$) in the first cycle, but increased to 190 mAh $g^{-1}$ in the initial 4 cycles. After the 4$^{th}$ cycle, it gradually decreased to 159 mAh $g^{-1}$ at the 100$^{th}$ cycle (capacity retention: 83.7%). On the other hand, in the diluted electrolyte, the initial capacity was high (197 mAh $g^{-1}$) and showed a good cycleability up to the 100$^{th}$ cycle. The capacity retention was 92.4 % at the 100$^{th}$ cycle and the average coulombic efficiency (99.0 %) for 100 cycles was higher than that of highly concentrated electrolyte (98.2%).

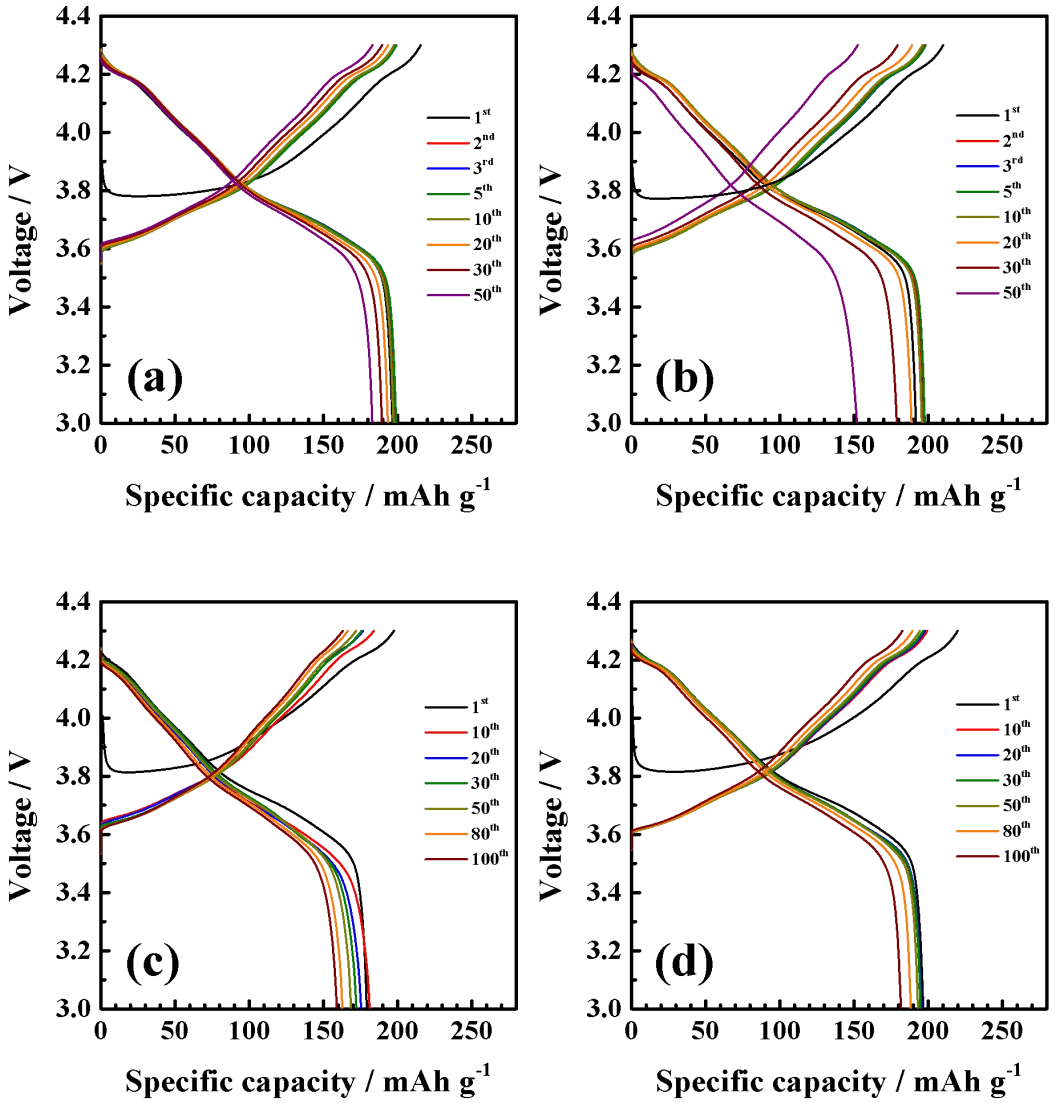


**Fig. 3-1.** Charge/discharge curves of $LiNi_{0.8}Co_{0.1}Mn_{0.1}O_2$ cathode in (a) 8.67 mol $kg^{-1}$ $LiBF_4$/DMC, (b) 0.96 mol $kg^{-1}$ $LiBF_4$/DMC+HFE (1:2 by volume), (c) 5.05 mol $kg^{-1}$ $LiPF_6$/DMC, and (d) 0.96 mol $kg^{-1}$ $LiPF_6$/DMC+HFE (1:2 by volume).

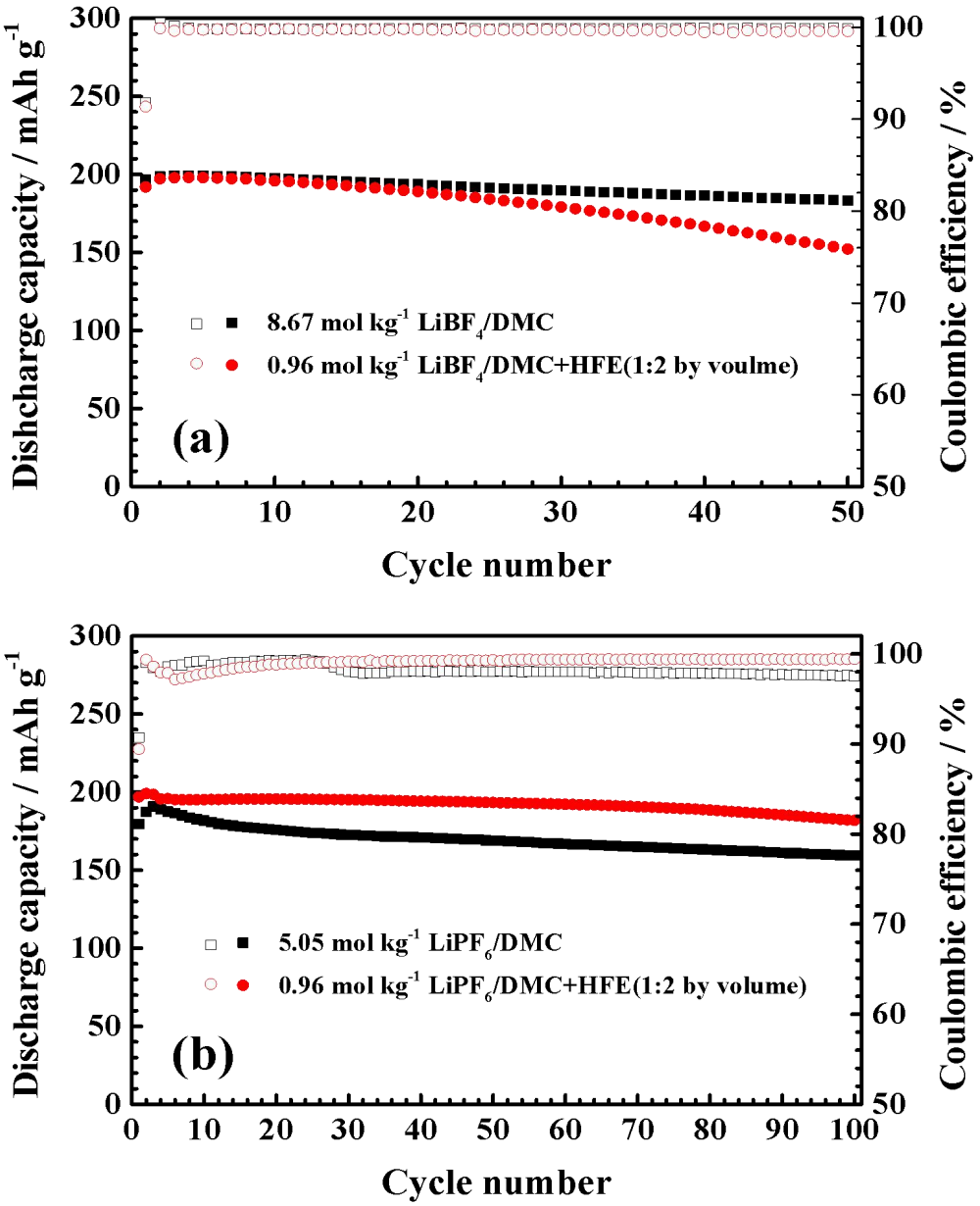


**Fig. 3-2.** Variations of discharge capacity and coulombic efficiency of $LiNi_{0.8}Co_{0.1}Mn_{0.1}O_2$ cathode cycled in (a) 8.67 mol $kg^{-1}$ $LiBF_4$/DMC and 0.96 mol $kg^{-1}$ $LiBF_4$/DMC (1:2 by volume) for 50 cycles, (b) 5.05 mol $kg^{-1}$ $LiPF_6$/DMC and 0.96 mol $kg^{-1}$ $LiPF_6$/DMC+HFE (1:2 by volume) for 100 cycles.

The dQ $dV^{-1}$ profiles obtained from the charge and discharge curves in Fig. 3-1 are shown in Fig. 3-3. In addition to the main redox peaks at around 3.9 V, a couple of redox peaks are seen at around 4.2 V on charging, which are assigned to the structural transformation from the hexagonal-2 (H2) to the hexagonal-3 (H3) phase. Li et al. reported that the H2/H3 phase transformation mostly affects the capacity fading of the $LiNi_{0.8}Co_{0.1}Mn_{0.1}O_2$.[35] In the diluted $LiBF_4$/DMC electrolyte (Fig. 3-3(b)), the peak separation increased more with an increase in cycle number. For example, the oxidation peak (on charging) was shifted up to 4.23 V at the 50$^{th}$ cycle, which was higher than 4.21 V of the nearly saturated $LiBF_4$/DMC (Fig. 3-3(a)). This result indicated that the dilution accelerated the deterioration of NCM811 particles, the reason of which will be discussed in later sections. In contrast, the redox peaks of the nearly saturated $LiPF_6$/DMC (Fig. 3-3(c)) and the dilute $LiPF_6$/DMC electrolyte (Fig. 3-3(d)) did not show remarkable peak shifts even at the 100$^{th}$ cycle. However, the peak intensity in the nearly saturated $LiPF_6$/DMC for NCM811 dropped more rapidly than that in the dilute $LiPF_6$/DMC electrolyte with an increase in cycle number, especially in the early stages. The reason is not clear, but the dilution with HFE has positive effects for suppressing the deterioration of NCM811 particles for the $LiPF_6$/DMC systems.

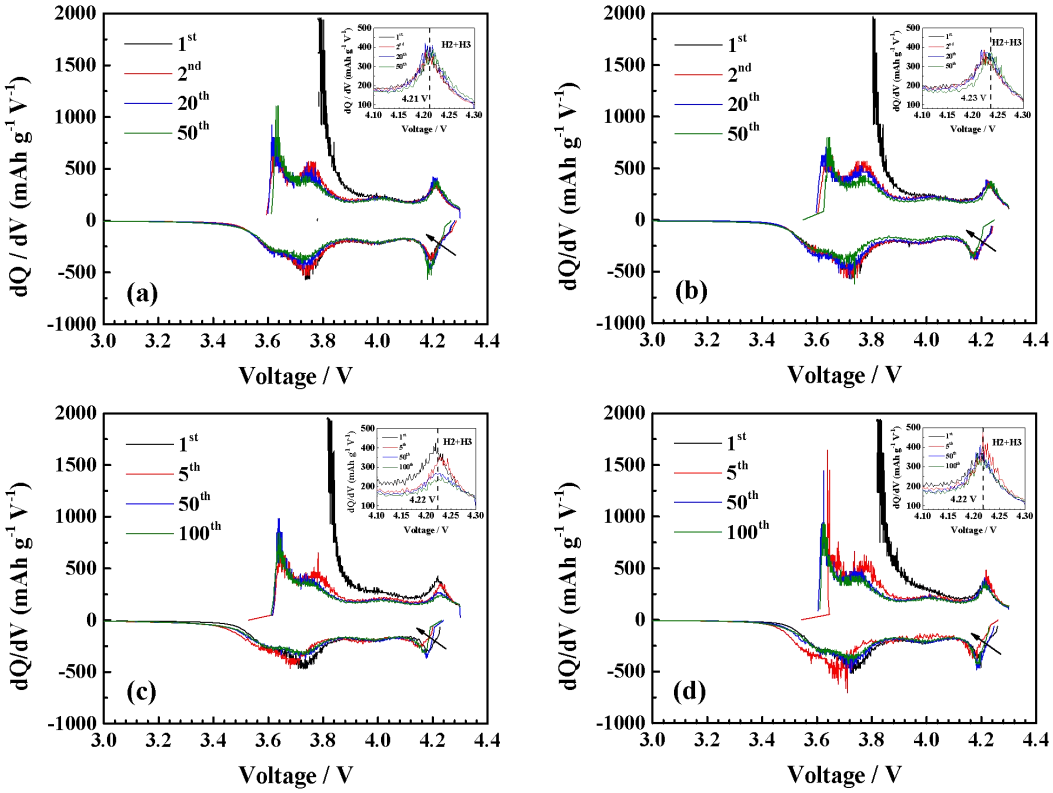


**Fig. 3-3.** The differential capacity curves (dQ $dV^{-1}$) profiles of (a) 8.67 mol $kg^{-1}$ $LiBF_4$/DMC, (b) 0.96 mol $kg^{-1}$ $LiBF_4$/DMC+HFE(1:2 by volume), (c) 5.05 mol $kg^{-1}$ $LiPF_6$/DMC and (d) 0.96 mol $kg^{-1}$ $LiPF_6$/DMC+HFE(1:2 by volume) at 0.1 C (30℃) in the voltage range of 3.0–4.3 V.

The rate performance of NCM811|Li cells using various electrolytes are shown in Fig. 3-4. The nearly saturated $LiBF_4$/DMC gave a better rate-capability than in the diluted $LiBF_4$/DMC+HFE. The diluted electrolyte gave a high capacity (190 mAh $g^{-1}$) comparable to the nearly saturated electrolyte (200 mAh $g^{-1}$) at a low rate of 0.1 C. However, at a high rate (2 C), the diluted electrolyte gave only one third of the capacity obtained in the nearly saturated electrolyte (150 mAh $g^{-1}$). This is because HFE suppressed the dissociation of $LiBF_4$ salt, which results in a low ionic conductivity (0.13 mS $cm^{-1}$) as shown in Table S3-1. For the $LiPF_6$/DMC system, the

diluted electrolyte gave a better rate-capability than the nearly saturated electrolyte. Though the ionic conductivity of the former (2.66 mS $cm^{-1}$) was slightly lower than that of the latter (2.78 mS $cm^{-1}$), a lower viscosity and a good separator wettability in the diluted electrolyte may improve the kinetics of the interfacial reactions, resulting in the observed increase in rate-capability. The temperature dependencies of the ionic conductivity of these two electrolytes are shown in Fig. S3-1 in Supporting Information. The activation energy for the ionic conductivity in the diluted electrolyte (11.2 kJ $mol^{-1}$) was much lower than that in the nearly concentrated electrolyte (28.7 kJ $mol^{-1}$). The lower activation energy may be also related to the enhancement of the kinetics of the interfacial reactions.

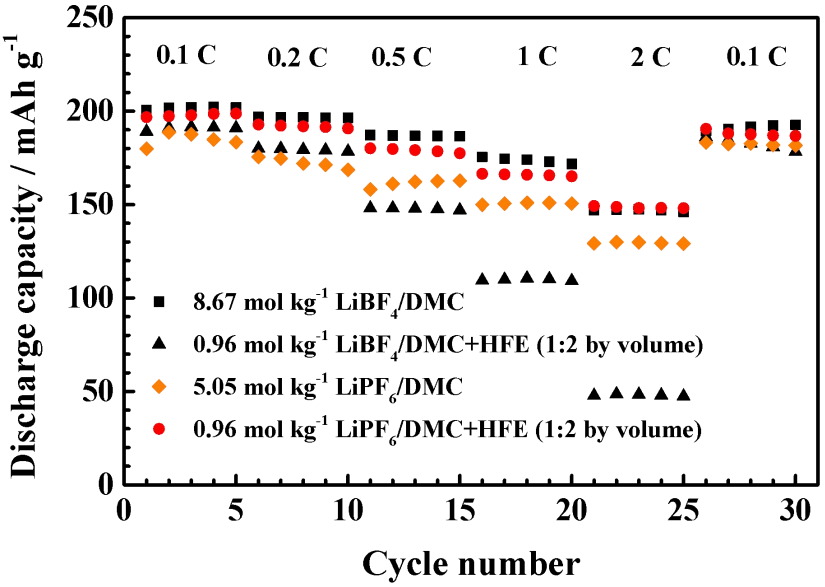


**Fig. 3-4.** Rate-capability of $LiNi_{0.8}Co_{0.1}Mn_{0.1}O_2$ cathode in 8.67 mol $kg^{-1}$ $LiBF_4$/DMC, 0.96 mol $kg^{-1}$ $LiBF_4$/DMC+HFE (1:2 by volume), 5.05 mol $kg^{-1}$ $LiPF_6$/DMC, and 0.96 mol $kg^{-1}$ $LiPF_6$/DMC+HFE (1:2 by volume).

We found that the dilution with HFE gives totally different effects between the $LiBF_4$/DMC and the $LiPF_6$/DMC systems. For the $LiBF_4$/DMC system, dilution with

HFE deteriorated the stability against oxidation and resulted in poor cycleability. It also deteriorated the rate-capability owing to a reduced ionic conductivity. In contrast, for the $LiPF_6$/DMC system, the dilution gave preferable effects on the cycleability and rate-capability. Because the main solvent is common (DMC), the difference should come from a difference in the local salt/solvent structure, such as solvation to $Li^+$ ions, cation-anion interactions (ion-pairing or aggregate formation), etc., of the electrolytes, which will be discussed in the following sections.

### *3.3.2 Raman spectroscopic analysis of $Li^+$/solvate structure*

Raman spectra were measured to investigate the effects of HFE dilution on the local salt/solvent structures in the electrolytes. Raman spectra (890-970 $cm^{-1}$) of pure DMC solvent and $LiBF_4$/DMC and $LiPF_6$/DMC electrolytes of different concentrations are shown in Fig. S3-2. In both systems, the band of solvating DMC (933 $cm^{-1}$) became stronger with an increase in the concentration of $LiBF_4$ or $LiPF_6$, while that of free DMC (916 $cm^{-1}$) became weaker, indicating less free DMC molecules in highly concentrated electrolytes. DMC dissolved more $LiBF_4$ (8.67 mol $kg^{-1}$, DMC/Li = 1.28) than $LiPF_6$ (5.05 mol $kg^{-1}$, DMC/Li = 2.2), and the reason is related with the coordination state of solvent/anion with $Li^+$ in highly concentrated electrolytes.

The fractions of solvated DMC in $LiBF_4$/DMC and $LiPF_6$/DMC of different concentrations, which were estimated by peak separation in Fig. S3-2, are plotted against the molar ratio of DMC/Li in Fig. S3-3(a). At a given DMC/Li, the fraction of

solvated DMC in $LiPF_6$/DMC was higher than that in $LiBF_4$/DMC. The coordination numbers of DMC toward $Li^+$ were evaluated from the data in Fig. S3-2 using the method described in Supporting Information and Fig. S3-4. The variations of the coordination number of DMC in $LiBF_4$/DMC and $LiPF_6$/DMC with the DMC/Li molar ratio are shown in Fig. S3-3(b). At low concentrations (i.e. high DMC/Li) up to 2.22 mol $kg^{-1}$ (DMC/Li = 5), the coordination numbers were close to 2 in $LiBF_4$/DMC and 4 in $LiPF_6$/DMC. With a further increase in concentration, the coordination number decreased and reached 1.2 in the saturated $LiBF_4$/DMC and 2.1 in the saturated $LiPF_6$/DMC. The lower coordination numbers suggest that $Li^+$ ions are coordinated with anions to make contact ion pairs and aggregates even at low concentrations in $LiBF_4$/DMC. This agrees well the fact that $LiBF_4$ is more associative than $LiPF_6$.[36]

Figure 3-5 compares Raman spectra (900-970 $cm^{-1}$) of the nearly saturated (8.67 and 5.05 mol $kg^{-1}$), moderately concentrated (3.70 mol $kg^{-1}$), and HFE-diluted (0.96 mol $kg^{-1}$) $LiBF_4$/DMC and $LiPF_6$/DMC, respectively. In the nearly saturated 8.67 mol $kg^{-1}$ $LiBF_4$/DMC (DMC/Li = 1.28), most of DMC molecules were solvating to $Li^+$ (916 $cm^{-1}$) and few free DMC (933 $cm^{-1}$) existed. However, the fraction of free DMC remarkably increased in the diluted 0.96 mol $kg^{-1}$ $LiBF_4$/DMC+HFE. This is partly owing to a higher DMC/Li ratio (3.00) of the diluted electrolyte. Because the miscibility of HFE and concentrated $LiBF_4$/DMC is poor, HFE-diluted electrolytes with a DMC/Li ratio higher than 3.00 cannot be obtained using the mixed DMC+HFE (1:2 by volume) solvent. The concentration of 0.96 mol $kg^{-1}$ was nearly saturated in

the diluted DMC+HFE (1:2 by volume) solvent, in which the DMC/Li ratio is equal to that in 3.70 mol $kg^{-1}$ $LiBF_4$/DMC (DMC/Li = 3.00). The fraction of solvating DMC in 0.96 mol $kg^{-1}$ $LiBF_4$/DMC+HFE (43.5%) was remarkably lower than that in 3.70 mol $kg^{-1}$ $LiBF_4$/DMC (61.5 %), even though the DMC/Li ratios were equal to each other. This fact suggested that HFE has negative influence on the solvation state for $LiBF_4$/DMC and increases the fraction of free DMC. This is the main reason for the poor cycleability of NCM811 in the diluted 0.96 mol $kg^{-1}$ $LiBF_4$/DMC+HFE in Figs. 3-1 and 3-2, because free DMC is more vulnerable to oxidation than solvating DMC.

In the $LiPF_6$/DMC system, HFE dilution also increased the fraction of free DMC as shown in Fig. 3-5. However, the fraction of solvating DMC molecules in 0.96 mol $kg^{-1}$ $LiPF_6$/DMC+HFE (92.7%) was much higher than that in 0.96 mol $kg^{-1}$ $LiBF_4$/DMC+HFE (43.5%), and was comparable to that comparing to the value (93.5%) in 3.70 mol $kg^{-1}$ $LiPF_6$/DMC (DMC/Li = 3.00). In contrast to the $LiBF_4$/DMC system, the dilution of HFE in the $LiPF_6$/DMC system gave very minor influence on the solvation state. This is because $LiPF_6$ is more dissociative than $LiBF_4$[31] and hence DMC molecules easily solvate to $Li^+$ ions in $LiPF_6$/DMC. Owing to the low fraction of free DMC, NCM811 showed good cycleability in the diluted 0.96 mol $kg^{-1}$ $LiPF_6$/DMC+HFE.

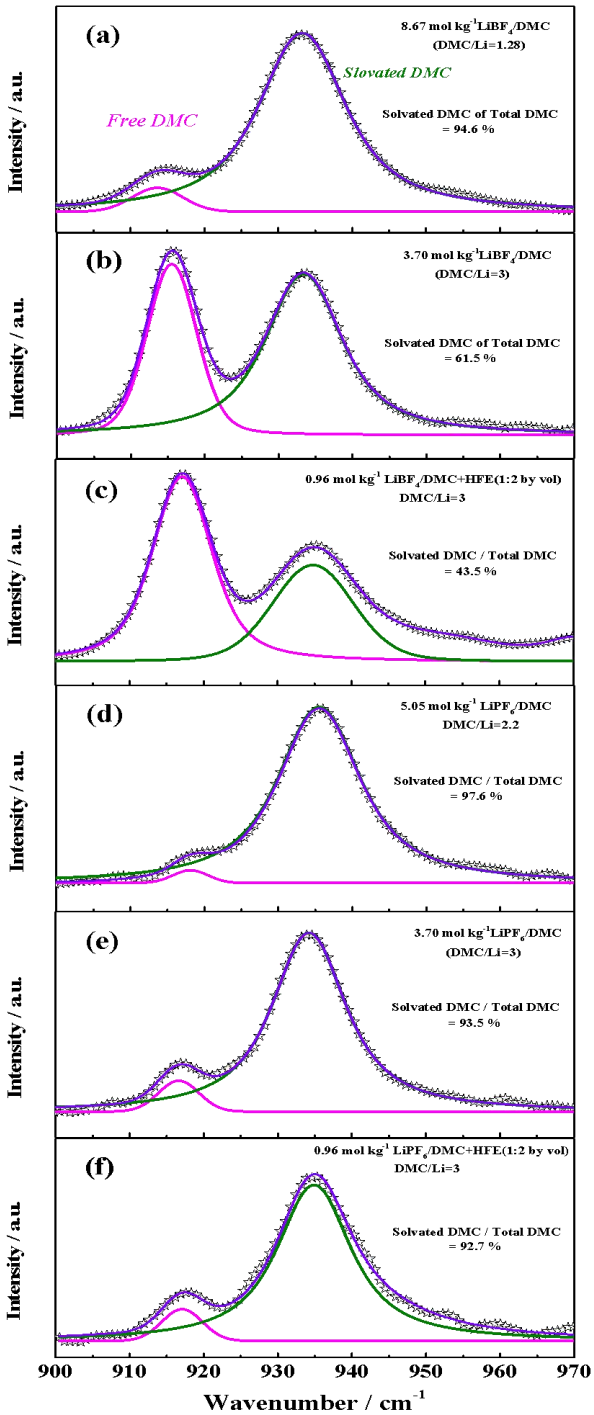


**Fig. 3-5.** Raman spectra of DMC in (a) 8.67 mol $kg^{-1}$ $LiBF_4$/DMC, (b) 3.70 mol $kg^{-1}$ $LiBF_4$/DMC, (c) 0.96 mol $kg^{-1}$ $LiBF_4$/DMC+HFE (1:2 by volume), (d) 5.05 mol $kg^{-1}$ $LiPF_6$/DMC, (e) 3.70 mol $kg^{-1}$ $LiPF_6$/DMC, and (f) 0.96 mol $kg^{-1}$ $LiPF_6$/DMC+HFE (1:2 by volume).

### *3.3.3 Raman spectroscopic analysis of anion structure*

Raman spectra of anions in $LiBF_4$/DMC (740-830 $cm^{-1}$) and $LiPF_6$/DMC (730-770 $cm^{-1}$) electrolytes of different concentrations are shown in Fig. 3-6. Three bands relating to the B-F symmetric vibrations of $BF_4^-$ anion were observed at 764, 773 and 781 $cm^{-1}$ (Fig. 3-6(a)). These bands can be assigned to the vibration modes of solvent-separated ion pairs (SSIPs), contact ion pairs (CIPs) and aggregates (AGGs), in which the anions are coordinated to zero, one, or more than one $Li^+$ cations, respectively.[37,38] In CIPs and AGGs, both the solvent molecules and the anions are coordinating to $Li^+$ ions. With an increase in concentration, $Li^+$ ions, $BF_4^-$ anions and DMC solvent molecules are likely to form aggregate clusters, indicating that not only $Li^+$-DMC interactions, but also $Li^+$-$BF_4^-$ interactions are enhanced. In contrast, $PF_6^-$ anions mainly existed as CIPs (743 $cm^{-1}$), and AGGs (751 $cm^{-1}$)[39] were hardly formed even at high concentrations (Fig. 3-6(b)), which explains the fact that $LiPF_6$ is less soluble in DMC than $LiBF_4$ though the former is more dissociative than the latter.

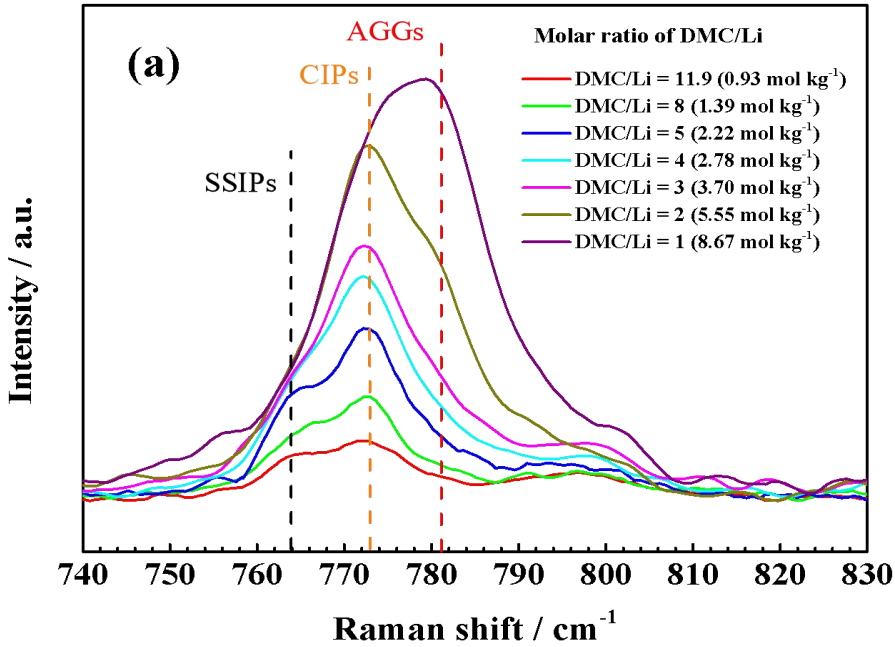


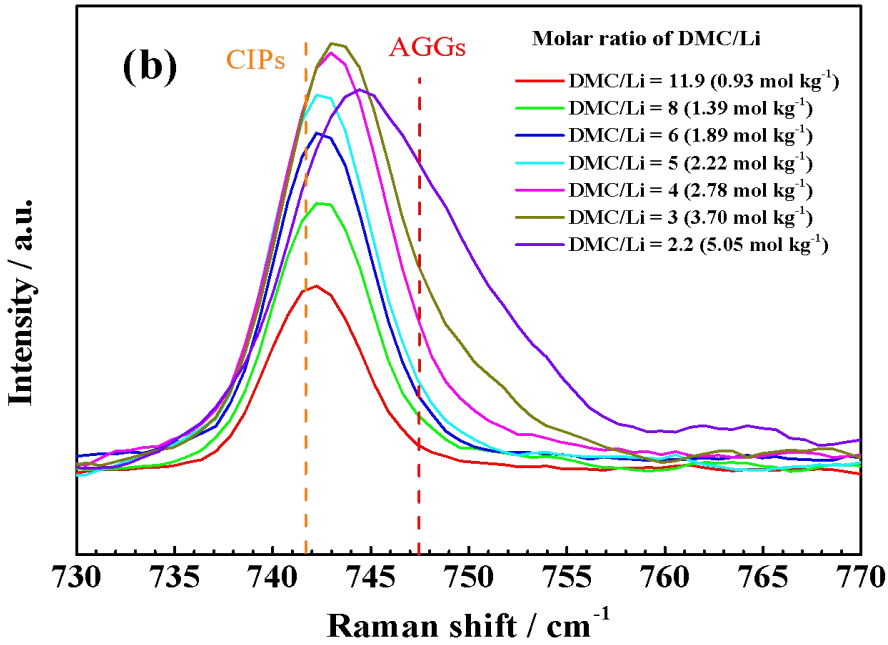


**Fig. 3-6.** Raman spectra of $BF_4^-$ anions in (a) $LiBF_4$/DMC and $PF_6^-$ anions in (b) $LiPF_6$/DMC at different DMC/Li molar ratios.

Figure 3-7 compares Raman spectra of $BF_4^-$ anions in 8.67 and 3.70 mol $kg^{-1}$ $LiBF_4$/DMC, 0.96 mol $kg^{-1}$ $LiBF_4$/DMC+HFE, and pure HFE. In the nearly saturated 8.67 mol $kg^{-1}$ $LiBF_4$/DMC (Fig. 3-7(a)), the fraction of AGGs was higher than that of CIPs, and SSIPs were not observed, indicating that the interactions among the solvent, $Li^+$ and the anion were very tight as was discussed in Fig. 3-6. However, in 3.70 mol $kg^{-1}$ $LiBF_4$/DMC (Fig. 3-7(b)), SSIPs appeared and the fraction of AGGs became smaller than that in 8.67 mol $kg^{-1}$ $LiBF_4$/DMC, suggesting that the interactions among the solvent, $Li^+$ and the anion became weak. In the diluted electrolyte (Fig. 3-7(c)), some bands from HFE overlap the bands from $BF_4^-$, and hence precise peak fitting of the $BF_4^-$ bands are difficult. However, it seems that the fraction of CIPs decreased, whereas the fraction of AGGs increased, though the DMC/Li ratio (3.00) is equal to that in 3.70 mol $kg^{-1}$ $LiBF_4$/DMC. These results suggest that the presence of HFE suppresses the dissociation of $LiBF_4$ owing to its low dielectric constant ($\varepsilon = 6.21$),[40] and thereby increases the fraction of free DMC that is vulnerable to oxidation as shown in Fig. 3-5.

Raman spectra of $PF_6^-$ anions in 5.05 and 3.70 mol $kg^{-1}$ $LiPF_6$/DMC, and 0.96 mol $kg^{-1}$ $LiPF_6$/DMC+HFE are shown in Fig. 3-8. The band intensities of $PF_6$ anions were obviously greater than those of HFE (Fig. 3-7(d)), hence, the bands of HFE can be ignored in Fig. 3-8(c). The fraction of AGGs in the diluted electrolyte was lower than that in 5.05 mol $kg^{-1}$ $LiPF_6$/DMC (Fig. 3-8(a)), which is due to an increase in the molar ratio of DMC/Li (from 2.2 to 3.0). The fractions of AGGs and CIPs in the diluted electrolyte were almost equal to those in 3.70 mol $kg^{-1}$ $LiPF_6$/DMC (Fig.

3-8(b)) that has the same DMC/Li ratio (3.00), indicating that the presence of HFE rarely affects the dissociation of $LiPF_6$ because $LiPF_6$ is more dissociative than $LiBF_4$. This is in good agreement with the fact in Fig. 3-5 that the fraction of solvating DMC only slightly changed after diluted with HFE.

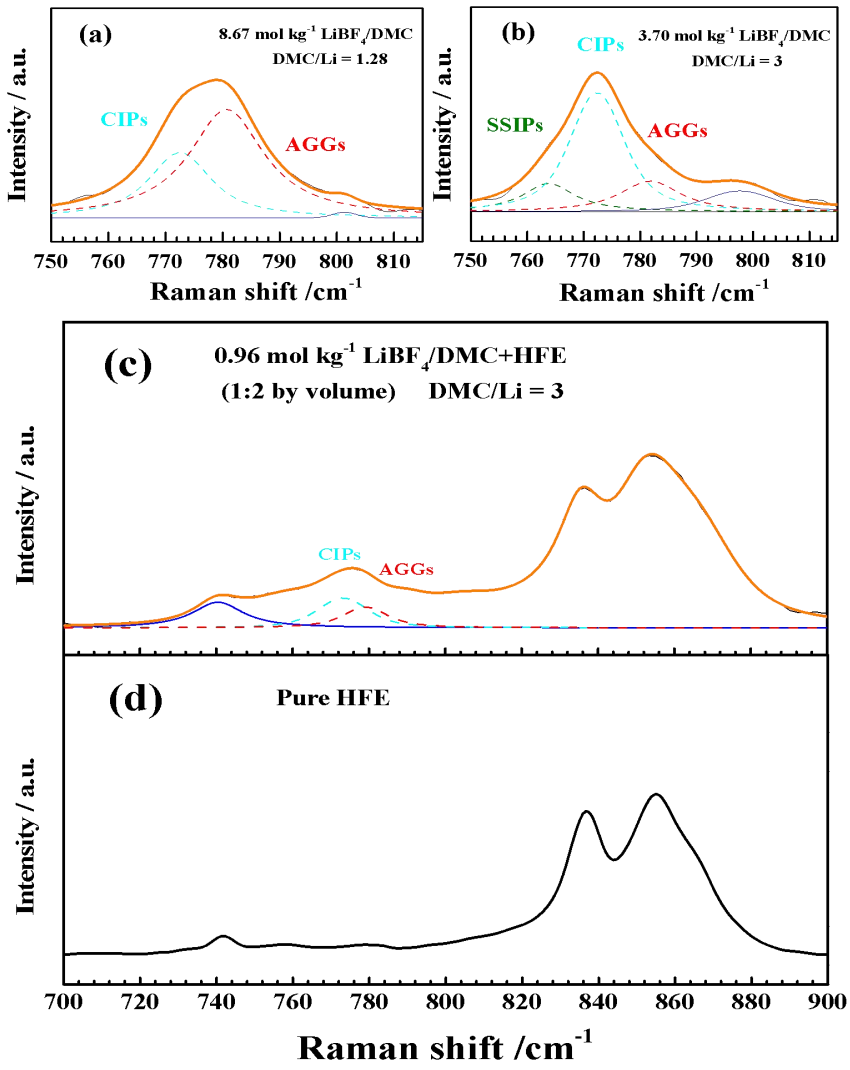


**Fig. 3-7.** Raman spectra of $BF_4^-$ anions in (a) 8.67 mol $kg^{-1}$, (b) 3.70 mol $kg^{-1}$ $LiBF_4$/DMC, (c) 0.96 mol $kg^{-1}$ $LiBF_4$/DMC+HFE (1:2 by volume) and (d) of pure HFE.

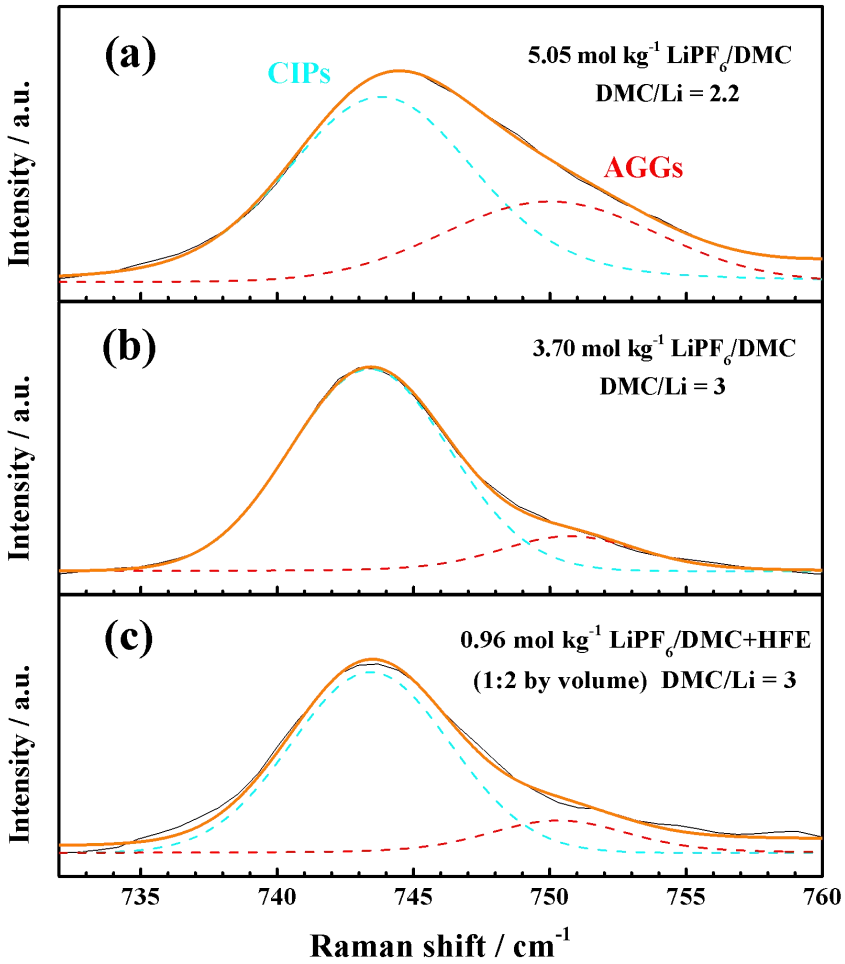


**Fig. 3-8.** Raman spectra of $PF_6^-$ anions in (a) 5.05 mol $kg^{-1}$, (b) 3.70 mol $kg^{-1}$ $LiPF_6$/DMC, and (c) 0.96 mol $kg^{-1}$ $LiPF_6$/DMC+HFE (1:2 by volume).

### *3.3.4 Anodic stability*

Linear sweep voltammograms on Pt electrode in different electrolytes are shown in Fig. 3-9. The nearly saturated 8.67 mol $kg^{-1}$ $LiBF_4$/DMC showed a high stability against oxidation up to 5.0 V, which is better than the nearly saturated 5.05 mol $kg^{-1}$ $LiPF_6$/DMC. However, in the diluted 0.96 mol $kg^{-1}$ $LiBF_4$/DMC+HFE (Fig. 3-9(a)), the oxidation current of electrolyte rose at around 3.9 V, indicating that the high stability against oxidation was spoiled by the dilution with HFE. This resulted from an

increased fraction of free DMC by the dilution with HFE as shown in Fig. 3-5. For the $LiPF_6$/DMC system (Fig. 3-9(b)), both the diluted and the nearly saturated electrolytes showed high stability against oxidation up to 4.3 V. This is because the dilution with HFE has little influence on the solvent-salt structure for the $LiPF_6$/DMC system as discussed above. The oxidation current increased significantly at potentials higher than 4.3 V in the diluted electrolytes, which is attributable to the oxidation of HFE because the increase in oxidation current at potentials higher than 4.3 V is also observed in the diluted 0.96 mol $kg^{-1}$ $LiBF_4$/DMC+HFE in Fig. 3-9(a). In Chapter 3, the upper potential for charge and discharge tests was fixed at 4.3 V vs. $Li/Li^+$, and the diluted $LiPF_6$/DMC+HFE gave good cycleabiltiy for NCM811 cathode. However, if the upper potential is raised to a potential higher than 4.3 V, decomposition of HFE will give harmful effects on the cycleability NCM811 or other Ni-rich NCM cathodes.

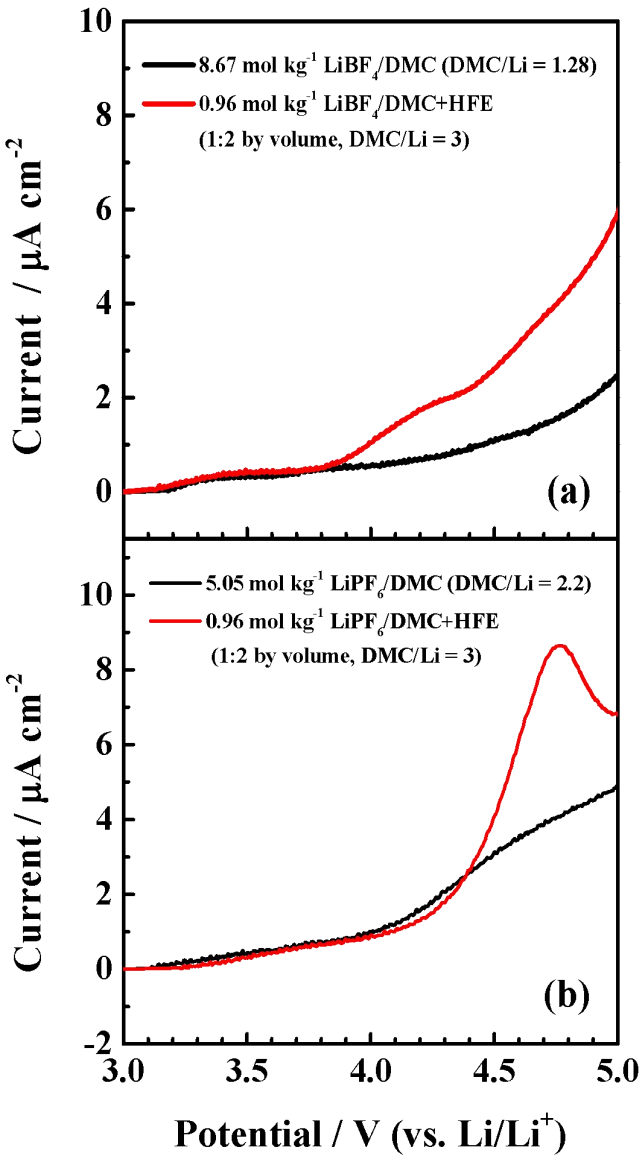


**Fig. 3-9.** Linear sweep voltammograms at Pt in (a) 8.67 mol $kg^{-1}$ $LiBF_4$/DMC and 0.96 mol $kg^{-1}$ $LiBF_4$/DMC+HFE (1:2 by volume) and (b) 5.05 mol $kg^{-1}$ $LiPF_6$/DMC and 0.96 mol $kg^{-1}$ $LiPF_6$/DMC+HFE (1:2 by volume). Sweep rate: 1 mV $s^{-1}$.

### *3.3.5 Particle fracture during cycling*

Figure 3-10 shows cross-sectional SEM images of the NCM811 particles after cycled in Fig. 3-2. NCM811 cathode particles usually suffer from severe crack formation and particle fracture when cycled in conventional electrolytes (e.g. 1 M EC-based electrolytes), which is a major reason for the poor cycleability of NCM811.

However, after cycled in highly concentrated 8.67 mol $kg^{-1}$ $LiBF_4$/DMC, crack formation was remarkably suppressed as shown in Figs. 3-10(a,b,c).[20] On the other hand, crack formation was significantly accelerated in the diluted $LiBF_4$/DMC+HFE (Figs. 3-10(d,f,e)). As was discussed in a previous report,[20] electrolyte solution penetrates through cracks and decomposes at the cracks to form decomposition products. The decomposition products accumulate at the cracks and accelerate particle disintegration. As shown by Raman analysis, the fraction of free DMC molecules, which are vulnerable to oxidation, increased by the dilution with HFE, and decomposition of the free DMC at cracks is the reason for the accelerated crack propagation (Figs. 3-10(d,e,f)) and capacity fading (Fig. 3-2(a)) in the diluted $LiBF_4$/DMC+HFE. In contrast, the particle fracture was remarkably inhibited in the diluted 0.96 mol $kg^{-1}$ $LiPF_6$/DMC+HFE (Figs. 3-10(j,k,l)), and the degree of the crack propagation was similar to that in 5.05 mol $kg^{-1}$ $LiPF_6$/DMC (Figs. 3-10(g,h,i)), suggesting that the diluted electrolyte had high stability against oxidation equally to the nearly saturated electrolyte. As discussed earlier, the dilution of HFE had little influence on the local salt/solvent structure for $LiPF_6$/DMC system and the fraction of free DMC was kept very low even in the diluted electrolyte, which resulted in the observed good cycleability and suppression of crack formation.

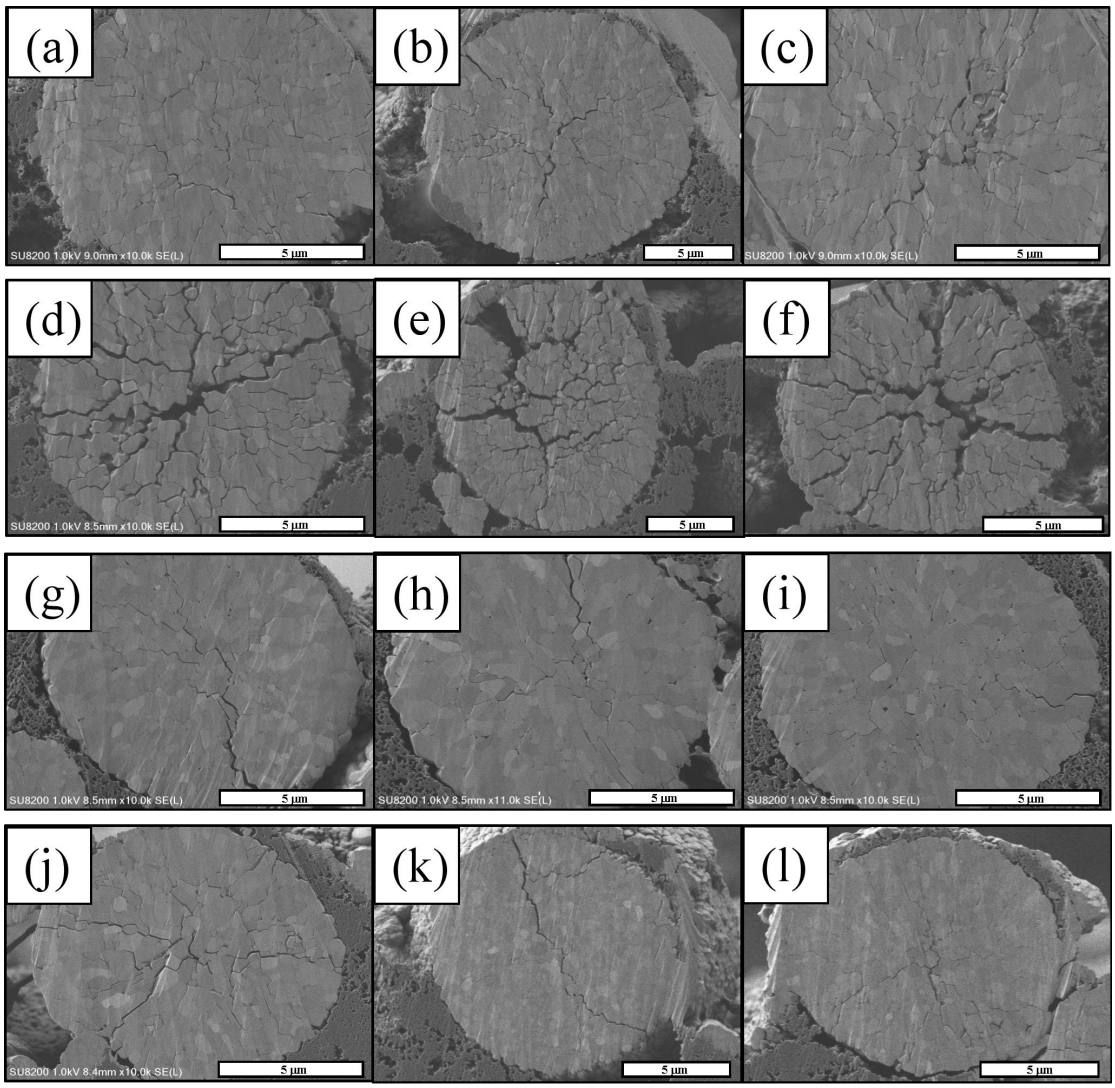


**Fig. 3-10.** Cross-sectional SEM images of $LiNi_{0.8}Co_{0.1}Mn_{0.1}O_2$ particles after 50 cycles in (a,b,c) 8.67 mol $kg^{-1}$ $LiBF_4$/DMC and (d,e,f) 0.96 mol $kg^{-1}$ $LiBF_4$/DMC+HFE (1:2 by volume), and after 100 cycles in (g,h,i) 5.05 mol $kg^{-1}$ $LiPF_6$/DMC and (j,k,l) 0.96 mol $kg^{-1}$ $LiPF_6$/DMC+HFE (1:2 by volume).

### 3.4 Conclusions

In Chapter 3, it was found that HFE to dilute the highly concentrated $LiBF_4$/DMC and $LiPF_6$/DMC electrolytes. However, the dilution with HFE for the $LiBF_4$/DMC system increased the fraction of free DMC, which is more vulnerable to oxidation than solvating DMC, because the dilution suppressed the dissociation of

$LiBF_4$. Consequently the cycling performance of NCM811 electrode decayed more quickly than that in the nearly saturated $LiBF_4$/DMC. Many cracks were formed after 50 cycles in the diluted electrolyte, which showed that the electrolyte decomposition within the cracks and accumulation of decomposed products are the main reason for the capacity fading. In contrast, the local salt/solvent structure was rarely affected by the dilution with HFE for $LiPF_6$/DMC system. Due to the highly dissociative character of $LiPF_6$, the dilution with HFE hardly changed the fraction of solvating DMC. Hence, the oxidation stability of the diluted electrolyte rarely deteriorated from that of the nearly saturated $LiPF_6$/DMC, and good cycle performance was obtained and crack formation was suppressed in the diluted electrolyte.

The results obtained in this work indicated that not only the choice of the diluents, but also lithium salt/diluent combination is an important factor for the dilution of concentrated electrolytes. It was found that the local salt/solvent structure in the electrolytes is strongly affected by the dissociative/associative character of the salts, which determines the stability against oxidation. In Chapter 4, a few kinds of fluorinated diluents that can be applied for the $LiBF_4$/DMC system are investigated to maintain a low molar ratio of DMC/Li and to obtain high anodic stability against higher potentials than 4.3 V.

**References**

[1] T. Nagaura, and K. Tozawa, "Lithium ion rechargeable battery." *Prog. Batteries Solar Cells*, **9**, A209 (1990).

[2] J. R. Dahn, U. Von Sacken, M. W. Juzkow, and H. Al-Janaby, "Rechargeable $LiNiO_2$/carbon cells." *J. Electrochem. Soc.*, **138**, A2207 (1991).

[3] K. Ozawa, "Lithium-ion rechargeable batteries with $LiCoO_2$ and carbon electrodes: the $LiCoO_2$/C system." *Solid State Ionics*, **69**, A212 (1994).

[4] J.-M. Tarascon, and M. Armand, "Issues and challenges facing rechargeable lithium batteries. *Nature*, **414**, A359 (2001).

[5] E. Antolini, and M. Ferretti, "Synthesis and thermai stability of $LiCoO_2$." *J. Solid State Chem*., **117**, A1 (1995).

[6] H. Wang, Y. Jang, B. Huang, D. R. Sadoway, and Y.-M Chiang, "TEM Study of Electrochemical Cycling-Induced Damage and Disorder in $LiCoO_2$ Cathodes for Rechargeable Lithium Batteries." *J. Electrochem. Soc.*, **146,** A473 (1999).

[7] C. Liu, G. Zachary, Neale, and G. Cao, "Understanding electrochemical potentials of cathode materials in rechargeable batteries." *Materials Today*, **19**, A109 (2016).

[8] Y. Baba, S. Okada, J. Yamaki, "Thermal stability of $Li_xCoO_2$ cathode for Lithium ion battery." *Solid Stare Ionics*, **148**, A311 (2002).

[9] T. Fang, J.-G. Duh, and S.-R. Sheenb, "Improving the Electrochemical Performance of $LiCoO_2$ Cathode by Nanocrystalline ZnO Coating." *J. Electrochem. Soc.*, 152, A1701 (2005).

[10] M. Yoshio, H. Noguchi, J.-i. Itoh, M. Okada, and T. Mouri, "Preparation and properties of $LiCo_yMn_xNi_{1-x-y}O_2$ as acathode for lithium ion batteries." *J. Power Sources,* **90**, A176 (2002).

[11] P. Y. Liao, J. G. Duh, and S. R. Sheen, "Effect of Mn Content on the Microstructure and Electrochemical Performance of $LiNi_{0.75-x}Co_{0.25}Mn_xO_2$ Cathode Materials." *J. Electrochem. Soc.*, **152,** A1695 (2005).

[12] H.-J. Noh, S. Youn, C. S. Yoon, and Y.-K. Sun, "Comparison of the structural and electrochemical properties of layered $Li[Ni_xCo_yMn_z]O_2$ (x=1/3, 0.5, 0.6, 0.7, 0.8 and 0.85) cathode material for lithium-ion batteries." *J. Power Sources*, **233**, A121 (2013).

[13] H.-R. Kim, S.-G. Woo, J.-H. Kim, W. Cho, and Y.-J Kim, "Capacity fading behavior of Ni-rich layered cathode materials in Li-ion full cells." *J. Electroanal. Chem.*, **782**, A168 (2016).

[14] Y. Liu, W. Yao, C. Lei, Q. Zhang, S. Zhong, and Z. Yan, "Ni-Rich Oxide $LiNi_{0.85}Co_{0.05}Mn_{0.1}O_2$ for Lithium Ion Battery: Effect of Microwave Radiation on Its Morphology and Electrochemical Property." *J. Electrochem. Soc.*, **166**, A1300 (2019).

[15] J. Li, H. Li,a W. Stone, R. Weber, S. Hy, and J. R. Dahn, "Synthesis of Single Crystal $LiNi_{0.5}Mn_{0.3}Co_{0.2}O_2$ for Lithium Ion Batteries." *J. Electrochem. Soc.*, **164**, A3529 (2017).

[16] Y.-S. Lee, Y.-K. Sun, S. Ota, T. Miyashita, and M. Yoshio, "Preparation and characterization of nano-crystalline $LiNi_{0.5}Mn_{1.5}O_4$ for 5 V cathode material by composite carbonate process." *Electrochem. Commun.*, **4**, A989 (2002).

[17] D. Aurbach, B. Markovsky, Y. Talyossef, G. Salitra, H-J. Kim, and S. Choi, "Studies of cycling behavior, ageing, and interfacial reactions of $LiNi_{0.5}Mn_{1.5}O_4$ and carbon electrodes for lithium-ion 5-V cells." *J. Power Sources*, **162**, A780 (2006).

[18] L.-J. Li, X.-H. Li, Z.-X. Wang, H.-J Guo, P. Yue, W. Chen, and L. Wu, "A simple and effective method to synthesize layered $LiNi_{0.8}Co_{0.1}Mn_{0.1}O_2$ cathode materials for lithium ion battery." *Powder Technology,* **206**, A353 (2011).

[19] X. Zheng, X. Li, B. Zhang, Z. Wang, H.Guo, Z. Huang, G. Yan, D. Wang, and Y. Xu, "Enhanced electrochemical performance of $LiNi_{0.8}Co_{0.1}Mn_{0.1}O_2$ cathode materials obtained by atomization co-precipitation method." *Ceramics International*, **42**, A644 (2016).

[20] Z. Cao, M, Hashinokuchi, T. Doi, and M. Inaba, "Improved cycle performance of $LiNi_{0.8}Co_{0.1}Mn_{0.1}O_2$ positive electrode material in highly concentrated $LiBF_4$/DMC." *J. Electrochem Soc.*, **166**, A82 (2019).

[21] K. Yoshida, M. Nakamura, Y. Kazue, N. Tachikawa, S. Tsuzuki, S. Seki, K. Dokko, and M. Watanabe, "Oxidative-stability enhancement and charge transpor mechanism in glyme-lithium salt equimolar complexes." *J. Am. Chem. Soc.,* **133**, A13121 (2011).

[22] D. W. McOwen, D. M. Seo, O. Borodin, J. Vatamanu, P. D. Boyled, and W. A. Henderson, "Concentrated electrolyte: decrypting electrolyte properties and reassessing Al corrosion mechanisms." *Energy Environ. Sci.,* **7**, A416 (2014).

[23] R. Petibona, C. P. Aiken, L. Ma, D. Xiong, and J. R. Dahn, "The use of ethyl acetate as a sole solvent in highly concentrated electrolyte for Li-ion batteries. *Electrochem. Acta*, **154**, A287 (2015).

[24] J. Wang, Y. Yamada, K. Sodeyama, E. Watanabe, K. Takada, Y. Tateyama, and A. Yamada, "Fire-extinguishing organic electrolytes for safe batteries." *Nature Energy*, **3**, A22 (2018).

[25] X. Ren, S. Chen, H. Lee, and K. Xu et al., " Localized High-Concentration Sulfone Electrolytes for High-Efficiency Lithium-Metal Batteries." *Chem.*, **4**, A1877 (2018).

[26] T. Doi, Y. Shimizu, M. Hashinokuchi, and M. Inaba, "$LiBF_4$-Based concentrated electrolyte solutions for suppression of electrolyte decomposition and rapid lithium-ion transfer at $LiNi_{0.5}Mn_{1.5}O_4$/electrolyte interface." *J. Electrochem Soc.*, **163**, A2211 (2016).

[27] T. Doi, M. Hahsinokuchi, and M. Inaba, "Solvation-controlled ester-based concentrated electrolyte solutions for high-voltage lithium-ion batteries." *Current Option in Electrochem.*, **9**, A49 (2018).

[28] T. Doi, Y. Shimizu, M. Hashinokuchi, and M. Inaba, "Low-Viscosity γ-Butyrolactone-Based Concentrated Electrolyte Solutions for $LiNi_{0.5}Mn_{1.5}O_4$ Positive Electrodes in Lithium-Ion Batteries." *Chem Electro Chem.*, **4**, A2398 (2017).

[29] T. Doi, R. Masuhara, M. Hashinokuchi, Y. Shimizu, and M. Inaba, "Concentrated $LiPF_6$/PC electrolyte solutions for 5-V $LiNi_{0.5}Mn_{1.5}O_4$ positive electrode in lithium-ion batteries." *Electrochim. Acta.,* **209**, A219 (2016).

[30] J. Wang, Y. Yamada, K. Sodeyama, C. H. Chiang, Y. Tateyama, and A. Yamada, "Superconcentrated electrolytes for a high-voltage lithium-ion battery." *Nature Commun.,* **7**, A12032 (2016).

[31] T. Doi, Y. Shimizu, M. Hashinokuchi, and M. Inaba, "Dilution of highly concentrated $LiBF_4$/propylene carbonate electrolyte solution with fluoroalkyl ethers for 5-V $LiNi_{0.5}Mn_{1.5}O_4$ positive electrodes." *J. Electrochem Soc.,* **164**, A6412 (2017).

[32] T. Doi, R. Matsumoto, Z. Cao, M. Hashinokuchi, and M. Inaba, "Fluoroalkyl ether-diluted dimethyl carbonate-based electrolyte solutions for high-voltage operation of $LiNi_{0.5}Co_{0.2}Mn_{0.3}O_2$ electrodes in lithium ion batteries." *Sustainable Energy Fuels,* **2**, A1197 (2018).

[33] S. Chen, J. Zheng, D. Mei, K. S. Han, M. H. Engelhard, W. Zhao, W. Xu, J. Liu, and J.-G. Zhang, "High-Voltage Lithium-Metal Batteries Enabled by Localized High-Concentration Electrolytes." *Adv. Mater*., **30**, A1706102 (2018).

[34] G. Ma, L. Wang, X. He, J. Zhang, H. Chen, W. Xu, and Y. Ding, "Pseudoconcentrated Electrolyte with High Ionic Conductivity and Stability Enables High-Voltage Lithium-Ion Battery Chemistry." *ACS Appl. Energy Mater.,* **1**, A5446 (2018).

[35] W. Li, J. N. Reimers, and J. R. Dahn, "In situ x-ray diffraction and electrochemical studies of $Li_{1-x}NiO_2$." *Solid State Ionics*, **67**, A123 (1993).

[36] K. Xu, "Electrolytes and Interphases in Li-Ion Batteries and Beyond." *Chem. Rev.*, **114**, A11503 (2014).

[37] N. Chapman, O. Borodim, T. Yoon, C. C. Nguyen, and B. L. Lucht,

"Spectroscopic and Density Functional Theory Characterization of Common Lithium Salt Solvates in Carbonate Electrolytes for Lithium Batteries." *J. Phys. Chem. C.*, **121**, A2135 (2017).

[38] D.M. Seo, O. Borodin, S.-D Han, Q, Ly, P. D. Boyle, and W. A. Henderson, "Electrolyte Solvation and Ionic Association." *J. Electrochem Soc.*, **159**, A553 (2012).

[39] S.-D. Han, S.-H. Yun, O. Borodin, D. Seo, R. Sommer V. Young, and W. Henderson, "Solvate Structures and Computational/Spectroscopic Characterization of $LiPF_6$ Electrolytes." *J. Phys. Chem. C.*, **119**, A8492 (2015).

[40] K. Dokko, N. Tachikawa, K. Yamauchi, M. Tsuchiya, A. Yamazaki, E. Takashima, J.-W. Park, K. Ueno, S. Seki, N. Serizawa, and M. Watanabe, "Solvate Ionic Liquid Electrolyte for Li‐S Batteries. *J. Electrochem. Soc.*,**160**, A1304 (2013) .

**Supporting Information**

**Table S3-1.** The viscosity and ionic conductivity data of various electrolytes.

| Conc. (mol kg$^{-1}$) | DMC/Li Molar ratio | Electrolyte | Solvent | Viscosity (mPa s) | Ionic conductivity (mS cm$^{-1}$) |
|---|---|---|---|---|---|
| 8.67 | 1.28 | $LiBF_4$ | DMC | 226 | 0.75 |
| 3.70 | 3.00 | | | 6.3 | 2.32 |
| 0.96 | 3.00 | | DMC+HFE (1:2 by volume) | 1.5 | 0.13 |
| 5.05 | 2.2 | $LiPF_6$ | DMC | 28 | 2.78 |
| 3.70 | 3.00 | | | 9.6 | 4.87 |
| 0.96 | 3.00 | | DMC+HFE (1:2 by volume) | 1.7 | 2.66 |

The viscosity of the electrolytes was measured with an Ubbelohde capillary viscometer at room temperature in an Ar-filled glove box (MDB-1NKP-DS, Miwa Mfg). The ionic conductivity was measured with an a.c. impedance analyzer (VersaSTAT 3, Princeton Applied Research) using a symmetrical cell consisting of two Pt plate electrodes.

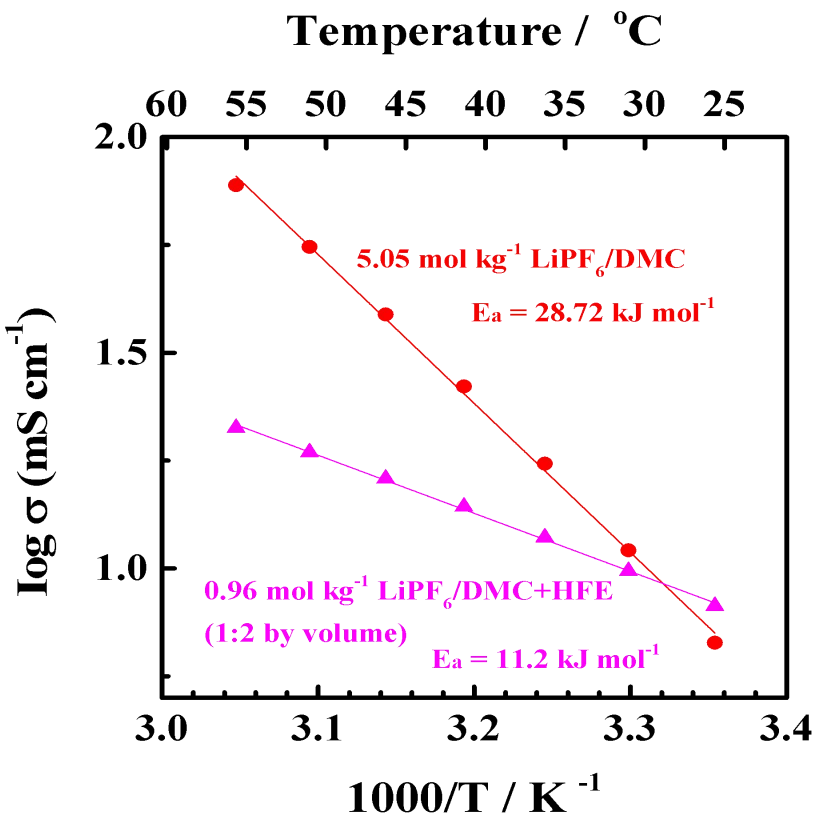


**Fig. S3-1.** Conductivities of 5.05 mol $kg^{-1}$ $LiPF_6$/DMC and 0.96 mol $kg^{-1}$ $LiPF_6$/DMC+HFE (1:2 by volume) electrolyte at different temperature.

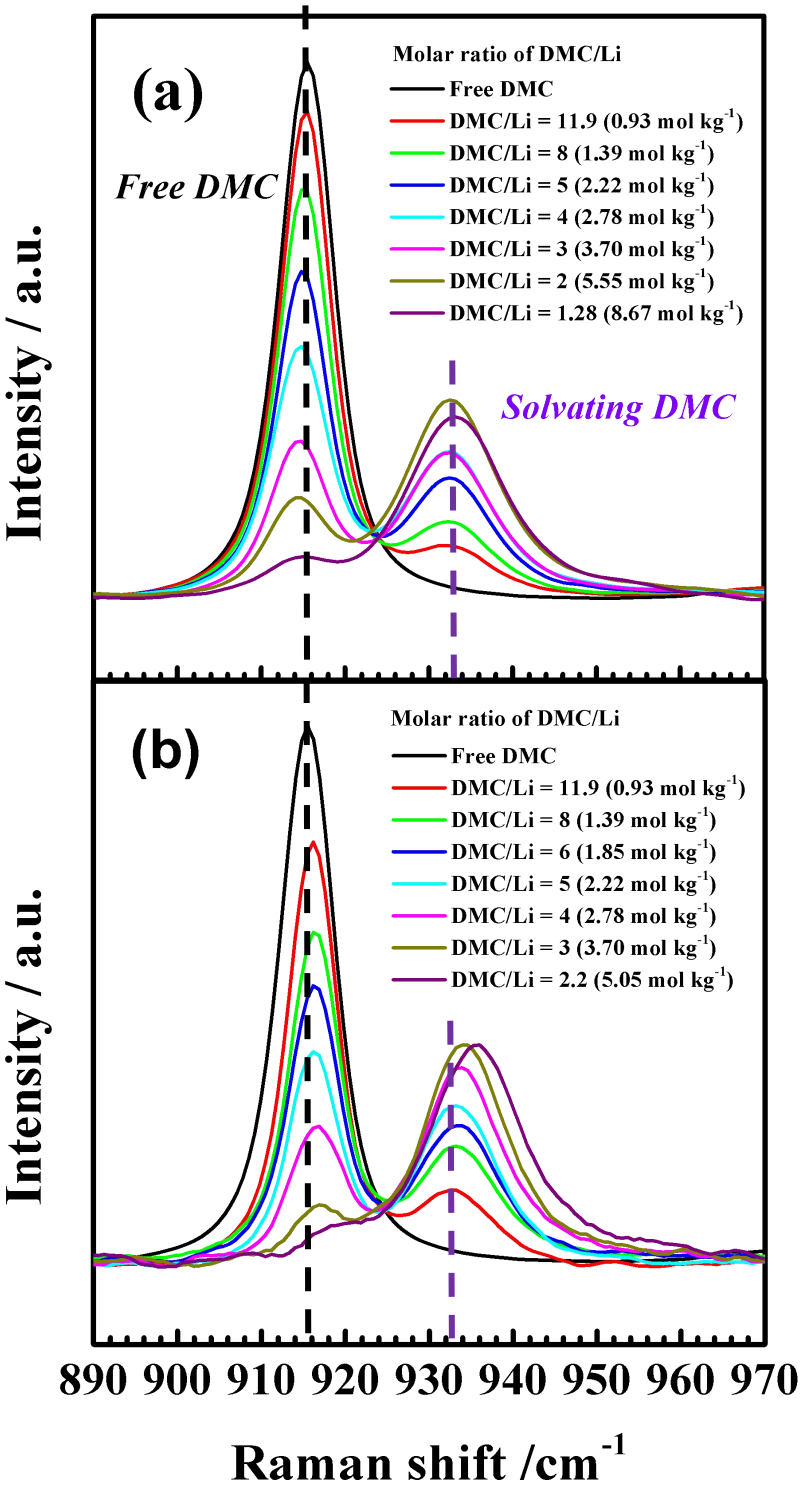


**Fig. S3-2.** Raman spectra (890-970 $cm^{-1}$) of pure DMC and (a) $LiBF_4$ and (b) $LiPF_6$ of different DMC/Li molar ratios.

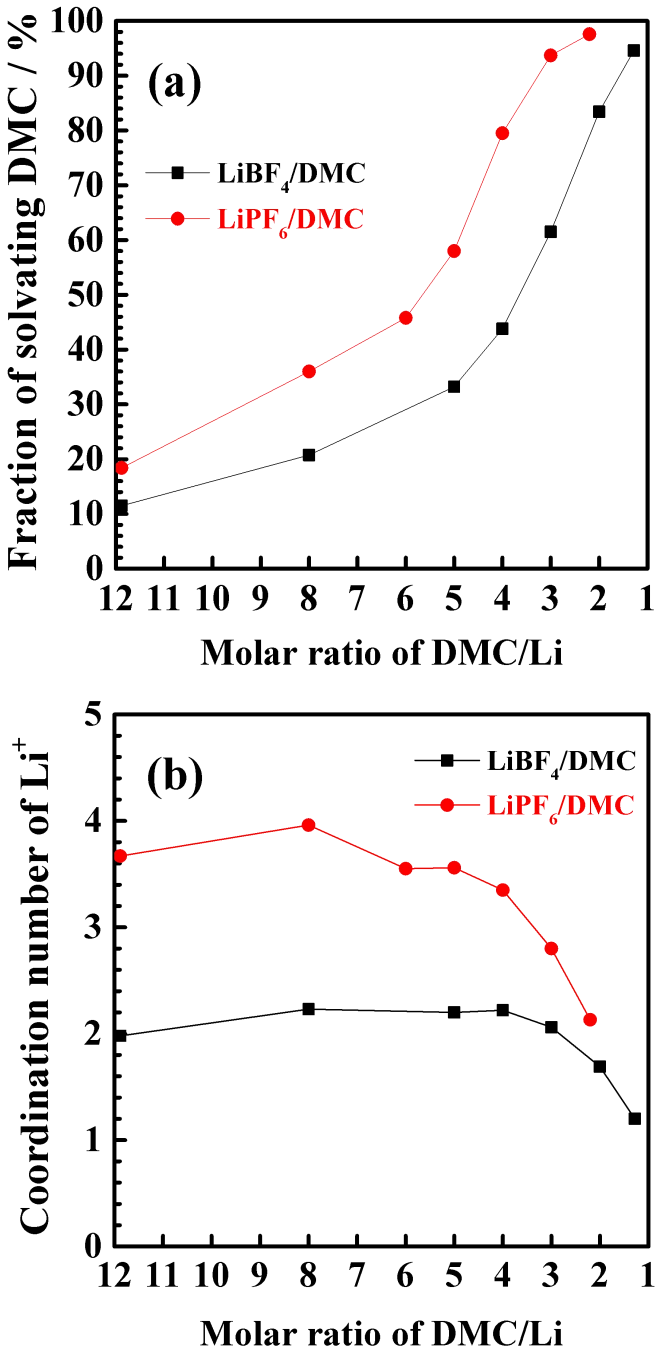


**Fig. S3-3.** (a) Fraction of solvating DMC and (b) calculated coordination number of $Li^+$ in $LiBF_4$/ and $LiPF_6$/DMC at different DMC/Li ratios.

***Determination of the coordinating number of DMC molecules toward $Li^+$***

The coordinating numbers of DMC molecules toward $Li^+$ were evaluated from the intensities of the bands at 916 and 934 $cm^{-1}$ (i.e., stretching vibration mode of free and coordinating DMC, respectively) using the method reported by Homma et al.,[S1] and Yamada et al.[S2] The Raman intensities of the bands at 916 $cm^{-1}$ ($I_{free}$) and 933 $cm^{-1}$ ($I_{coordinating}$) were determined by the numbers of free DMC molecules ($N_{free}$) and coordinating DMC molecules ($N_{coordinating}$), respectively, per one $Li^+$ in the solution as:

$$N_{total} = N_{free} + N_{coordinating} \quad \text{(S3-1)}$$

$$I_{free} = \sigma_{free} N_{free} \quad \text{(S3-2)}$$

$$I_{coordinating} = \sigma_{coordinating} N_{coordinating} \quad \text{(S3-3)}$$

where $N_{total}$ denotes the total number of DMC molecules per $Li^+$, and $\sigma_{free}$ and $\sigma_{coordinating}$ the Raman scattering coefficients for free and coordinating DMC molecules, respectively. For calculation, we need the Raman intensity of a band that is not affected by coordination, and here we employed a Raman band at 690 $cm^{-1}$ that is assigned to the $OCO_2$ rocking mode of DMC.[S3] The Raman intensity of the unaltered 690 $cm^{-1}$ band ($I_{unaltered}$) is given by the product of $N_{total}$ and the Raman scattering coefficient ($\sigma_{unaltered}$) of the 690 $cm^{-1}$ band as:

$$I_{unaltered} = \sigma_{unaltered} N_{total} \quad \text{(S3-4)}$$

From Eqs (S3-1) ,(S3-2) and (S3-3), the following equation (Eq. (S3-5)) is given:

$$N_{coording} = N_{total} \frac{\dfrac{I_{coordinating}}{\sigma_{coordinating} / \sigma_{free}}}{\dfrac{I_{coordinating}}{\sigma_{coordinating} / \sigma_{free}} + I_{free}} \quad \text{(S3-5)}$$

The value of $N_{coordinating}$ can be calculated by the ratio of $\sigma_{coordinating}/\sigma_{free}$. From Eqs.

(S3-2) ,(S3-3) and (S3-4), the following equation (Eq. (S3-6)) is given:

$$\frac{I_{coordinating}}{I_{unaltered}} = -\frac{\sigma_{coordinating}}{\sigma_{free}}\frac{I_{free}}{I_{unaltered}} + \frac{\sigma_{coordinating}}{\sigma_{unaltered}} \qquad \text{(S3-6)}$$

Here, the intensities of $I_{\mathrm{coordinating}}$ and $I_{\mathrm{free}}$ are normalized by the intensity of $I_{unaltered}$ at 690 $cm^{-1}$. The slope of the $I_{coordinating}/I_{unaltered}$ *vs* $I_{free}/I_{unaltered}$ plot gives the value of the $\sigma_{coordinating}/\sigma_{free}$ value (Fig. S3-1) and imported the value into Eq. (S3-5) to obtain $N_{coordinating}$ of DMC in different concentrated $LiBF_4$/DMC and $LiPF_6$/DMC electrolyte solutions are shown in Fig. S3-4.


[S1] O. Homma, Y. Amino, T. Miyajima, T. Enta, E. Murotani, and Y. Onozaki, *Res. Reports Asahi Glass Co., Ltd*. **67**, A33 (2017) (in Japanese).

[S2] Y. Yamada, Y. Takazawa, K. Miyazaki, and T. Abe, "Electrochemical Lithium Intercalation into Graphite in Dimethyl Sulfoxide-Based Electrolytes: Effect of Solvation Structure of Lithium Ion." *J. Phys. Chem. C*, **114**, A11680 (2010).

[S3] L. Doucey, M. Evault, A. Lautié, A. Chaussé, and R. Messina, "A study of the $Li/Li^+$ couple in DMC and PC solvents: Part 1: Characterization of $LiAsF_6$/DMC and $LiAsF_6$/PC solutions." *Electrochim. Acta,* **44**, A2371 (1999).

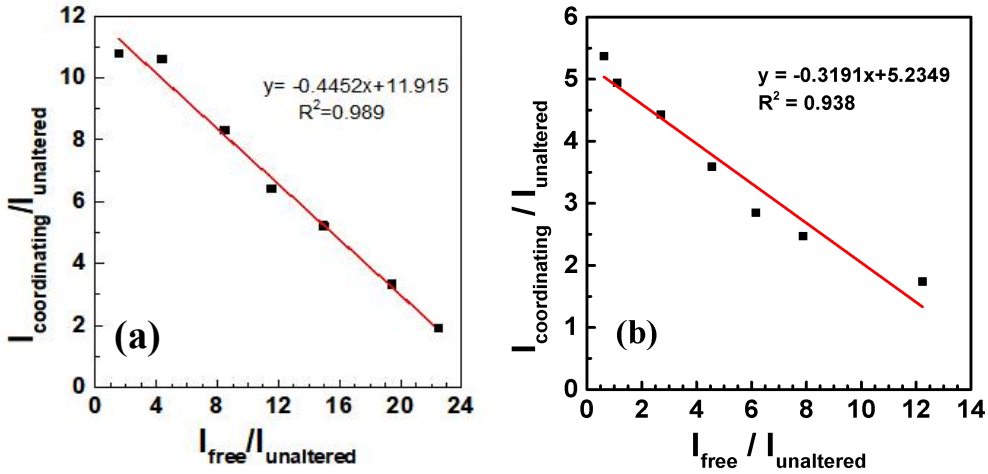


**Fig. S3-4.** $I_{coordinating}$ / $I_{unaltered}$ vs. $I_{free}$ / $I_{unaltered}$ polt of DMC molecules in (a)$LiBF_4$/DMC and (b) $LiPF_6$/DMC of different molar ratios.

# CHAPTER 4

# Dilution Effects of Highly Concentrated $LiBF_4$/DMC with Fluorinated Esters on Charge/Dishcharge Properties of Ni-rich $LiNi_{0.8}Co_{0.1}Mn_{0.1}O_2$ Positive Electrode

## 4.1 Introduction

Nickel-rich layered lithium transition metal oxides such as $LiNi_{0.8}Co_{0.1}Mn_{0.1}O_2$ (NCM811) are promising as positive electrode materials in advanced lithium ion batteries (LIBs), because they exhibit a higher specific capacity (close to 200 mAh $g^{-1}$) when charged to 4.3 V and higher vs $Li/Li^+$.[1-5] However, conventional 1 mol $dm^{-3}$ (M)-level electrolytes are not suitable for the Ni-rich layered metal oxide cathodes to be charged to 4.3 V and higher because of parasitic surface reactions (such as oxidative decomposition of the electrolyte solution). The side reactions lead to a structural degradation (such as crack formation) of the cathode particles, which results in poor cycle performance.[6,7] Several mitigation methods, such as electrolyte additives to form a stable cathode/electrolyte interphase (CEI)[8-11] and surface oxide coating[12-15], have been reported to suppress these side reactions. The use of highly concentrated

electrolytes is a simple method for improving the resistance of oxidative decomposition at high potentials that has been developed in recent years.[16-25] The highly concentrated electrolyte solutions have chemical windows wider than the conventional electrolytes. In the highly concentrated electrolytes, most of solvent molecules coordinate tightly to $Li^+$ ions and can reduce the fraction of free solvent molecules that are vulnerable to oxidation. In Chapter 2, NCM811 positive electrode exhibited that a much better cycling performance in a highly concentrated 8.67 mol $kg^{-1}$ $LiBF_4$/dimethylcarbonate (DMC) than 1 mol $dm^{-3}$ (M)-level conventional electrolytes when charged to 4.3 V.[26] In Chapter 3, in order to solve the problems of the highly concentrated $LiBF_4$/DMC electrolyte, that is, low ionic conductivity and high viscosity, we diluted it with hydrofluoroether (1,1,2,2‐tetrafluoroethyl 2,2,3,3‐tetrafluoropropyl ether, HFE), because HFE has good properties as a diluent, such as a high stability against oxidation and a low donor number (DN) that hinders the solvation of the diluent molecules to $Li^+$ ion.[27-29] Unfortunately, the cycling performance of NCM811 electrode decayed more quickly in the HFE-diluted electrolyte than the highly concentrated electrolyte in Chapter 3.[30] The reason was mainly because the presence of HFE suppressed the dissociation of $LiBF_4$, which is poorly dissociative, and thereby increased the fraction of free DMC in the diluted electrolyte. The results indicated that not only the choice of the diluents, but also lithium salt/diluent combination is an important factor for the dilution of concentrated electrolytes.

In Chapter 4, fluorinated esters were focused as diluents to dilute the highly concentrated $LiBF_4$/DMC electrolyte. Here we used methyl fluoropropionates of different numbers of F atoms: methyl 3,3,3-trifluoropropionate ($CF_3CH_2COOCH_3$, 3FMP), methyl tetrafluoropropionate ($CF_3CHFCOOCH_3$, 4FMP), and methyl perfluoropropionate ($CF_3CF_2COOCH_3$, 5FMP). Molecular structure of fluorinated esters were shown in the Figure 1. Highly electronegative fluorine atoms decrease the electron density of oxygen atoms of the ester group, so that not only the stability against oxidation, but also the coordinating strength of the O atoms can be adjusted by the number of F atoms. Charge/discharge characteristics of NCM811 positive electrode was investigated in highly concentrated $LiBF_4$/DMC diluted with these fluorinated esters. We found that 4FMP gave better cycling performance of NCM811 as a diluent than 3FMP and 5FMP. Raman spectroscopy was used to analyze the solution structure such as cation solvation and anion aggregation. The correlation between the charge/discharge characteristics and the solution structure was discussed in order to understand the important factors for diluents of highly concentrated electrolytes.

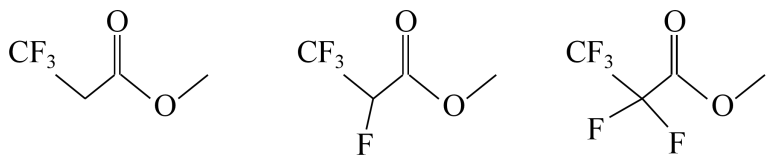


a. 3FMP b. 4FMP c. 5FMP

**Fig. 4-1.** Molecular structures of fluorinated esters: (a) methyl 3,3,3-trifluoropropionate (3FMP); (b) methyl tetrafluoropropionate (4FMP); (c) methyl perfluoropropionate (5FMP).

## 4.2 Experimental

### *4.2.1 Preparation of electrolyte solution*

$LiBF_4$ (Kishida Chemical), DMC (Kishida Chemical), 3FMP (Tokyo Chemical Industry), 4FMP, (MolPort), and 5FMP (Tokyo Chemical Industry) were of lithium battery grade and used without further purification. DMC and each diluent were mixed at 1:2 by volume, and $LiBF_4$ was added to the mixtures to obtain nearly saturated electrolytes: 1.0 mol $kg^{-1}$ $LiBF_4$/DMC+5FMP, 1.8 mol $kg^{-1}$ $LiBF_4$/DMC+4FMP and 3.3 mol $kg^{-1}$ $LiBF_4$/DMC+3FMP, in which the DMC/Li molar ratios were 3.0, 1.8, and 1.0, respectively. All electrolytes were prepared in an Ar filled glove box (DBO-1.5KP-DID, Miwa Mfg) with oxygen and water contents below 0.1 ppm.

### *4.2.2 Characterization of electrolyte solutions*

The viscosity of the electrolytes was measured with an Ubbelohde capillary viscometer at room temperature in an Ar-filled glove box (MDB-1NKP-DS, Miwa Mfg). The solution structure was studied with a Raman spectrometer (LabRAM HR Evolution, Horiba) equipped with a multichannel charge coupled device detector. The spectra were recorded using a 785-nm semiconductor laser (100 mW) through an objective lens.

The ionic conductivity was measured with an a.c. impedance analyzer (VersaSTAT 3, Princeton Applied Research) using a symmetrical cell consisting of two Pt plate electrodes. The stability of the electrolytes against oxidation was

evaluated on a Pt disk working electrode (10 mm in diameter) by linear sweep voltammetry (LSV) at a scan rate of 1 mV $s^{-1}$ between 3.0 and 5.0 V (vs. $Li/Li^+$) using a three-electrode cell with two Li foils as a reference and a counter electrode.

### *4.2.3 Preparation of NCM811 electrode*

A slurry consisting of 80 mass% $LiNi_{0.8}Co_{0.1}Mn_{0.1}O_2$ powder as an active material, 10 mass% graphitized Ketjenblack (FD-7001D, Lion Specialty Chemicals) as a conductor, 10 mass% poly[(vinylidenefluoride)-co-chorotrifluoroethylene] (P(VdF-CtFE)) as a binder and 1-methyl-2-pyrrolidone (NMP) as a solvent was cast onto an aluminum foil. The sheet was dried at 80°C for 18 h in a vacuum oven, and was punched into discs of 13 mm in diameter. The active material mass loading was 1.6-2.3 mg $cm^{-2}$ and the electrode thickness was 15-20 μm.

### *4.2.4 Charge and discharge tests*

The disc working electrode was used to assemble a two-electrode coin-type cell with a lithium foil (Honjo Metal, 15 mm in diameter) as a counter electrode. A glass filter (GF/D, Whatman®) was used as a separator and dipped in the electrolyte prior to assembling the coin-type cells in the Ar-filled glove box. Charge and discharge tests were performed between 3.0 V and 4.3 V vs $Li/Li^+$ at 30°C using a battery test system (TOSCAT-3100, Toyo system Co., Ltd.) at a C/10 rate unless otherwise noted. After charge and discharge tests, the cell was disassembled in the Ar-filled glove box. The NCM811 electrode was washed with pure DMC to remove residual solvent and Li salt,

and then dried overnight in the glove box. Surface morphology observation and elemental analysis of the NCM811 electrode were carried out with a scanning electron microscope (SEM) (SU8220, HITACHI Ltd.) equipped with an energy dispersive X-ray spectroscopy (EDX, XFlash5060FQ, Bruker).

## 4.3. Result and Discussion

### *4.3.1 Ionic conductivity and Raman spectroscopic analysis of the electrolytes*

The ionic conductivity data of the diluted electrolytes used in this study are summarized in Table 4-1. The ionic conductivity and viscosity of non-diluted, nearly saturated 8.67 mol $kg^{-1}$ $LiBF_4$/DMC were 0.75 mS $cm^{-1}$ and 226 mPa s, respectively.[26] The dilution with 3FMP, 4FMP, and 5FMP significantly lowered the viscosity (< 10 mPa s), which is acceptable for practical use. On the other hand, the effects on the conductivity were very minor. Of the three diluted electrolytes, 1.8 mol $kg^{-1}$ $LiBF_4$/DMC+4FMP (1:2) showed the highest ionic conductivity.

**Table 4-1.** Ionic conductivity and viscosity data of $LiBF_4$/DMC and diluted electrolytes.*

| Conc. (mol $kg^{-1}$) | Li salt | Solvent | Diluent | Volume ratio | Molar ratio (DMC/Li) | Ionic conductivity (mS $cm^{-1}$) | Viscoity (mPa s) |
|---|---|---|---|---|---|---|---|
| 8.67 | $LiBF_4$ | DMC | - | - | 1.28 | 0.75 | 226 |
| 1.0 | | | 5FMP | 1:2 | 3.0 | 0.44 | 1.86 |
| 1.8 | | | 4FMP | | 1.8 | 0.78 | 2.41 |
| 3.3 | | | 3FMP | | 1.0 | 0.72 | 5.62 |

*The concentration of $LiBF_4$ was nearly saturated in each electrolyte.

Raman spectra (890 - 960 $cm^{-1}$) of the three electrolytes are shown in Fig. 4-2,

together with those of the neat fluorinated esters. Free DMC showed only one peak at around 916 $cm^{-1}$ and the peak of DMC coordinated with Li ion appeared at around 933 $cm^{-1}$.[31] The fractions of solvating DMC in these electrolytes were estimated by peak fitting, and were 40.7 %, 63.1 % and 72.8 % in 1.0 mol $kg^{-1}$ $LiBF_4$/DMC+5FMP, 1.8 mol $kg^{-1}$ $LiBF_4$/DMC+4FMP and 3.3 mol $kg^{-1}$ $LiBF_4$/DMC+3FMP electrolytes, respectively. The fraction of solvating DMC in 1.0 mol $kg^{-1}$ $LiBF_4$/DMC+5FMP was significantly lower than those in the other two electrolytes, which is the reason for poor stability against oxidation discussed later

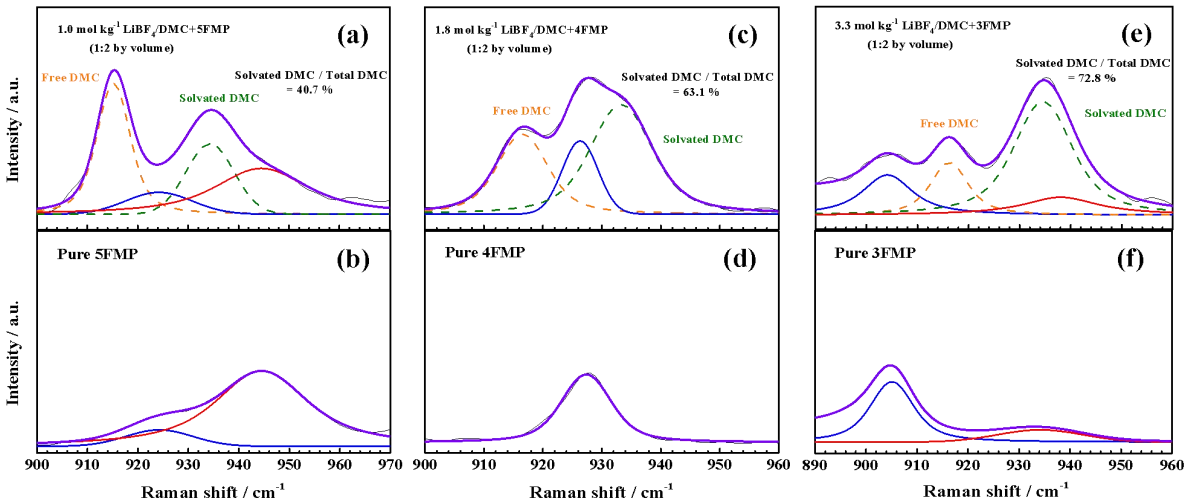


**Fig. 4-2.** Raman spectra of DMC in (a) 1.0 mol $kg^{-1}$ $LiBF_4$/DMC+5FMP (1:2 by volume), (c) 1.8 mol $kg^{-1}$ $LiBF_4$/DMC+4FMP (1:2 by volume) and (e) 3.3 mol $kg^{-1}$ $LiBF_4$/DMC+3FMP (1:2 by volume), and of neat (b) 5FMP, (d) 4FMP and (f) 3FMP diluent solvents.

Raman spectra (750-800 $cm^{-1}$) of anions in these electrolytes are shown in Fig. 4-3. Only two bands relating to the B-F symmetric vibration of $BF_4^-$ anion were observed at 773 and 781 $cm^{-1}$. These bands are assigned to the vibration modes of contact ion pairs (CIPs) and aggregates (AGGs), respectively.[32] Solvent-separated ion

pairs (SSIPs) was not be observed at 764 $cm^{-1}$ in these electrolytes,[32] suggesting that both DMC molecules and $BF_4^-$ anions coordinated to $Li^+$ ions in these electrolytes. The fraction of AGGs increased gradually with increasing the concentration of $LiBF_4$, and it was highest in 3.3 mol $kg^{-1}$ $LiBF_4$/DMC+3FMP, indicating that the interactions among $Li^+$ ions, $BF_4^-$ anions and DMC solvent molecules enhanced.

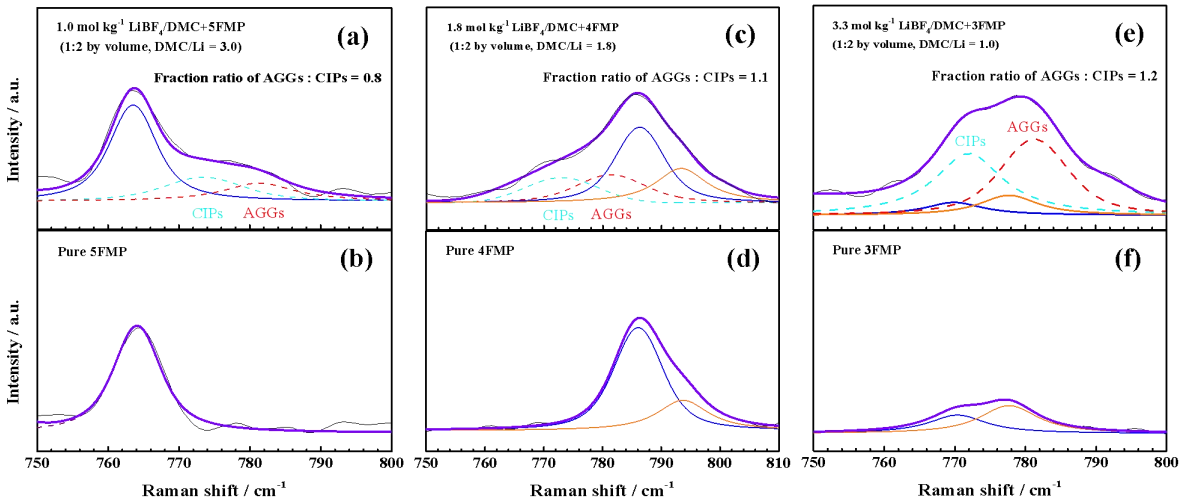


**Fig. 4-3.** Raman spectra of $BF_4^-$ anions in (a) 1.0 mol $kg^{-1}$ $LiBF_4$/DMC+5FMP (1:2 by volume), (c) 1.8 mol $kg^{-1}$ $LiBF_4$/DMC+4FMP (1:2 by volume) and (e) 3.3 mol $kg^{-1}$ $LiBF_4$/DMC+3FMP (1:2 by volume) and of neat (b) 5FMP, (d) 4FMP and (f) 3FMP diluent solvents.

### *4.3.2 Linear sweep voltammetry*

The anodic stability of 1.0 mol $kg^{-1}$ $LiBF_4$/DMC+5FMP, 1.8 mol $kg^{-1}$ $LiBF_4$/DMC+4FMP, and 3.3 mol $kg^{-1}$ $LiBF_4$/DMC+3FMP were investigated by LSV, and the results are shown in Fig. 4-4. The anodic stability of 1.8 mol $kg^{-1}$ $LiBF_4$/DMC+4FMP and 3.3 mol $kg^{-1}$ $LiBF_4$/DMC+3FMP exhibited better oxidation resistance than 1.0 mol $kg^{-1}$ $LiBF_4$/DMC+5FMP. The oxidation current in 1.0 mol $kg^{-1}$ $LiBF_4$/DMC+5FMP started to flow at around 3.9 V, whereas it started at around 4.0 V

in the other two electrolytes. At potentials higher than 4.2 V, the current increased significantly in 1.0 mol kg$^{-1}$ $LiBF_4$/DMC+5FMP; however, the increase in current was remarkably suppressed in the other two electrolytes. These results confirm that the decrease of free DMC by increasing of $LiBF_4$ concentration is effective for improving the anodic stability of the electrolytes. As shown in Fig. 4-2, 1.0 mol kg$^{-1}$ $LiBF_4$/DMC+5FMP showed a high fraction of free DMC (59.3%) than the other diluted electrolytes. This is because the electron density of the O atoms of the ester group decreases with the number of strongly electronegative F atoms, which decreases the coordination ability of the O atoms with $Li^+$ ions and resulted in the low solubility of $LiBF_4$ in DMC+5FMP.

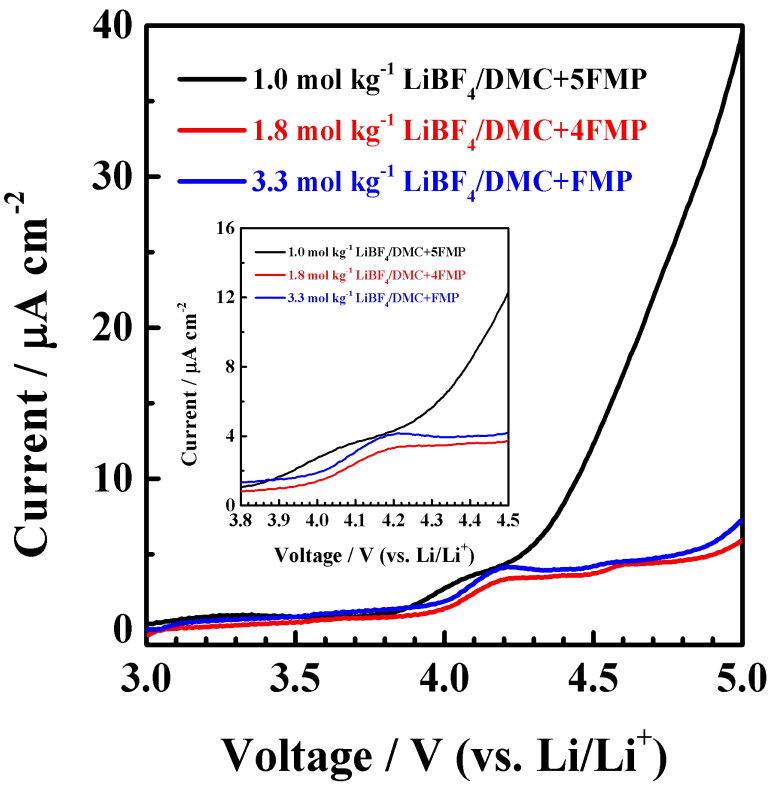


**Fig. 4-4.** Linear sweep voltammograms at Pt in 1.0 mol kg$^{-1}$ $LiBF_4$/DMC+5FMP (1:2 by volume), 1.8 mol kg$^{-1}$ $LiBF_4$/DMC+4FMP (1:2 by volume) and 3.3 mol kg$^{-1}$ $LiBF_4$/DMC+3FMP (1:2 by volume). Sweep rate: 1 mV s$^{-1}$.

Though the fraction of free DMC (36.9%) in 1.8 mol $kg^{-1}$ $LiBF_4$/DMC+4FMP was higher than that (27.2%) in 3.3 mol $kg^{-1}$ $LiBF_4$/DMC+3FMP, the former electrolyte showed a slightly higher stability against oxidation than the latter electrolyte. This may be mainly due to a lower anodic stability of 3FMP than 5FMP, which will be discussed later.

### *4.3.3 Charge and discharge characteristics*

Figure 4-5 shows the charge/discharge curves and the dQ $dV^{-1}$ profiles of NCM811|Li cells in 1.0 mol $kg^{-1}$ $LiBF_4$/DMC+5FMP, 1.8 mol $kg^{-1}$ $LiBF_4$/DMC+4FMP and 3.3 mol $kg^{-1}$ $LiBF_4$/DMC+3FMP. The initial charge and discharge capacities and coulombic efficiencies of NCM811 in these electrolytes are summarized in Table 4-2. The initial discharge capacity was close to 200 mAh $g^{-1}$ in each electrolyte, which is typical of NCM811 charged up to 4.3 V. The initial coulombic efficiency (90.3 %) in 1.8 mol $kg^{-1}$ $LiBF_4$/DMC+4FMP was slightly higher than 87.9 % and 89.5 % in 1.0 mol $kg^{-1}$ $LiBF_4$/DMC+5FMP and 3.3 mol $kg^{-1}$ $LiBF_4$/DMC+3FMP, respectively. The lower coulombic efficiency arose from the oxidative decomposition of the electrolyte. In addition, rapid capacity fading was observed in 1.0 mol $kg^{-1}$ $LiBF_4$/DMC+5FMP and 3.3 mol $kg^{-1}$ $LiBF_4$/DMC+3FMP accompanied by an increase in polarization on cycling, which implies that the electrolyte decomposition deteriorated the NCM811 particles as discussed later.

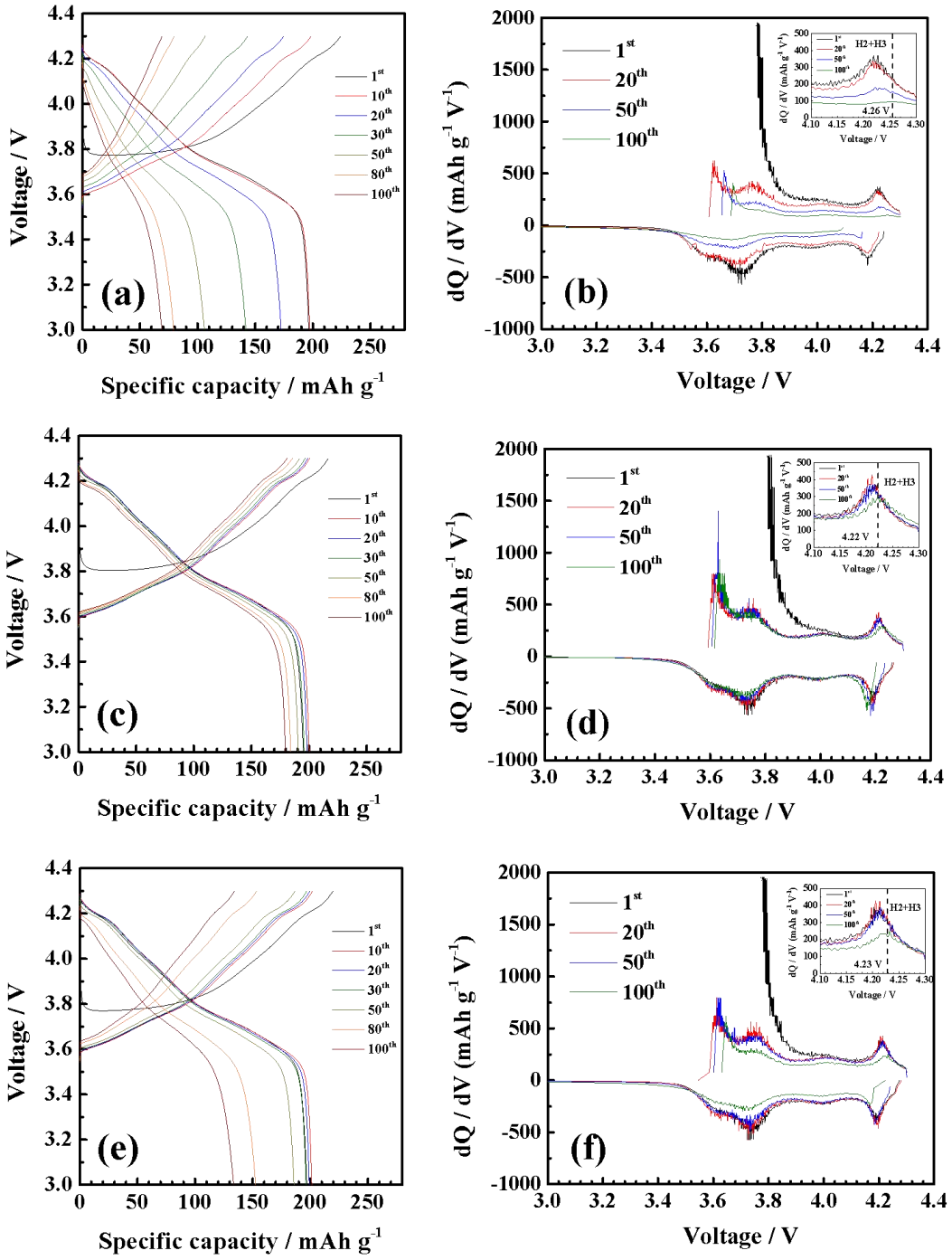


**Fig. 4-5.** Charge/discharge curves (a, c, e) and differential capacity curves (dQ $dV^{-1}$) profiles (b, d, f) of $LiNi_{0.8}Co_{0.1}Mn_{0.1}O_2$ in (a, b) 1.0 mol $kg^{-1}$ $LiBF_4$/DMC+5FMP (1:2 by volume), (c, d) 1.8 mol $kg^{-1}$ $LiBF_4$/DMC+4FMP (1:2 by volume) and (e, f) 3.3 mol $kg^{-1}$ $LiBF_4$/DMC+3FMP (1:2 by volume) at C/10.

**Table 4-2.** Initial charge/discharge performance of NCM811|Li cells using 1.0 mol $kg^{-1}$ $LiBF_4$/DMC+5FMP (1:2 by volume), 1.8 mol $kg^{-1}$ $LiBF_4$/DMC+4FMP (1:2 by volume) and 3.3 mol $kg^{-1}$ $LiBF_4$/DMC+3FMP (1:2 by volume).

| Conc. (mol $kg^{-1}$) | Electrolyte | Charge capacity (m Ah $g^{-1}$) | Dicharge capacity (m Ah $g^{-1}$) | Irreversible capactiy (m Ah $g^{-1}$) | Coulombic efficiency (%) |
|---|---|---|---|---|---|
| 1.0 | $LiBF_4$/DMC+5FMP | 224 | 197 | 27 | 87.9 |
| 1.8 | $LiBF_4$/DMC+4FMP | 216 | 195 | 21 | 90.3 |
| 3.3 | $LiBF_4$/DMC+3FMP | 220 | 197 | 23 | 89.5 |

On the dQ $dV^{-1}$ profiles, in addition to the main redox peaks at around 3.7 V, a couple of redox peaks are seen at around 4.2 V, the latter of which are assigned to the structural transformation from the H2 to the H3 phase. It has been reported that the H2/H3 phase transformation mostly affects the capacity fading of NCM811 cathodes because it is accompanied by a large volume change.[33-36] The variation of the H2/H3 peak is informative on what happened during cycling. In 1.0 mol $kg^{-1}$ $LiBF_4$/DMC+5FMP (Fig. 4-5(d)), the intensity of the oxidation peak (on charging) dropped rapidly on cycling, while the peak was shifted up to 4.26 V at the $100^{th}$ cycle, indicating that the deterioration of NCM811 particles was very serious. In 3.3 mol $kg^{-1}$ $LiBF_4$/DMC+3FMP (Fig. 4-5(f)), the drop of the peak intensity did not change up to the $50^{th}$ cycle; however, it decreased remarkably at the $100^{th}$ cycle. In addition, the oxidation peak was shifted up to 4.23 V after 100 cycles. In 1.8 mol $kg^{-1}$ $LiBF_4$/DMC+4FMP (Fig. 4-5(e)), the peak intensity did not appreciably change up to the $100^{th}$ cycle, and the peak shift was the smallest (4.22 V at the $100^{th}$ cycle). These

results imply that the deterioration of NCM811 particles by crack formation and the resulting particle fracture were eased in 1.8 mol kg$^{-1}$ $LiBF_4$/DMC+4FMP.

Figure 4-6 shows the variations of discharge capacity and coulombic efficiency of NCM811|Li cells for 100 cycles. In the initial 20 cycles, high capacities of ca. 200 mAh g$^{-1}$ were obtained in each electrolyte. In 1.0 mol kg$^{-1}$ $LiBF_4$/DMC+5FMP, however, the capacity significantly decreased after the 10$^{th}$ cycle, and dropped to 34.7 % of the initial capacity at the 100$^{th}$ cycle. In 3.3 mol kg$^{-1}$ $LiBF_4$/DMC+3FMP, the capacity was stable up to the 40$^{th}$ cycle, but after that it decreased gradually to 66.2 % at the 100$^{th}$ cycle. In contrast, good capacity retention was obtained in 1.8 mol kg$^{-1}$ $LiBF_4$/DMC+4FMP up to the 100$^{th}$ cycle (90.1%). The average coulombic efficiency for 100 cycles in 1.8 mol kg$^{-1}$ $LiBF_4$/DMC+4FMP (99.5 %) was also higher than those in 1.0 mol kg$^{-1}$ $LiBF_4$/DMC+5FMP (99.2 %) and 3.3 mol kg$^{-1}$ $LiBF_4$/DMC+3FMP (99.4 %). These results indicated that oxidative decomposition of electrolyte was suppressed in 1.8 mol kg$^{-1}$ $LiBF_4$/DMC+4FMP.

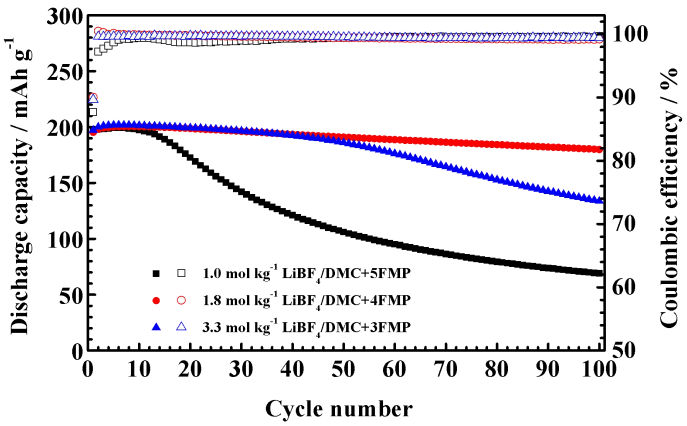


**Fig. 4-6.** Variations of discharge capacity and coulombic efficiency of $LiNi_{0.8}Co_{0.1}Mn_{0.1}O_2$ cathode cycled in 1.0 mol kg$^{-1}$ $LiBF_4$/DMC+5FMP (1:2 by volume), 1.8 mol kg$^{-1}$ $LiBF_4$/DMC+4FMP (1:2 by volume) and 3.3 mol kg$^{-1}$ $LiBF_4$/DMC+3FMP (1:2 by volume).

The rate performance of NCM811|Li cells using various electrolytes are shown in Fig. 4-7. 1.0 mol kg$^{-1}$ $LiBF_4$/DMC+5FMP exhibited the worst rate-capability in these electrolytes and the discharge capacity at 2 C was only 63 mAh g$^{-1}$. This is partly because 5FMP suppressed the dissociation of $LiBF_4$ salt, which resulted in a low ionic conductivity (0.44 mS cm$^{-1}$) as shown in Table 4-1. In addition, the thick CEI formation, which will be discussed later, may be another reason for the poor rate-capability in 1.0 mol kg$^{-1}$ $LiBF_4$/DMC+5FMP. On the other hand, both 1.8 mol kg$^{-1}$ $LiBF_4$/DMC+4FMP and 3.3 mol kg$^{-1}$ $LiBF_4$/DMC+3FMP gave higher rate performance than $LiBF_4$/DMC+5FMP. At low rates, the NCM811 positive electrode in $LiBF_4$/DMC+4FMP exhibited slightly higher discharge capacities than that in $LiBF_4$/DMC+3FMP. However, both electrolytes gave similarly high discharge capacity of 156 mAh g$^{-1}$ at 2 C. Though the ionic conductivity of $LiBF_4$/DMC+3FMP (0.72 mS cm$^{-1}$) was a little lower than $LiBF_4$/DMC+4FMP (0.78 mS cm$^{-1}$), the higher concentration of $Li^+$ ions in 3.3 mol kg$^{-1}$ $LiBF_4$/DMC+3FMP contributed to an improved charge-transfer kinetics.

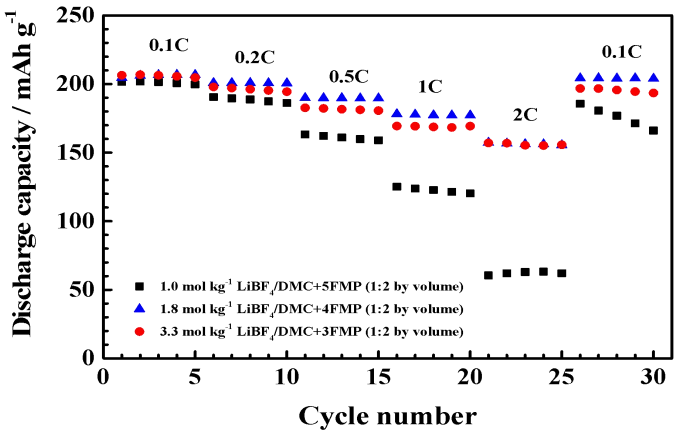


**Fig. 4-7.** Rate-capability of $LiNi_{0.8}Co_{0.1}Mn_{0.1}O_2$ cathode in 1.0 mol kg$^{-1}$ $LiBF_4$/DMC+5FMP (1:2 by volume), 1.8 mol kg$^{-1}$ $LiBF_4$/DMC+4FMP (1:2 by volume) and 3.3 mol kg$^{-1}$ $LiBF_4$/DMC+3FMP (1:2 by volume).

### *4.3.4 SEM images and EDX F-mapping profiles after cycled*

Figure 4-8 shows SEM images and EDX F-mapping profiles of the surface of NCM811 positive electrodes before cycling and after 100 cycles in the three electrolytes. The contents of B, C, O and F elements on the particle surface estimated by EDX mapping are shown in Table 4-3. The NCM811 particles (average diameter: 10 μm) consisted of smaller primary particles of several hundred nm. The surface of the secondary particle was dense and cracks were not observed before cycling (Fig. 4-8(a)). After 100 cycles, many cracks were formed on the NCM811 particles cycled in $LiBF_4$/DMC+5FMP (Fig. 4-8(c)) and $LiBF_4$/DMC+3FMP (Fig. 4-8(g)). However, crack formation in $LiBF_4$/DMC+4FMP after 100 cycles (Fig. 4-8(e)) were much less remarkable than those cycled in the other two electrolytes.

EDX F-mapping profiles revealed that the content of F element on the NCM811 particles after 100 cycles increased in the order of $LiBF_4$/DMC+5FMP, $LiBF_4$/DMC+4FMP, and $LiBF_4$/DMC+3FMP. It is reasonable to think that the F element came from decomposition products of the diluents because the content of boron did not change appreciably in Table 4-3. The number of electron-withdrawing fluorine atoms decreases in the order of 5FMP, 4FMP and 3FMP, and hence 3FMP is the most vulnerable to oxidative decomposition. Therefore 3FMP easily decomposed during cycling not only on the particle surface, but also within the cracks formed inside the NCM811 particles as discussed in previous studies.[26] This accelerated crack formation as shown in Fig. 4-8(g), and resulted in the serious capacity fading after the $40^{th}$ cycle in Fig. 4-6. Though the effects of $BF_4^-$ anion decomposition may not be

minor in this study, the content of B element slightly decreased in the order of $LiBF_4$/DMC+5FMP, $LiBF_4$/DMC+4FMP and $LiBF_4$/DMC+3FMP in Table 4-3. It is known that AGGs have higher stability against oxidation than CIPs and SSIPs.[25,26] Hence these results agree with the order of the fraction of AGGs in Fig. 4-3.

**Table 4-3.** The content of different elements on the surface of NCM811 electrode cycled in different electrolytes after 100 cycles.

| Electrolyte solution | Element content (wt %) | | | |
|---|---|---|---|---|
| | B | C | O | F |
| 1.0 mol $kg^{-1}$ $LiBF_4$/DMC+5FMP | 2.93 | 5.31 | 70.81 | 20.95 |
| 1.8 mol $kg^{-1}$ $LiBF_4$/DMC+4FMP | 2.76 | 5.78 | 68.96 | 22.46 |
| 3.3 mol $kg^{-1}$ $LiBF_4$/DMC+3FMP | 2.49 | 4.84 | 65.28 | 27.38 |

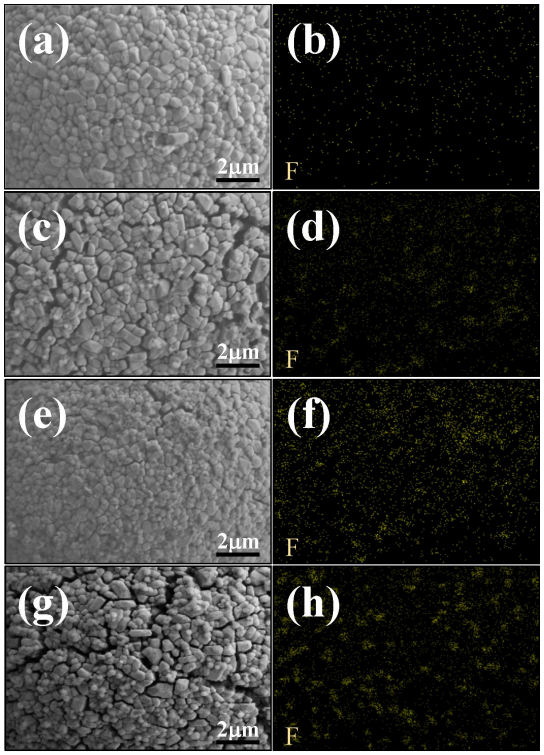


**Fig. 4-8.** SEM images (a, c, e, g) and EDX F-mapping profiles (b, d, f, h) of the surface of NCM811 positive electrodes before cycling (a, b) and after 100 cycles in (c, d)1.0 mol $kg^{-1}$ $LiBF_4$/DMC+5FMP, (e, f) 1.8 mol $kg^{-1}$ $LiBF_4$/DMC+4FMP and (g, h) 3.3 mol $kg^{-1}$ $LiBF_4$/DMC+3FMP.

5FMP has the highest anodic stability because of the highest number of F atoms and actually the content of F element on the particle surface was the lowest after cycled in $LiBF_4$/DMC+5FMP in Fig. 4-8. However, the miscibility with concentrated $LiBF_4$/DMC electrolyte was low, and the solubility (saturated concentration) in $LiBF_4$/DMC+5FMP was lower (ca. 1.0 mol $kg^{-1}$, DMC/Li = 3.0) than the other two electrolytes. Hence the fraction of free DMC, which is vulnerable to oxidation, in $LiBF_4$/DMC+5FMP was the highest as shown in Fig. 4-2. This is very similar to the case of the HFE diluent reported previously.[30] Free DMC easily decomposed and accumulated during cycling on the particle surface and in the cracks within the particles, which is the main reason for the poor capacity retention in $LiBF_4$/DMC+5FMP. Because free DMC in $LiBF_4$/DMC+5FMP was much more vulnerable to oxidation than 3FMP as shown by LSVs in Fig. 4-4, the capacity started to drop much earlier (after the $10^{th}$ cycle) than in $LiBF_4$/DMC+3FMP in Fig. 4-6. 4FMP has a higher miscibility with concentrated $LiBF_4$/DMC than 5FMP, and the number of fluorine atoms is higher than 3FMP. The former property suppressed the oxidative decomposition of DMC, and the latter property enhanced the stability of 4FMP against oxidation. These factors cooperatively contributed to the good capacity retention $LiBF_4$/DMC+4FMP of in Fig. 4-6 and less crack formation in Fig. 4-8.

## 4.4 Conclusions

In Chapter 4, dilution effect of highly concentrated $LiBF_4$/DMC electrolyte with three kinds of methyl fluoropropionates (5FMP, 4FMP and 3FMP) with different F atoms on the charge/discharge characteristics of NCM811 positive electrode was investigated. All the electrolytes had low viscosities lower than 10 mPa s, which are affordable for practical use. The nearly saturated 1.8 mol $kg^{-1}$ $LiBF_4$/DMC+4FMP exhibited good cycling performance, whereas severe capacity fading was observed for 1.0 mol $kg^{-1}$ $LiBF_4$/DMC+5FMP and 3.3 mol $kg^{-1}$ $LiBF_4$/DMC+3FMP, though the latter two were also nearly saturated. In the case of $LiBF_4$/DMC+5FMP, a large amount of free DMC molecules, which are vulnerable to oxidation, were formed by the dilution with 5FMP. In the case of $LiBF_4$/DMC+3FMP, the diluent 3FMP molecules are not stable against oxidation because the number of electron-withdrawing F atoms of 3FMP is smaller than those of the other two diluents. The miscibility of 4FMP with concentrated $LiBF_4$/DMC is higher than 5FMP, and hence the resulting higher concentration (1.8 mol $kg^{-1}$, DMC/Li = 1.8) suppressed the formation of free DMC molecules. On the other hand, the oxidation resistance of 4FMP is higher than 3FMP, suppressing the deterioration of NCM811 electrode due to the oxidative decomposition of 4FMP. As a compromise, $LiBF_4$/DMC+4FMP showed the best performance. It is concluded that the compatibility of a good miscibility and a high anodic stability is important for exploring good diluents for highly concentrated $LiBF_4$/DMC.

**References**

[1] Y. Ding, R. Wang, L. Wang, K. Cheng, Z. Zhao, D. Mu, and B. Wu, "A short review on layered $LiNi_{0.8}Co_{0.1}Mn_{0.1}O_2$ positive electrode material for lithium-ion batteries." *Energy Procedia*, **105**, A2941 (2017).

[2] J.-H. EoM, M.-G. Kim, and J. Cho. "Storage characteristics of $LiNi_{0.8}Co_{0.1+x}Mn_{0.1-x}O_2$ (x=0, 0.03, and 0.06) cathode materials for lithium batteries." *J. Electrochem Soc.*, **155**, A239 (2008).

[3] M.-H. Kim, H.-S. Shin, D. Shin, and Y.-K. Sun, "Synthesis and electrochemical properties of $LiNi_{0.8}Co_{0.1}Mn_{0.1}O_2$ and $LiNi_{0.8}Co_{0.2}O_2$ via co-precipitation." *J. Power Sources*, **159**, A1328 (2006).

[4] C. S. Yoon, K.-J. Park, U.-H. Kim, K. H. Kang, H.-H. Ryu, and Y.-K. Sun, "High-Energy Ni-Rich $Li[Ni_xCo_yMn_{1-x-y}]O_2$ Cathodes via Compositional Partitioning for Next-Generation Electric Vehicles." *Chem. Mater.*, **29**, A10436 (2017).

[5] D.-L. Vua, J.-Y. Choia, W.-B. Kima, J. Leeb, and J.-W. Lee, "Layered $LiNi_{0.8}Co_{0.1}Mn_{0.1}O_2$ Prepared through Calcination in Air with Preoxidized Precursor." *J. Electrochem Soc.*, **164**, A2670 (2017).

[6] S. Wang, J. Liu, X. Yu, J. Liu, J. Rong, C. Zhu, Q. Wang, Z. Yuan, and Y. Zhang "Electrochemical Behavior of 3,4-ethylenedioxythiophene as an Anti-overcharge Additive for Lithium-ion Batteries." *Int. J. Electrochem. Sci.*, **14,** A9527 (2019).

[7] J. Laveda, J. Low, F. Pagani, E. Stilp, S. Dilger, V. Baran, M. Heere, and C. Battaglia, "Stabilizing Capacity Retention in NMC811/Graphite Full Cells via TMSPi Electrolyte Additives." *Appl. Energy Mater.*, **2**, A7036 (2019).

[8] Y. K. Han, J. Yoo, and T. Yim, "Why is tris(trimethylsilyl) phosphite effective as an additive for high-voltage lithium-ion batteries?" *J. Mater. Chem. A*, **3**, A10900 (2015).

[9] C. Peebles, R. Sahore, J. A. Gilbert, J. C. Garcia, A. Tornheim, J. Bareno, H. Iddir, C. Liao, and D. P. Abraham, "Tris(trimethylsilyl) Phosphite (TMSPi) and Triethyl Phosphite (TEPi) as Electrolyte Additives for Lithium Ion Batteries: Mechanistic Insights into Differences during $LiNi_{0.5}Mn_{0.3}Co_{0.2}O_2$-Graphite Full Cell Cycling." *J. Electrochem. Soc.*, **164,** A1579 (2017).

[10] W. D. Qiu, J. Xia, L. P. Chen, and J. R. Dahn, "A study of methyl phenyl carbonate and diphenyl carbonate as electrolyte additives for high voltage $LiNi_{0.8}Mn_{0.1}Co_{0.1}O_2$/graphite pouch cells." *J. Power Sources*, **318**, A228 (2016).

[11] D. Y. Wang, J. Xia, L. Ma, K. J. Nelson, J. E. Harlow, D. J. Xiong, L. E. Downie, R. Petibon, J. C. Burns, A. Xiao, W. M. Lamanna, and J. R. Dahn, "A Systematic Study of Electrolyte Additives in $Li[Ni_{1/3}Mn_{1/3}Co_{1/3}]O_2$ (NMC)/Graphite Pouch Cells." *J. Electrochem. Soc.,* **161**, A1818 (2014).

[12] B. Zhang, P. Dong, H. Tong, Y. Yao, J. Zheng, W. Yu, J. Zhang, and D. Chu, "Enhanced electrochemical performance of $LiNi_{0.8}Co_{0.1}Mn_{0.1}O_2$ with lithium-reactive $Li_3VO_4$ coating." *J. Alloys Compd.*, **706**, A198 (2017)

[13] X. Xiong, Z. Wang, G. Yan, H. Guo, and X. Li, "Role of $V_2O_5$ coating on $LiNiO_2$-based materials for lithium ion battery." *J. Power Sources*, **245**, A183 (2014).

[14] W. Cho, S. M. Kim, J. H. Song, T. Yim, S. G. Woo, K. W. Lee, J. S. Kim, and Y. J. Kim, "Improved electrochemical and thermal properties of nickel rich

$LiNi_{0.6}Co_{0.2}Mn_{0.2}O_2$ cathode materials by $SiO_2$ coating." *J. Power Sources*, **282**, A45 (2015).

[15] Y. Xu, Y. Liu, Z. Lu, H. Wang, D. Sun, and G. Yang, "The preparation and role of $Li_2ZrO_3$ surface coating $LiNi_{0.5}Co_{0.2}Mn_{0.3}O_2$ as cathode for lithium-ion batteries." *Appl. Surf. Sci.*, **361**, A150 (2016).

[16] K. Yoshida, M. Nakamura, Y. Kazue, N. tachikawa, S. Tsuzuki, S. Seki, K. Dokko, and M. Watanabe, "Oxidative-stability enhancement and charge transport mechanism in glyme-lithium salt equimolar complexes." *J. Am. Chem. Soc.*, **133**, A13121 (2011).

[17] X. Ren et al., "High-Concentration Ether Electrolytes for stable High-Voltage Lithium Metal Batteries." *ACS Energy letters*, **4**, 896 (2019).

[18] D. W. McOwen, D. M. Seo, O. Borodin, J. Vatamanu, P. D. Boyled, and W. A. Henderson, "Concentrated electrolyte: decrypting electrolyte properties and reassessing Al corrosion mechanisms." *Energy Environ. Sci.*, **7**, A416 (2014).

[19] R. Petibon, C. P. Aiken, L. Ma, D. Xiong, and J. R. Dahn, "The use of ethyl acetate as a sole solvent in highly concentrated electrolyte for Li-ion batteries." *Electrochem. Acta*, **154**, A287 (2015).

[20] J. Wang, Y. Yamada, K. Sodeyama, E. Watanabe, K. Takada, Y. Tateyama, and A. Yamada, "Fire-extinguishing organic electrolytes for safe batteries." *Nature Energy*, **3**, A22 (2018).

[21] T. Doi, Y. Shimizu, M. Hashinokuchi, and M. Inaba, "$LiBF_4$-Based concentrated electrolyte solutions for suppression of electrolyte decomposition and rapid

lithium-ion transfer at $LiNi_{0.5}Mn_{1.5}O_4$/electrolyte interface." *J. Electrochem Soc.*, **163**, A2211 (2016).

[22] T. Doi, M. Hahsinokuchi, and M. Inaba, "Solvation-controlled ester-based concentrated electrolyte solutions for high-voltage lithium-ion batteries." *Current Option in Electrochem.*, **9**, A49 (2018).

[23] T. Doi, Y. Shimizu, M. Hashinokuchi, and M. Inaba, "Low-Viscosity γ-Butyrolactone-Based Concentrated Electrolyte Solutions for $LiNi_{0.5}Mn_{1.5}O_4$ Positive Electrodes in Lithium-Ion Batteries." *Chem Electro Chem.*, **4**, A2398 (2017).

[24] T. Doi, R. Masuhara, M. Hashinokuchi, Y. Shimizu, and M. Inaba, "Concentrated $LiPF_6$/PC electrolyte solutions for 5-V $LiNi_{0.5}Mn_{1.5}O_4$ positive electrode in lithium-ion batteries." *Electrochim. Acta.*, **209**, A219 (2016).

[25] J. Wang, Y. Yamada, K. Sodeyama, C. H. Chiang, Y. Tateyama, and A. Yamada, "Superconcentrated electrolytes for a high-voltage lithium-ion battery." *Nature Commun.*, **7**, A12032 (2016).

[26] Z. Cao, M. Hashinokuchi, T. Doi, And M. Inaba, "Improved cycle performance of $LiNi_{0.8}Co_{0.1}Mn_{0.1}O_2$ positive electrode material in highly concentrated $LiBF_4$/DMC." *J. Electrochem Soc.,* **166**, A82 (2019).

[27] T. Doi, Y. Shimizu, M. Hashinokuchi, and M. Inaba, "Dilution of highly concentrated libf4/propylene carbonate electrolyte solution with fluoroalkyl ethers for 5-V $LiNi_{0.5}Mn_{1.5}O_4$ positive electrodes." *J. Electrochem Soc.*, **164**, A6412 (2017).

[28] T. Doi, R. Matsumoto, Z. Cao, M. Hashinokuchi, and M. Inaba, "Fluoroalkyl ether-diluted dimethyl carbonate-based electrolyte solutions for high-voltage

operation of $LiNi_{0.5}Co_{0.2}Mn_{0.3}O_2$ electrodes in lithium ion batteries." *Sustainable Energy Fuels*, **2**, A1197 (2018).

[29] K. Dokko, N. Tachikawa, K. Yamauchi, M. Tsuchiya, A. Yamazaki, E. Takashima, J.-W. Park, K. Ueno, S. Seki, N. Serizawa, and M. Watanabe, "Solvate Ionic Liquid Electrolyte for Li-S Batteries." *J. Electrochem. Soc.*, **160**, A1304 (2013).

[30] Z. Cao, M. Hashinokuchi, T. Doi. And M. Inaba, "Dilution Effects of Highly Concentrated Dimethyl Carbonate-based Electrolytes with a Hydrofluoroether on Charge/Discharge Properties of $LiNi_{0.8}Co_{0.1}Mn_{0.1}O_2$ Positive Electrode." *J. Electrochem. Soc.*, **166**, A4005 (2019).

[31] N. Chapman, O. Borodim, T. Yoon, C. C. Nguyen, B. and L. Lucht, "Spectroscopic and Density Functional Theory Characterization of Common Lithium Salt Solvates in Carbonate Electrolytes for Lithium Batteries." *J. Phys. Chem. C*, **121**, A2135 (2017).

[32] D. M. Seo, O. Borodin, S.-D Han, Q, Ly, P. D. Boyle, and W. A. Henderson, "Electrolyte Solvation and Ionic Association." *J. Electrochem Soc.*, **159**, A553 (2012).

[33] W. Li, J.N. Reimers, and J. R. Dahn, "In situ x-ray diffraction and electrochemical studies of $Li_{1-x}NiO_2$, *Solid State Ionics."* **67**, A123 (1993).

[34] W. Zhu, X. Huang, T. Liu, Z. Xie, Y. Wang, K. Tian, L. Bu, H. Wang, L. Gao, and J. Zhao, "Ultrathin $Al_2O_3$ Coating on $LiNi_{0.8}Co_{0.1}Mn_{0.1}O_2$ Cathode Material for Enhanced Cycleability at Extended Voltage Ranges." *Coatings*, **9**, 92 (2019).

[35] R. Jung, M. Metzger, F. Maglia, C. Stinner, and H. A. Gasteiger, "Oxygen Release and Its Effect on the Cycling Stability of $LiNi_xMn_yCo_zO_2$ (NMC) Cathode

Materials for Li-Ion Batteries." *J. Electrochem. Soc.*, **164**, A1361 (2017).

[36] Y. Liu, W. Yao, C. Lei, Q. Zhang, S. Zhong, and Z. Yan, "Ni-Rich Oxide $LiNi_{0.85}Co_{0.05}Mn_{0.1}O_2$ for Lithium Ion Battery: Effect of Microwave Radiation on Its Morphology and Electrochemical Property." *J. Electrochem. Soc.*, **166**, A1300 (2019).

# CHAPTER 5
# General Conclusions and Publication List

## 5.1 General Conclusions

In this thesis, the author focused on highly concentrated electrolytes and their diluted electrolytes with fluorinated solvents to improve the cycling performance of a Ni-rich ternary $LiNi_{0.8}Co_{0.1}Mn_{0.1}O_2$ (NCM811) positive electrode for practical application. Dilution effects of the concentrated electrolytes on the charge/discharge properties of NCM811 were discussed in detail from the viewpoint of the solvation structure of the electrolyte. The results obtained in this thesis will be important keys for the development of new electrolyte systems for high energy lithium ion batteries in the near future. The main achievements in this thesis are summarized as follows:

In Chapter 2, the effects of the concentration of lithium tetrafluroborate ($LiBF_4$)/dimethylcarbonate (DMC) electrolytes on the charge/discharge characteristics of nickel-rich $LiNi_{0.8}Co_{0.1}Mn_{0.1}O_2$ positive electrode were investigated. NCM811

exhibited better cycling performance in the nearly saturated (8.67 mol $kg^{-1}$) $LiBF_4$/DMC electrolyte than 0.93 (ca. 1 M) and 2.22 mol $kg^{-1}$ electrolytes. Raman spectra indicated that free DMC gradually decreased, while the solvated DMC increased with increasing the concentration of $LiBF_4$. $BF_4^-$ anions were likely to form aggregates (AGGs) with $Li^+$ ions and DMC in the highly concentrated electrolyte. These results suggested the interactions between DMC, $Li^+$ and $BF_4^-$ were so strong that the AGGs can hardly be oxidized. The study of linear sweep voltammetry (LSV) proved that the anodic stability of electrolyte increased with increasing the concentration of $LiBF_4$. Furthermore, cross-sectional SEM images and EDX mapping profiles revealed that the highly concentrated electrolyte effectively suppressed not only oxidative decomposition of the electrolyte on the particle surface, but also the particle fracture caused by crack propagation within the particles.

In Chapter 3, in order to decrease the high viscosity of highly concentrated electrolytes, hydrofluoroether (1,1,2,2-tetrafluoroethyl 2,2,3,3-tetrafluoropropyl ether (HFE) was used as a diluent. Dilution effects of highly concentrated $LiBF_4$/DMC and $LiPF_6$/DMC with HFE on cycling performance of NCM811 positive electrode material were investigated. The cycle performance of NCM811 remarkably was deteriorated in 0.96 mol $kg^{-1}$ $LiBF_4$/DMC+HFE electrolyte comparing to that in highly concentrated $LiBF_4$/DMC electrolyte. Raman spectra indicated that the fraction of free DMC increased in the diluted electrolyte, which led to instability against oxidation. In contrast, the fraction of free DMC had rarely increased after diluted with

HFE in the $LiPF_6$/DMC system. Due to the highly dissociative character of $LiPF_6$, the dilution with HFE hardly changed the fraction of solvating DMC. 0.96 mol $kg^{-1}$ $LiPF_6$/DMC+HFE electrolyte showed a high stability against oxidation comparable to the nearly saturated $LiPF_6$/DMC electrolyte, and NCM811 showed an excellent cycle performance in the diluted electrolyte. These results indicated that not only the choice of the diluents, but also lithium salt/diluent combination is an important factor for the dilution of concentrated electrolytes.

In Chapter 4, methyl 3,3,3-trifluoropropionate ($CF_3CH_2COOCH_3$, 3FMP), methyl tetrafluoropropionate ($CF_3CHFCOOCH_3$, 4FMP), and methyl perfluoropropionate ($CF_3CF_2COOCH_3$, 5FMP) were used as diluents to decrease the viscosity of highly concentrated $LiBF_4$/DMC electrolyte. The cycling performance of NCM811 positive electrode in these diluted electrolytes was investigated. In the nearly saturated 1.8 mol $kg^{-1}$ $LiBF_4$/DMC+4FMP, NCM811 exhibited good cycling performance compared to 1.0 mol $kg^{-1}$ $LiBF_4$/DMC+5FMP and 3.3 mol $kg^{-1}$ $LiBF_4$/DMC+3FMP. Due to a lower miscibility of 5FMP with concentrated $LiBF_4$/DMC than that of 4FMP, a larger amount of free DMC molecules in $LiBF_4$/DMC+5FMP were observed in Raman spectra. The oxidative decomposition of free DMC in the $LiBF_4$/DMC+5FMP caused a rapid drop in the capacity of NCM811 positive electrode. On the other hand, Raman spectra indicated that more solvated DMC molecules existed in $LiBF_4$/DMC+3FMP than $LiBF_4$/DMC+4FMP; however, the capacity fading of NCM811 was faster in $LiBF_4$/DMC+3FMP electrolyte. This is because 3FMP is less stable against oxidation

than the other two diluents, the oxidative decomposition of 3FMP on the surface of NCM811 particle led to the deterioration of NCM811 positive electrode during cycling. As a compromise, $LiBF_4$/DMC+4FMP showed the best cycling performance. It was concluded that the compatibility of a good miscibility and a high anodic stability is important for exploring good diluents for highly concentrated $LiBF_4$/DMC.

In this thesis, the author clarified the change in the physical-chemical property of $LiBF_4$/DMC electrolyte with increasing the concentration and successfully improved the cycling performance of NCM811 positive electrode in highly concentrated $LiBF_4$/DMC electrolyte. In order to reduce the viscosity, the author chose fluorinated solvents to dilute the highly concentrated $LiBF_4$/DMC electrolyte and successfully reduced the viscosity of electrolyte to below 10 mPa s, which is applicable for practical cells. By analyzing the dilution effects of highly concentrated electrolyte with fluorinated solvents on the charge-discharge characteristics of NCM811 positive electrode, the author found that a good miscibility and a high anodic stability of the diluent are important for maintaining the solvation structure of electrolyte, while keeping high stability against oxidation comparable to the highly concentrated electrolyte. Unfortunately, the ionic conductivity of the diluted electrolytes did not increase remarkably though the viscosity of electrolytes decreased to a practical level. For realizing rapid charging-discharging properties of lithium ion batteries for automotive use, it is necessary to explore other diluents that can improve the ionic conductivity of the diluted electrolytes in the future research.

## 5.2 Publication List

Chapter 2

"Improved cycle performance of $LiNi_{0.8}Co_{0.1}Mn_{0.1}O_2$ positive electrode material in highly concentrated $LiBF_4$/DMC."

Ziyang Cao, Z Michihiro Hashinokuchi, Takayuki Doi, and Minoru Inaba, *J. Electrochem. Soc.*, **166**, A82 (2019).

Chapter 3

"Dilution Effects of Highly Concentrated Dimethyl Carbonate-based Electrolytes with a Hydrofluoroether on Charge/Discharge Properties of $LiNi_{0.8}Co_{0.1}Mn_{0.1}O_2$ Positive Electrode."

Ziyang Cao, Masakazu Haruta, Takayuki Doi, and Minoru Inaba, *J. Electrochem. Soc.*, **166**, A4005 (2019).

Chapter 4

"Dilution Effects of Highly Concentrated $LiBF_4$/DMC with Fluorinated Esters on Charge/Dishcharge Properties of Ni-rich $LiNi_{0.8}Co_{0.1}Mn_{0.1}O_2$ Positive Electrode."

Ziyang Cao, Masakazu Haruta, Takayuki Doi, and Minoru Inaba, *J. Electrochem. Soc.*, **167**, 040508 (2020).

Publications not included in this thesis

"Fluoroalkyl Ether-diluted Dimethyl Carbonate-based Electrolyte Solutions for High-voltage Operation of $LiNi_{0.5}Co_{0.2}Mn_{0.3}O_2$ Electrodes in Lithium Ion Batteries."

Takayuki Doi, Ryo Matsumoto, Ziyang Cao, Michihiro Hashinokuchi, and Minoru Inaba, *Sustainable Energy & Fuels*, **2**, A1197 (2018).

"Effect of Lithium Silicate Addition on the Microstructure and Crack Formation of $LiNi_{0.8}Co_{0.1}Mn_{0.1}O_2$ Cathode Particles."

Satoshi Hashigami, Yukihiko Kato, Kei Yoshimi, Akihiro Fukumoto, Ziyang Cao, Hiroyuki Yoshida, Toru Inagaki, Michihiko Hashinokuchi, Takayuki Doi, and Minoru Inaba, *ACS Appl. Mater. & Interfaces*, **11**, A39910 (2019).

"Extension of anodic potential window of ester-based electrolyte solutions for high-voltage lithium-ion batteries."

Takayuki Doi, Ryo Matsumoto, Takatsugu Endo, Taishin Sato, Ziyang Cao, Masakazu Haruta, Michihiro Hashinokuchi, Yoshifumi Kimura, and Minoru Inaba, *ACS Appl. Energy Mater.*, **2**, A7728 (2019).

# Acknowledgements

How fast time flies! Without knowing it, five years of doctoral course have passed. The successful completion of the thesis is inseparable from the patient guidance and sincere help of Professor Minoru Inaba and Associate Professor Takayuki Doi at Department of Molecular Chemistry and Biochemistry, Doshisha University. The author is greatly indebted to Professor Yoshifumi Kimura and Professor Takuya Goto at Graduate School of Science and Engineering, Doshisha University, for their helpful discussion and comments.

The author would also like to thank Dr. Michihiro Hashinokuchi, Dr. Masakazu Haruta and Dr. Hideo Daimon for their useful advice and discussion, and all the members of Electrochemistry Laboratory, especially Yusuke Shimizu, Ryo Masumoto, Taccori Romain Jun, Taishin Sato, Ryo Fujii, Taihei Ishihama for their assistance.

Finally, the author is very grateful to his parents and his family for their support and contribution, especially his wife, Yuchen Yang.

Ziyang Cao

March, 2020